Wheel Slip Control in ABS Brakes using Gain Scheduled Optimal Control with Constraints

by

Idar Petersen

Thesis submitted for the degree of
Doktor Ingeniør

Department of Engineering Cybernetics
Norwegian University of Science and Technology
Trondheim, Norway

2003

Norwegian University of Science and Technology
Faculty of Information Technology, Mathematics and Electrical Engineering
Department of Engineering Cybernetics
N-7491 Trondheim
Norway

Dr.ing. thesis 2003:43
ITK Report 2003:1-W

ISBN 82-471-5593-1
ISSN 0809-103X

Preface

This thesis is submitted in partial fulfillment of the requirements for the degree Doktor Ingeniør at the Norwegian University of Science and Technology (`NTNU`) and is based on research done in the period of February 1998 through May 2002.

The doctoral project has been accomplished at SINTEF Automatic Control and the Department of engineering cybernetics, `NTNU`. My supervisor and coadvisor have been professor Tor A. Johansen and professor Bjarne A. Foss respectively. One semester of the doctoral project was spent at the Department of Electrical Engineering and Computer Science at Case Western Reserve University in Cleveland, USA, under the supervision of professor Michael Branicky. The research was sponsored by the European Commission under the ESPRIT LTR-project 28104 H_2C.

Acknowledgments

First and foremost, I would like to thank my advisor professor Tor A. Johansen for his rich source of ideas, practical insight and support throughout the entire research. I am grateful for having been given the opportunity to work on an industrial problem within the framework of a doctoral degree. This close co-operation with my supervisor and the industry has resulted in a book chapter, two journals and several conference papers. This H_2C project and its team dinners will be missed very much.

I would like to acknowledge the cooperative spirit and helpfulness that I have experienced within the H_2C project, specially from Jens Lüdemann and Jens Kalkkuhl at DaimlerChrysler.

Sincere thanks go to Dr.Ing. Kai Hofsten and PhD student Petter Tøndel whom I have been sharing office with. They are duely thanked for their insightful comments and for (always) having a twisted view on life in general - there have been some hilarious, non-academic dialogues in that 'think-box-office'! I would also like to thank a former colleague, Dr.Ing. Olav Slupphaug for his help and 'Trøndersk' humour and Dr.Ing. Lars Imsland for our LMI discussions. I would like to thank all my colleagues and specially the members of the process control group at NTNU, headed by professor Bjarne A. Foss, for an inspiring and social environment.

I am very grateful for the help I have received from Helen Griffiths (from Wales) in proofreading the most important chapters in this thesis.

I would like to thank SINTEF and Sture Holmstrøm for supporting me, and Britt Ottem for all possible help with the administrative paper work. A special thank you to Kjell Eidem for his highly admired service attitude on unix and other network issues.

I am very grateful for the support from my parents and my extended family, the Brennans, which I had the pleasure to stay with during my six months research period in Cleveland. To my beloved wife, Sobah, who has helped me with the editing, has always (almost) been kind and supportive, patient and encouraging, and for your patience at my delayed arrivals for dinner and in waiting for me late at night, I dearly love and respect you deeply. And finally, my dearest daughter Hannah, for all the fantastic moments. If I could only be as awake and happy as you when you wake up in the middle of the night!

Thank you all, this thesis would never have been possible without your contributions.

Idar Petersen

Trondheim, May, 2003

Summary

In a conventional antilock brake system (ABS), the wheel slip will oscillate around a "critical slip" within some given thresholds. This oscillation will have as side effects a noticeable vibration for the driver and limitations in ABS performance. Thus, the actual friction force between tyre and road will oscillate around a "maximum" point. The level of complexity present in current production ABS systems has serious limitations for further development and analysis.

This thesis looks at the analysis and design of an ABS controller using a continuously adjustable electromechanical actuator where the ABS aims to control the slip of the wheel to arbitrary setpoints provided by a higher level control system such as the electronic stability program (ESP). Thus, maximum friction force can be obtained together with a vibration free braking.

This thesis contributes to stability and robustness analysis of a nonlinear ABS controller with respect to uncertainty in the road/tyre friction using Lyapunov theory, frequency analysis and experiments with a test vehicle. A communication delay between the ABS controller and the electromechanical actuator together with the actuator dynamics introduce phase losses and the effect of these performance limitations are also analysed.

This thesis contributes to model-based nonlinear wheel slip controller design, as an explicit gain scheduled LQR design method was used for controller design.

Full-scale results are presented for a Mercedes car (E220) equipped with a brake-by-wire system and electromechanical actuators for various test scenarios, which show that high performance and robustness are achieved. The test scenarios consist of straight-line braking on different road surfaces (ice, snow, dry asphalt, wet asphalt and inhomogeneous asphalt/plastic coated surface) and a single experiment for braking in a turn on dry asphalt.

The main results of this dissertation have been published in international journals, at international conferences and as a book chapter.

Abbrevations

ABC	Active body control
ABS	Antilock brake system
ACC	Adaptive cruise control
BAS	Brake assist system
BbW	Brake by wire
BBWM	Brake by wire manager
CA	Collision avoidance
CRC	Cyclic redundancy check
DbW	Drive by wire
EBD	Electronic brakeforce distribution
ECU	Electronic control unit
EHB	Electrohydraulic brakes
EKF	Extended Kalman filter
EMB	Electromechanical brakes
EMS	Electromechanical steering
ESP	Electronic stability program
ETC	Electronic traction control
HCU	Hydraulic control unit
ISO	International Organization for Standardization
LPV	Linear parameter-varying
OEM	Automotive original equipment
LQR	Linear quadratic regulation
LQRC	LQR with constraints
PM	Power manager
SAE	Society of Automotive Engineers
SbW	Steer by wire
TCS	Traction control system
TDMA	Time division multiple access
TTP	Time-triggered protocol

Contents

Chapter 1

Introduction

> "Braking is to be done as hard and late as possible to ensure that your ABS kicks in, giving a nice, relaxing foot massage as the brake pedal pulsates. For those of you without ABS, it's a chance to stretch your legs." Unknown

The motivation for an anti-lock braking system (ABS) is that it can provide improvements in the performance of the vehicle under braking compared to a conventional brake system (SAE 1992). Performance improvement is typically sought in the areas of stability, steerability and stopping distance. An ABS controls the slip of each wheel to prevent it from locking such that a high friction is achieved and steerability is maintained. ABS controllers are characterized by robust adaptive behaviour with respect to highly uncertain tyre characteristics and fast changing road surface properties (SAE 1992; Burckhardt 1993).

This chapter gives an overview of ABS (history and its function), followed by a literature review on ABS controllers. To prepare the reader for the research presented in this thesis, information on x-by-wire and electromechanical brakes is then provided. This chapter ends with a summary of the contributions found in this thesis, together with the layout of this thesis.

1.1 An anti-lock braking system overview

The current hydraulic ABS systems were conceived from systems developed for trains in the early 1900's. Next, anti-lock brakes were developed to assist aircrafts stop straight and quickly on slippery runways. In 1947, the first use of anti-lock brakes on aeroplanes was on B-47 bombers to avoid tire blowout on dry concrete and spin-outs on icy runways. The first automotive use of ABS was in 1954 on a limited number of Lincolns which were fitted with an ABS from a French aircraft. In the late 60's, Ford, Chrysler, and Cadillac offered ABS on very few models. These very first systems used analog computers and vacuum-actuated modulators. Since the vacuum-actuated modulators cycled so slowly, the vehicle's actual stopping distance increased. Legal concerns then literally put the development on hold in the US, while the European companies took the lead in the next 10-20 years. In the late 70's, Mercedes and BMW introduced electronically-controlled ABS systems. By 1985, Mercedes, BMW and Audi had introduced Bosch ABS systems and Ford introduced its first Teves system. By the late-80's, ABS systems were offered on many high-priced luxury and sports cars. Today, braking systems on most passenger cars and many light-duty vehicles have become complex, computer-controlled systems. Since the mid-80's, vehicle manufacturers have introduced dozens of anti-lock braking systems. These systems differ in their hardware configurations as well as in their control strategy (SAE 1992; Burckhardt 1993).

Any production ABS incorporates a number of subsystems and in most ABS systems there will be a slip controller subsystem, the objective of which is to avoid locking the wheels under a braking manoeuvre, either by ensuring that the slip stays within a specified range or at a given setpoint. Note that not all ABS systems estimate and control the wheel slip explicitly, but work on speed and acceleration instead. Among these subsystems, the logic responsible for coordinating the four wheel slip controllers is of particular importance. The wheel slip controllers for each wheel are (as safety devices) only active in critical situations. Thus, each controller is switched off and the brake is set to manual operation when the wheel is no longer in danger of being locked. On the other hand, the slip controller has to be switched on early enough to prevent the wheel from locking. Thus, the corresponding switching logic is crucial for the functionality of the ABS.

The basic control-philosophy (Burckhardt 1993; Hattwig 1993; Maisch, Mergenthaler, and Sigi 1993; Maier and Müller 1995; Wellstead and Pettit 1997) for conventional ABS systems, is a combination of

- slip control and
- wheel acceleration control.

Wheel acceleration control uses the measured wheel angular velocities to control indirectly the slip by regulating the acceleration/decelration of the wheels. The actuator used in conventional ABS systems is a hydraulic solenoid valve which has three brake pressure modes:

- increase
- hold
- reduce

The controller is switched on when the deceleration of the wheel drops below a specified value for a given period of time. As long as the ABS is active, the switching between the different actuator modes (increase, hold or reduce) is controlled either using several slip and acceleration thresholds or by defining a switching surface using a weighted sum of slip and acceleration. By appropriately selecting these thresholds, the slip will oscillate around the “critical slip”. Thus, the friction force between the tyres and the road surface will be close to its maximum value and the braking distance is minimized. This kind of algorithm will have vibrations as a side effect which are noticeable while braking (Burckhardt 1993).

Slip control works satisfactorily for non-decreasing tyre force characteristics while wheel acceleration control tends to work better for tyre characteristics which have a pronounced maximum. This is due to the fact that a larger wheel acceleration/deceleration can be obtained in the pronounced maximum case. ABS controllers have been shown to be highly adaptive since they can tolerate a considerable amount of uncertainty in the tyre force characteristics and the friction coefficient.

Conventional ABS systems have some limitations in control and performance. One of the most significant disadvantages of these systems is their disability in slip control and tracking of a specified desired slip in an acceptable range.

Today’s production ABS is a rule-based control system that has exhaustive tables for different braking scenarios. The controllers are tuned in a trial and error manner using simulations and exhaustive field testing. The level of complexity of these systems is a serious limitation for the analysis and further development of the current production ABS systems.

1.2 Literature review

Different control methods have been tested for their performance in ABS. The model-based approach in (Drakunov, Özgüner, Dix, and Ashrafi 1995) applies a search for the optimum brake torque via sliding modes. This approach requires the tyre force, hence, a sliding observer is used to estimate it. The approach is tested in a simplified simulation environment. Sliding mode control has been tested in a hardware in the loop simulator (Kawabe, Nakazawa, Notsu, and Watanabe 1997) and also in a vehicle. A derivative part depending on the rotational acceleration is introduced in order to reduce the chattering of the sliding controller. The sliding controller proposed by (Choi and Cho 1998) is mainly used to show the advantage of a PWM controlled actuator. (Wu and Shih 2001) design an ABS controller (without slip-feedback) which integrates sliding-mode control with PWM. Sliding mode control is also considered in (Schinkel and Hunt 2002).

Another theoretical approach is presented by (Freeman 1995). Freeman designs an adaptive Lyapunov-based nonlinear wheel slip controller. This controller has been extended in (Yu 1997) by introducing speed dependence of the Lyapunov function and also including a model of the hydraulic circuit dynamics. Neither of these two latter approaches have been tested in simulation or in a real vehicle. Another Lyapunov based nonlinear adaptive tyre slip controller is presented in (Lüdemann 2002) using Sontag's formula (Sontag 1989; Krstić, Kanellakopoulos, and Kokotović 1995). No actuator dynamics have been included in this analysis.

Feedback linearization to design a slip controller is suggested by (Liu and Sun 1995) where gain scheduling is used to handle the variation of the tyre friction curve with respect to speed.

A maximum tyre/road friction approach using optimal control theory is proposed in (Tsiotras and Canudas de Wit 2000) based on a static friction model.

An adaptive emergency braking controller designed to achieve near-maximum braking effort is suggested in (Yi, Alvarez, Horowitz, and Canudas de Wit 2000).

(Wellstead and Pettit 1997) formulate a conventional ABS controller as a piecewise linear controller including analysis of the switching cycles. Investigations on a variable desired slip can be found in (Fajdiga and Janičijevič 1992). The desired slip is varied according to the side slip angle.

(Taheri and Law 1991) design a simple PD wheel slip controller by the Ziegler-Nichols rule, focusing on the desired slip value. The desired slip is estimated by evaluating the switching of a conventional ABS. Additionally, a modification of the desired slip according to the steering angle is also proposed.

A robust PID controller based on loop-shaping and a nonlinear PID, where the nonlinear function gives a low/high gain for large/small errors respectively, are proposed in (Jiang 2000) together with simulation results for a heavy vehicle. Other PID-type approaches to wheel slip control are considered in (Jun 1998; Wang, Schmitt-Hartmann, Schinkel, and Hunt 2001; Solyom and Rantzer 2002).

Conventional ABS control is compared against PID, sliding and fuzzy controllers in (Jun 1998). The PID algorithm adapts very slowly on different road surfaces. A combination of the model-based approaches should give good performance; but this has not been tested.

1.3 X-by-Wire

There is an increasing demand on automotive original equipment manufacturers (OEM) to increase vehicle safety and performance, while simultaneously reducing manufacturing costs and maximizing efficiencies in the design process (Leen and Heffernan 2002). The introduction of x-by-wire (XBW) systems into the automotive environment is gaining rapid momentum, and XBW examines the global movement toward replacing hydraulics and mechanical systems with electronics for safety-critical applications. The "x" in "x-by-wire" represents the basis of any safety-related application, such as steering, braking, power train, suspension, throttle control or multi-airbag systems. These applications aim to increase overall vehicle safety and performance by liberating the driver from routine tasks and assisting the driver to find solutions in critical situations.

Integrating by-wire systems will create both functional and infrastructure improvements. Functional improvements include (Delphi 2002):

- Improved ride and handling - By-wire computer control of chassis dynamics allows steering, braking, and suspension to work together.
- Enhanced stability control - Sensors and controllers work together to detect then correct increased yaw movements that could result in spinouts or rollovers.
- Safety-enhancing systems - By-wire technology provides the communication link necessary to enable safety systems like lane keeping and collision avoidance.

Through modular design and the elimination of hardware, x-by-wire offers several infrastructure improvements (Delphi 2002):

- Increased modularity - Fully functional by-wire modules reduce OEM assembly time and cost.

- Improved driver interface - The elimination of mechanical connections to the steering column gives OEMs more flexibility in designing the driver interface with regard to location, type, feel, and performance.

- Enhanced passive safety - An x-by-wire cockpit can simplify and improve occupant restraint management.

- Added flexibility - Vehicle designers will have more flexibility in the placement of hardware under the hood and in the interior to support alternative powertrains, enhance styling and improve interior functionality.

- Lead-time reduction - OEMs will be able to use a laptop computer to perform soft tuning capabilities instead of manually adjusting mechanical components.

The following paragraph has been extracted from (Leen and Heffernan 2002). In the past few years there has been a tendency in vehicle construction to increase the safety of vehicles by introducing intelligent assistance systems (e.g. ABS, Brake-Assistant (BA), Electronic Stability Program (ESP), etc.) that help the driver to cope with critical driving situations. Typical for these functions is the active control of the driving dynamics by distributed assistant systems, which therefore need a communication network. The electronic components which control these functions are safety-critical. However, the assistance functions deliver only an add-on service in accordance to a fail-safe strategy for the electronic components. If there is any doubt about the correct behavior of the assistance system, it will be shut down. For by-wire systems without a mechanical backup, a new dimension of safety requirements for automotive electronics is reached. After a fault, the system has to be fail-operational until a safe state (e.g. vehicle stand still) is reached.

Figure 1.1 shows how dynamic driving-control systems have been steadily adopted since the 1920's.

1.3.1 Electromechanical brakes

Brake-by-wire means that there is no hydraulic or mechanical connection between the brake pedal and the brake actuators. The driver's brake command results in an electrical signal that is communicated via micro-controllers to the actuator. Such technologies require new types of brake actuators such as electromechanical, (Hedenetz and Belschner 1998; Schwarz 1999; Isermann,

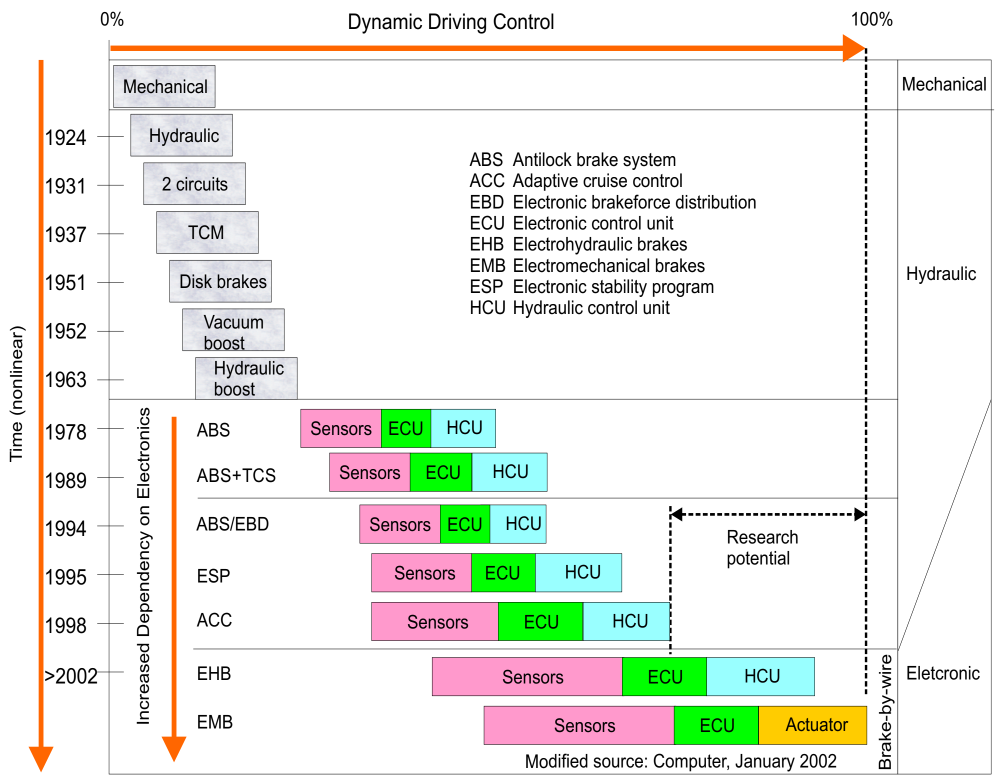

Figure 1.1: Past and projected progress in dynamic driving control systems.

Schwarz, and Stölzl 2002), or electro-hydraulic brakes. A main feature of electromechanical and electro-hydraulic brakes compared to conventional brakes with solenoid valves is that they allow accurate continuous adjustment of the brake force.

Electromechanical Braking systems (EMB), also referred to as brake-by-wire, takes the place of conventional hydraulic braking systems with a completely ‘dry’ electrical component system by replacing conventional actuators with electric motor-driven units. EMB is designed to improve connectivity with other vehicle systems, thus enabling simpler integration of higher level functions such as traction control (ETS), acceleration skid control (ASR), ESP and BA. This integration may vary from embedding the function within the EMB system, as in ABS, to interfacing to these additional systems using communication links.

This move to electronic control helps to eliminate many of the manufacturing, maintenance, and environmental concerns associated with hydraulic systems. The potential benefits of the EMB systems include:

- Assistance functions (ABS, BA, ESP,...) which could be realized by software and sensors, and without additional mechanical or hydraulic components.
- Benefit due to electrical interfaces instead of hydraulic interfaces, which allow easier adapting of assistance systems.
- A reduction in system weight resulting in improved vehicle performance and economy.
- Simpler maintenance as maintenance requirements are reduced.
- Ecological as there is a reduction in pollutant sources reduction through the elimination of corrosive and toxic hydraulic fluids.
- Comfort as pedal ergonomics are adaptable.
- Nearly rest torque-free.
- No mechanical links between the brake components and the engine compartment, improving passive safety.
- No perceptible noise emission when braking.
- Reduced costs for assembly during line production due to simpler and faster assembly of the system into the host vehicle.
- Intelligent error response
- The supervisory monitoring system will not interfere with the pedal movement (no pulsating effect felt).
- Implementation of features such as 'hill hold'.

Another advantage is the elimination of the large vacuum booster found in conventional systems which helps simplify the production of right and left-hand drive vehicle variants.

To satisfy the fail-operational requirement, an additional redundancy in the control components, sensors, software, power supply and the communication system has to be included. Nevertheless, there are still good reasons (as listed above) to introduce by-wire functions for brake systems.

As mentioned earlier, production ABS uses the wheel acceleration to control the slip to maximize the friction force. In the next generation of brake-by-wire systems where EMB's are used, it may be beneficial to introduce a shift from wheel acceleration/deceleration control to slip setpoint control. The slip setpoint is supposed to be provided by a higher level control system (e.g. ESP) which can be used to stabilize the lateral dynamics of the vehicle while braking. In this way, the control objective is shifted to maintain a specified slip for each of the vehicle's wheels. This makes wheel slip control an interesting alternative to conventional ABS systems, where the control logic usually does not include an explicit wheel slip controller (SAE 1992; Maier and Müller 1995; Wellstead and Pettit 1997). The target slip may also be based on automatic monitoring of the road conditions, e.g. (Gustafsson 1997).

1.3.2 The H_2C project

Heterogenous Hybrid Control (H_2C) is an European Commission ESPRIT LTR-project which was started in late 1998 consisting of participants from DaimlerChrysler (Germany), Glasgow University (Scotland), Lund University (Sweden) and SINTEF (Norway). One major research part of the project was to study wheel slip control for an ABS system, where DaimlerChrysler provided a vehicle (a Mercedes E220) fitted with EMB. The following paragraph describes briefly the methods used in designing wheel slip controllers by the project participants in the H_2C project.

The electro-mechanical wheel brake by Continental Teves (Schwarz 1999; Lüdemann 2002) is a disk brake working on the floating caliper-principle. (Lüdemann 2002) formulates two possible hybrid ABS controllers: a Lyapunov-based nonlinear PI-type controller and a nonlinear adaptive slip control using Sontag's formula (Sontag 1998; Krstić, Kanellakopoulos, and Kokotović 1995) which both have been tested. (Schinkel and Hunt 2002) formulate an ABS control using a sliding mode approach. A linearization of a nonlinear model is used in (Wang, Schmitt-Hartmann, Schinkel, and Hunt 2001), where a SSP(simultaneous stabilisation problem) approach is used to design an ABS controller. In (Solyom and Rantzer 2002), a model-based design method for gain scheduled robust nonlinear PI(D) controllers is described and tested. It should be noted that the controller performance by the different controller design methods implemented and tested in the H_2C project, were shown to converge by the end of the project (Lüdemann 2002), but are not conclusive. This is due to the fact that there are no scenarios containing complete test data for well-tuned controllers.

There are several more producers of electromechanical brake actuators from companies such as Siemens, Delphi, Lucas, Bosch, Honda. Due to the industrial property rights and very strict proprietary policies within the automotive industry, very little has been published around automotive EMB. There is no literature describing tests and performance results of EMB beside those that have been carried out through the H_2C project.

1.3.3 Requirements for brake-by-wire systems

There are several requirements for brake-by-wire systems, which are listed below (the terms Safety, Reliability, Maintainability and Availability are used in accordance with the definition of (Laprie 1995)). First, some common requirements for automotive by-wire systems (Hedenetz and Belschner 1998):

- Safety - after one arbitrary fault, the system must be available in a satisfying manner e.g., the brakes have to work with an adequate brake force.
- Reliability - the reliability of a by-wire system must be at least as high as a comparable mechanical system.
- Availability - the availability must be at least as high as present systems.
- Maintainability - the maintainability intervals must be at least as long as present systems.
- Lifetime - the lifetime must be at least as long as present systems. The Society of Automotive Engineers (SAE) classified in-vehicle communication systems into three categories, class A-C (SAE 1993). For safety-related communication systems, class C is required.
- Costs - must be not more than to those of conventional systems.
- Compartment - must be small enough for easy integration of the components.
- Legal aspects - must be fulfilled (Council 1971) (EU has set tolerance guidelines for brake systems. When the braking performance falls within these tolerance levels, the system is considered safe).

Then, the special requirements for brake-by-wire systems:

- Actuators - the brake actuator must be free of braking torque in case of power loss.
- Sensors - triple redundancy shall be used for the pedal sensors to get one valid pedal measurement by the loss of one sensor.
- Power supply - two independent power supplies must be used.
- Communication - the communication system must be fail-operational after one fault.
- Software - the software must be certified (eg. ISO).

To reach these requirements, new technologies had to be developed for the actuators (Schwarz 1999; Lüdemann 2002), communication (FlexRay 2002; Hedenetz and Belschner 1998; Kopetz and Grünsteidl 1994) and electronic components (Flemming 2001; Leen and Heffernan 2002).

1.4 Contributions

The introduction of advanced functionality such as ESP, drive-by-wire and more sophisticated actuators and sensors offers both new opportunities and requirements for a higher performance in ABS brakes. The main motivation for this research has been to analyze and design an ABS controller on an automotive vehicle fitted with a new electromechanical actuator, rather than a hydraulic actuator, which allows continuous adjustment of the clamping force. The main contributions of this thesis can be summarized as:

- Model-based nonlinear wheel slip controller design.
- Lyapunov stability and robustness analysis.
- Full-scale verification tests.

1.4.1 Model-based nonlinear wheel slip controller design

The wheel slip dynamics are highly nonlinear. Despite this, the wheel slip controller design used in this research work is based on an explicit linear quadratic regulation (LQR) design method developed recently, which takes into account the input and state constraints (Johansen, Petersen, and Slupphaug 2000a; Johansen, Petersen, and Slupphaug 2002). The control design relies on local linearization and gain scheduling. My contribution to the design method is mostly on the implementation and the verification of the design method. Two modifications were developed and tested which improved the initial transient response: controller initialization and off-equilibrium design. This constrained LQR will hereafter be referred to as LQRC. The full paper (Johansen, Petersen, and Slupphaug 2002), that describes the controller design method LQRC, is included in Appendix A. In addition, a MATLAB toolbox was developed for the LQRC controller design method (Johansen and Petersen 2001).

Proceeding results were reported in (Branicky, Johansen, Petersen, and Frazzoli 2000; Johansen, Kalkkuhl, Lüdemann, and Petersen 2001).

1.4.2 Lyapunov stability and robustness analysis

As the control design relies on local linearization and gain scheduling, the effects of this simplification are analyzed with a somewhat idealized Lyapunov-based nonlinear stability and robustness analysis, taking into account uncertain tyre friction nonlinearities. The Lyapunov function is derived using the Riccati equation solution. Robust stability is shown for a wide range of slip, tyre friction and expected speed values (Petersen, Johansen, Kalkkuhl, and Lüdemann 2001; Petersen, Johansen, Kalkkuhl, and Lüdemann 2002).

In order to also investigate the effects of sampling, communication delays, actuator dynamics and the fundamental limitations in performance, this analysis is complemented by a classical frequency analysis in (Johansen, Petersen, Kalkkuhl, and Lüdemann 2003). The model used in the three previous references has been extended to include actuator dynamics in (Petersen, Johansen, Kalkkuhl, and Lüdemann 2003). Here, a parameter-dependent Lyapunov function for the nominal closed loop was found by solving an linear matrix inequality (LMI) problem and this function was used to investigate the robustness with respect to uncertainty in the road/tyre friction characteristic. Lyapunov stability and robustness analysis are treated in Chapter 4.

1.4.3 Full-scale verification tests

This research work contains detailed experimental evaluation using a test vehicle, a Mercedes E220, provided by DaimlerChrysler. The test results included in this thesis are from a series of successful experiments carried out for a straight-line braking manoeuvre on different road surfaces (ice, snow, dry asphalt, wet asphalt and inhomogeneous asphalt/plastic coated surface) and braking in a turn on dry asphalt. The results have in part been published in (Petersen, Johansen, Kalkkuhl, and Lüdemann 2001; Petersen, Johansen, Kalkkuhl, and Lüdemann 2002; Johansen, Petersen, Kalkkuhl, and Lüdemann 2003; Petersen, Johansen, Kalkkuhl, and Lüdemann 2003) and are analyzed in Chapter 6.

1.4.4 Scope and organization of H_2C project

The LQRC controller design method was chosen by the H_2C project as the method seemed promising with respect to handling input and state constraints. Half-way through the project, the test vehicle was fitted with a new and faster electromechanical brake-actuator. As a consequence of this upgrade, the need for a design method handling constraints became less important.

The H_2C project was organized such that the test vehicle was provided by DaimlerChrysler with their software and hardware implementations. An important issue to mention is that the extended Kalman-filter was provided by DaimlerChrysler. Time was spent on software programming for basic support function like controller logging and making the application software flexible to allow toggling of active controller and setting of parameters on-line without requiring a recompilation of the run-time software code. The main software provided by the other project participants was their respective wheel slip controller.

DaimlerChrysler also provided a vehicle simulator and a tyre friction model. The simulator was used extensively for thorough testing of the wheel slip controller before being implemented into the test vehicle.

1.5 Outline

Chapter 2 gives an overview of the vehicle with its sensors and computer system. In addition, to provide an insight into the fault tolerance and safety of the ABS used, descriptions of the TTP communication and the brake-by-wire-/power-manager are given. A detailed description of the state-of-the-art electromechanical brake actuator and its discretized model are also included.

Chapter 3 presents the wheel slip dynamics and the quarter car model. Friction curves are presented showing the variation of tyre/road friction as a function of wheel slip for various road conditions. This chapter also gives an introduction to friction modelling together with estimation of friction curves based on experimental data. Finally, dynamics caused by the vehicle pitching is discussed.

Chapter 4 describes why gain scheduled control is suitable for ABS control and presents a linearization of wheel slip dynamics and its properties. Gain scheduled LQ designs with Lyapunov analysis for three cases are provided: (i) slip dynamics without integral action, (ii) slip dynamics with integral action, (iii) slip dynamics with integral action and actuator dynamics.

Chapter 5 explains the implementation, redesign and tuning of the wheel slip controller. An overview of the controller structure, the ABS supervisory logic and the controller states is given. An introduction is then given to the controller design method, LQRC, and its constraint specification. A further analysis of the effects of choice of slip setpoint, sampling, communication delays, actuator dynamics and performance limitations is provided by a classical frequency analysis. Two redesigns that improved the initial transient response (controller initialization and off-equilibrium design) are described. The implementation of anti-windup and bumpless transfer due to gain switching are described in detail.

Chapter 6 describes and discusses in detail all test scenarios and test results that have been conducted. Straight-line braking manoeuvres are shown for surfaces like ice, snow, dry asphalt, wet asphalt and on an inhomogeneous asphalt/plastic coated surface. Experiments where braking was carried out while turning on dry asphalt and the verification of improved initial transient responses are also shown.

Chapter 7 provides discussion and conclusions of this research.

Appendix A is a reprint of (Johansen, Petersen, and Slupphaug 2002).

The notation is consistent throughout the thesis.

Chapter 2

Test Vehicle

This chapter briefly states the computer system used in the vehicle and a concise functional overview of relevant sensors. An extensive description of the EMB, its dynamics and limitations are provided. Further, a brief insight into the TTP communication, the brake-by-wire manager (BBWM) and the power manager/supply unit (PM) are also provided as to explain the safety aspects and why there are inherent physical limitations imposed on the ABS controller bandwidth.

The experimental vehicle is a Mercedes E220 equipped with four electromechanical disk brake actuators supplied by Continental Teves and a brake-by-wire system. Figure 2.1 shows a photo of the test vehicle.

2.1 Computer system and limitations

Figure 2.2 shows the hardware architecture of the vehicle. It consists of four servo controllers for the brakes, a monitoring unit, a BBWM and a PM. These systems communicate via a TTP (time-triggered protocol) bus and the main computer system (for BBWM) consisted of a Motorola 68060 CPU with a floating-point coprocessor. Three major system limitations are listed below having a direct impact on the ABS controller:

i. Limited available processing capacity by the BBWM-CPU for controller processing. This limitation is mainly due to the extended Kalman filter, which required most of the CPU's processing capacity.

ii. Limited available memory for applications running on BBWM. This has a directly limitation on how large the ABS controller software can

Figure 2.1: The experimental vehicle

be.

iii. Phase losses are introduced by the TTP communication delay between the BBWM and the electronic control unit (ECU). This imposes fundamental performance limitations.

2.2 Vehicle sensors

The vehicle is equipped with the following sensors:

- Four wheel speed sensors.
- A sensor for the steering wheel angle.
- Sensors for the position of the brake pedal and the force applied to the brake pedal.
- Two accelerometers for longitudinal and lateral acceleration respectively.
- A yaw rate sensor.

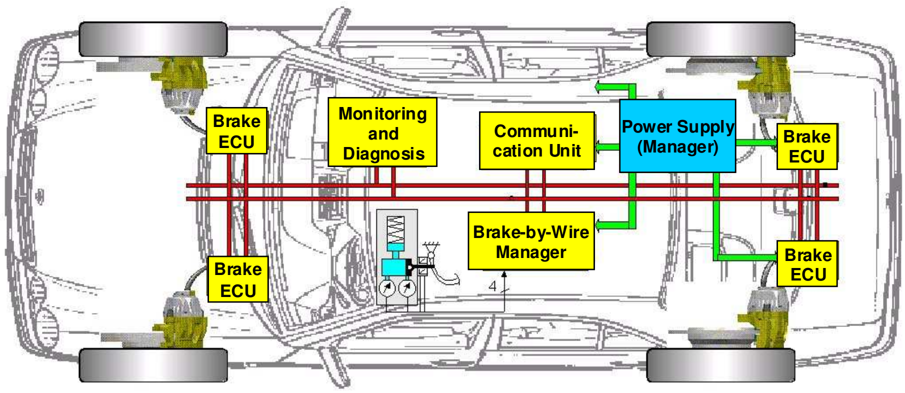

Figure 2.2: Diagram of test vehicle with brake-by-wire

- Four Hall sensors for measuring the clamping forces at each brake.

To determine the driver's intent, the information about the angle of the steering wheel is needed, which is typically delivered from a variable-photosensitivity wheel that interrupts a light beam.

Several sensors are used to track the actual vehicle response to the driver's inputs. Vehicle speed can be estimated from the anti-lock brake wheel-speed sensors. The on-board computer makes an estimate of the coefficient of friction between the tires and the road surface using the estimated vehicle acceleration (from the engine-management system) and the actual lateral acceleration. This estimated coefficient of friction is factored into the driver's inputs and vehicle speed to calculate a nominal sideslip and yaw rate for the vehicle. During this process, special circumstances like inclinations, road crowns, and split-friction-coefficient surfaces are taken into account.

The vehicle was scraped when the H_2C projected ended and therefore a detailed description of the type of electronics used in the vehicle cannot be made. The following sensor information is from (Flemming 2001) and describes the ABS related sensors functionalities and the inherent physical limitations a wheel-speed sensor suffer from.

2.2.1 Wheel-speed sensor

It is from the wheel-speed sensor signals that the ECU derives the wheel's rotation rates. The operating concept is a inductive wheel-speed sensor system.

The inductive wheel-speed sensor's stator pole with its coil winding is installed directly above a reluctor ring (pulse rotor) attached to the wheel hub. This stator pole is linked to a permanent magnet projecting a magnetic field toward and into the reluctor ring. The continuously alternating sequence of teeth (96 in total) and gaps that accompanies the wheel's rotation induces corresponding fluctuations in the magnetic field through the stator pole. These pulse-like variations in the magnetic force field also affect the coil by inducing an alternating current suitable for monitoring at the ends of its windings. The frequency of this alternating current is proportional to the wheel speed.

Various stator-pole pin configurations and installation options are available to adapt the system to the different conditions encountered with various wheels, but regardless of the version, precise alignment between stator pole and reluctor ring is vital. The amplitude of the voltage induced in the windings of the inductive wheel speed sensor is proportional to wheel speed. As this implies, the induced voltage is zero when the wheel is stationary. The minimum detectable rotation rate is defined by such factors as tooth geometry, gap, voltage rise rate and the ECU's sensitivity to incoming signals. The corresponding wheel speed coincides with the minimum switch-off speed available for the ABS application.

In some experiments (see Figures 6.3, 6.4, 6.8, 6.19, 6.20, 6.22, 6.23) at low wheel speeds it can be seen that the wheel slip or the wheel speed has unexpected spikes. This may be due to the fact that there might not be sufficient signals generated within the sampling time to ensure a reliable wheel speed estimate or the generated signal is too weak. To ensure a interference-free signal detection, the gap separating the wheel speed sensor and the reluctor ring is only approximately $1mm$, thus, the installation tolerances are narrow. The wheel-speed sensor is also installed on a stable mounting to prevent mechanic oscillation patterns in the vicinity of the brakes from distorting the sensor's signals. In some experiments (see Figures 6.19 and 6.15) the wheel speed estimate is observed containing repeating noisy spikes and this occurred even before braking was commenced. Finally, the wheel speed sensor also receives a coating of grease prior to installation to protect it from the dirt and water spray common around the wheels.

2.3 Electromechanical brake actuator

The electromechanical actuator is a disk brake working on the caliper-principle. The actuator's housing is connected firmly to the vehicle‘s steering knuckle. Both brake pads are fixed to the fist with one degree of freedom towards the active line of the clamping force. Figure 2.3 shows a photo of the EMB and its mounting in the vehicle.

Figure 2.3: Photo of the electromechanical brake

Figure 2.4 shows a sectional drawing of the brake. The electromechanical converter is a brushless DC motor. At the pad-sided end, the rotor gear forms the sun wheel of the planetary gear. The planet wheels of the planetary gear are in mesh with the internal-geared wheel, bolted in the brake cabinet and which power the planet carrier. A planetary roller gear transforms the rotary motion into a translatory motion. The planetary gear's spindle is hollow and contains a force measurement device as well as a pressure pin for the decoupling of rotating movements acting on the spindle. When activating the brake, the drive end brake-pad will be moved through the pad support, whereas the pressure pin and the force sensor will be shifted towards the brake disk, caused by the spindle‘s motion. The above description of the EMB is extracted from (Lüdemann 2002).

2.3.1 EMB model

The model of the electromechanical brake consists of a model of an electric motor and a gearbox that transforms the rotational movement into a translatory movement. A nonlinear characteristic for the conversion of the

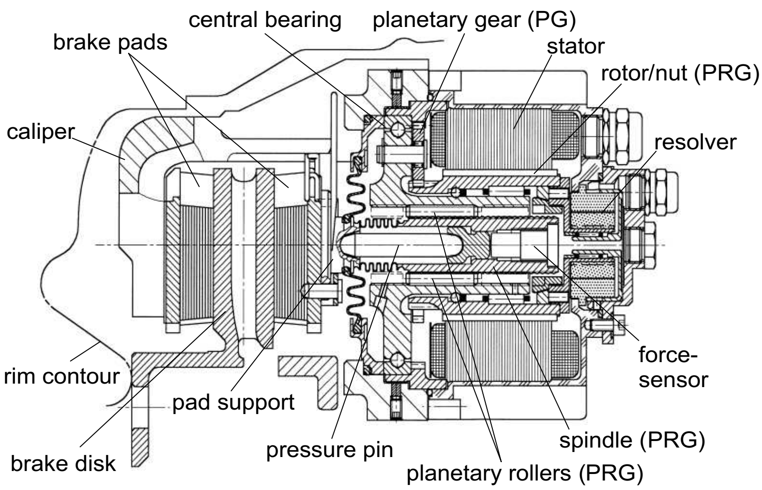

Figure 2.4: Cross-section diagram of electromechanical brake

movement into a force as well as a nonlinear friction model is taken into account. Figure 2.5 shows the structure of the physical model of the brake where the symbols have the following meaning:

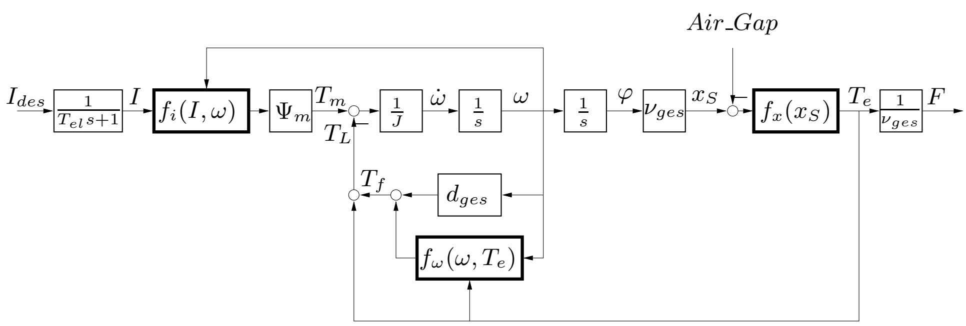

Figure 2.5: Physical EMB model

Air_Gap	:	Air gap between brake disk and brake pads
d_{ges}	:	Overall viscous friction
$f_i(I, \omega)$	:	Feedback of the motor on the current
$f_x(x_S)$	:	Transfer function between spindle position and clamping force
$f_\omega(\omega, T_e)$	:	Transfer function between angle of rotation and friction torque
F	:	Clamping force
I	:	Motor current
J	:	Overall inertia
T_e	:	Available torque
T_f	:	Friction torque
T_L	:	Available load torque $\quad T_L = T_e + T_f$
T_m	:	Electric torque
T_{el}	:	Electric time constant of the motor
x_S	:	Spindle position
ν_{ges}	:	Transmission factor
φ	:	Rotation angle
Ψ_m	:	Magnetic flux
ω	:	Angular velocity

The electromechanical brake is servo controlled by a cascade PID-controller, which consists of a current controller, an angular velocity controller and a force controller as shown in Figure 2.6. The index m denotes the measured values of the clamping force F_m, ω denotes the angular velocity and I the current. Index b indicates the reference signal. From the brake pedal measurements (brake-wish) the brake-by-wire system computes a desired clamping force (F_d) for each brake actuator. After F_d has passed through an anti-windup routine, the slip controller output F_b is passed to the EMB servo controller. Thus, the control output F_b cannot become larger than the desired clamping force F_d. F_b is the reference clamping force signal provided to the brake servo controllers of each wheel.

The EMB model is from (Schwarz 1999; Lüdemann 2002).

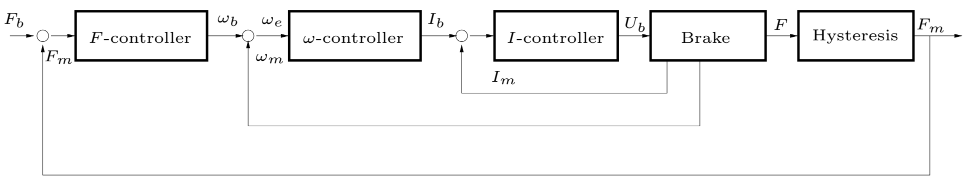

Figure 2.6: Cascade structure of the EMB servo controller

2.3.2 Actuator dynamics

The electromechanical actuator has its own internal dynamics as seen in Section 2.3.1 and a discretized transfer function is described by

$$h_2(z^{-1}) = \frac{0.1572z^{-1} - 0.0254z^{-2}}{1 - 1.5222z^{-1} + 0.6549z^{-2}} \tag{2.1}$$

An approximation of the second order transfer function (2.1) to a first order discrete-time linear transfer function with sufficient accuracy for control design gives:

$$h_1(z^{-1}) = \frac{b_{act}z^{-1}}{1 - a_{act}z^{-1}} \tag{2.2}$$

Its corresponding first order discrete-time linear state space model (with sampling interval $T_s = 7ms$) is

$$T_b(t+1) = a_{act}T_b(t) + b_{act}\tilde{T}_b(t) \tag{2.3}$$

with $\tilde{T}_b$ being the commanded brake torque to the actuator, $a_{act} = 0.6$ and $b_{act} = 0.4$ which makes it equivalent to alow-pass filter. The transfer function has a phase of -18.6 degrees at $f = 3Hz$ and -61.7 degrees at $f = 11.8Hz$, cf. Figure 2.7. Sinusoidal experimental results (Lüdemann 2002) show that the EMB actuator has a phase of approximately -20 degrees at $f = 3Hz$ and -60 degrees at $f = 10Hz$.

Figure 2.8 shows step responses of the actual EMB actuator and its two models, a first order (2.2) and a nonlinear (from Figure 2.5). The step responses of the first order and the non-linear models are similar (cf. Figure 2.8), but the nonlinear model is better. The nonlinear brake model is only used for simulation. A corresponding continuous first order transfer function for equation (2.2) is

$$h_1(s) = \frac{a}{s+a} \tag{2.4}$$

where the parameter $a = 72$ rad/s is the bandwidth of the actuator.

There are limitations on the clamping force that can be applied to the brake pads by the actuator during braking. The (small) minimum force is to ensure that the brake pads are positioned close to the brake disk with no air-gap. The maximum force is what the actuator is capable of. Maximum braking force with the EMB 4.0 actuator is 30 kN. The control input is the clamping force F_b that is related to the brake torque as $T_b = k_bF_b$, where the constant k_b depends on the friction between the brake pads and the brake

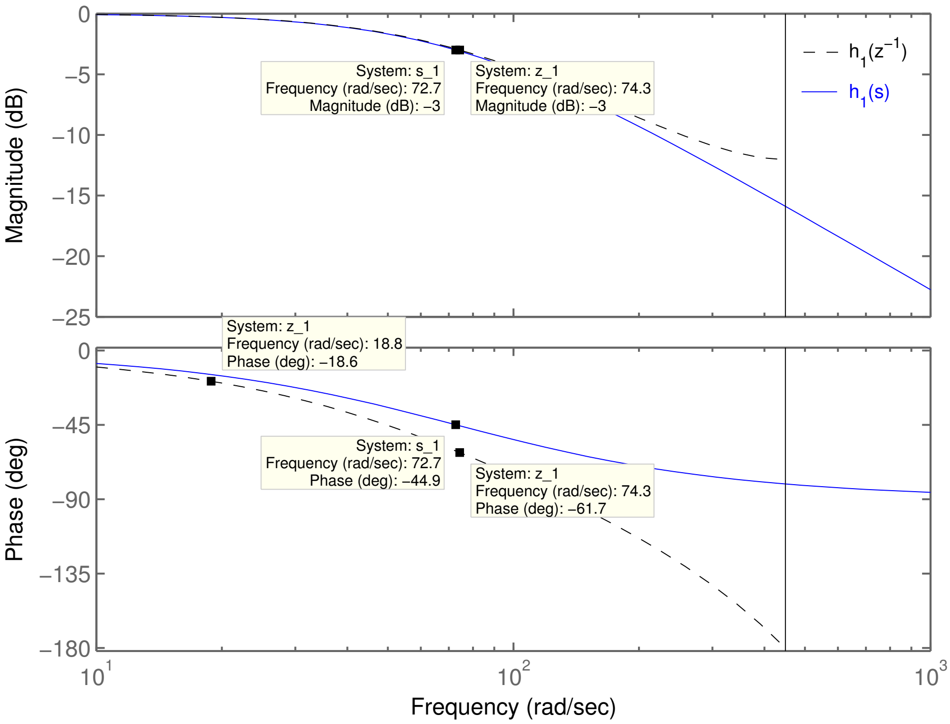

Figure 2.7: Bode plot of $h_1(z^{-1})$, $h_1(s)$

disc. This leads to the actuator constraint (see Section 5.5.3 for further implementation details):

$$T_b^{max} = 0.1056m \cdot 30kN \; = \; 3017Nm \tag{2.5}$$

There is also a rate limit at how fast the torque can be changed by the actuator:

$$\dot{T}_b^{max} = 250kNm/s \tag{2.6}$$

2.4 TTP Communication

Designed for realtime distributed systems that are hard and fault tolerant, the time-triggered protocol ensures that there is no single point of failure (Kopetz and Grünsteidl 1994). The protocol has been proposed for systems that replace mechanical and hydraulic braking and steering subsystems. TTP is an offshoot of the European Union's Brite-Euram X-by-wire

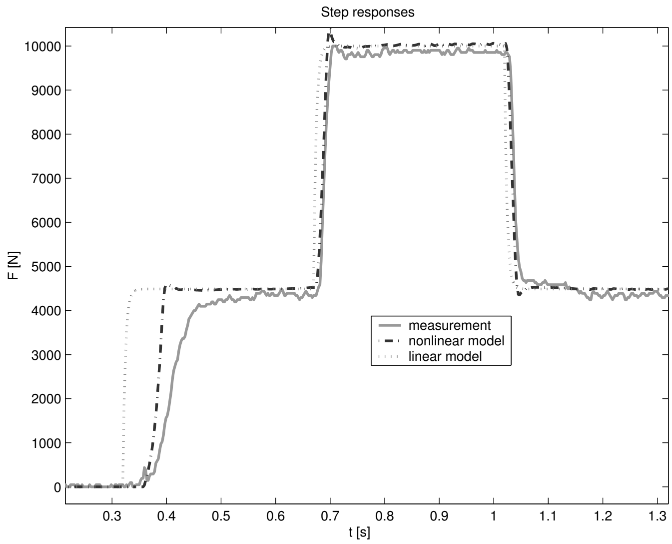

Figure 2.8: Verification of the brake models

project. In contrast to an event triggered system, a TTP system is built up by defining first the static message schedule (Hedenetz and Belschner 1998). Figure 2.9 shows the communication matrix of the brake-by-wire network in the test vehicle. The lower part of Figure 2.9 shows the static synchronous TDMA (time division multiple access) schedule and its constraint where each subsystem has to send exactly once in a TDMA cycle. The messages shown with 'I' are called I-Frames and are used for synchronization of lost members. I-Frames do not transmit information for the application layer, therefore they are not shown in the upper part of the matrix where the receivers of the transmitted messages are located.

All communication between the BBWM, the PM and the ECU's is based on the fault tolerant TTP bus. The BBWM and the PM send their messages in vice versa time slots. In this way short burst errors can be recovered. A BBWM slot has a length of about $0.88msec$.New set points for the brake force can be sent every $7msec$. The brake control ECU's send their status and the current brake force. These messages are not so time critical as the transmission of the brake force set points. The brake ECU's send their messages only once in a cluster cycle, which is 16 slots. In the available slots, the brake ECU's send I-Frames for the network management.

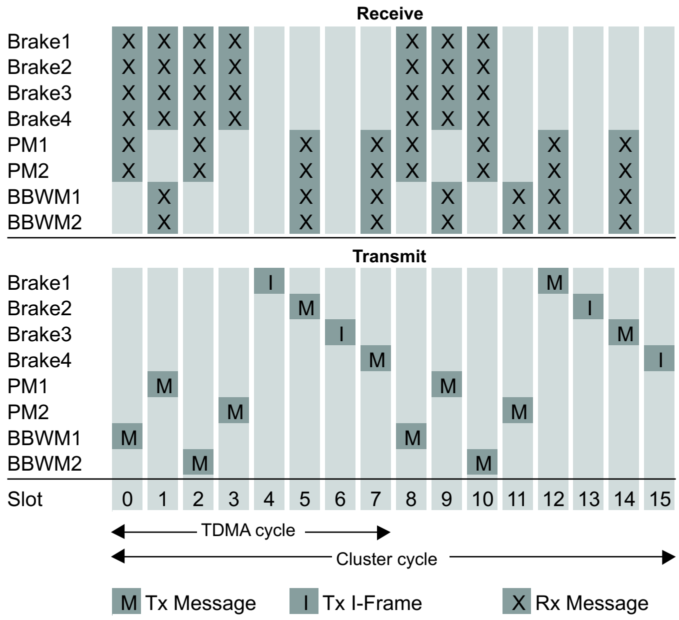

Figure 2.9: Communication Matrix of the Brake-by-wire

2.5 Brake-By-Wire-Manager and Power Manager

The BBWM functionality is to read the values from the brake pedal sensors, the revolution counters of the wheels, the yaw-sensor, the acceleration sensors and to calculate from all these values the brake force (set points) for the four brake actuators. The BBWM can manage higher assistance functions like ABS, traction and driving dynamic control.

The ECU assumes all the system's electrical, electronic and closed-loop control functions. These include

- Power supply for all the system sensors
- Registration of operating conditions
- Data conversion (input/output drivers, A/D conversion)
- Data conditioning (calculation of manipulated variables using stored program maps)
- Data transmission (amplification and relay of signals to the system actuators)

- CAN network linkage to other ECU's.

The PM controls the battery charger, proceeds active power management and monitors the status of the power supply. If the generator or one of the redundant power circuits should fail or the charge of the batteries is getting low, the PM generates a warning signal. Each of the four brake actuators have one brake ECU to control the electric motor of the brake actuator.

Figure 2.10 shows the schedule, which is periodically executed in the BBWM:

i. Pedal Signal Measurement - of the pedal signals from the three pedal sensors.

ii. Pedal Signal Plausibility Checks - from the three pedal signals, one valid value is selected. This task is executed three times to detect faults.

iii. Voter - a task votes over the result of the three plausibility check tasks.

iv. Brake Force Control - the brake forces for the four actuators are calculated. This task is also executed three times.

v. Voter - a task votes over the result of the three brake force control tasks.

vi. TTP Communication - the brake forces are send to the brakes via the TTP communication network.

vii. Diagnose - a diagnostic task.

viii. Diagnose Output - the diagnose values are transmitted to an external diagnosis device.

The Pedal Signal Plausibility Checks and the Brake Force Control are both executed three times (due to being safety-related tasks) to discover possible faults. These two tasks are safety-related since they handle and manipulate data variables, while the other tasks i.e. Pedal Signal Measurement, TTP-Communication, Diagnose and Diagnose Output, only handle messages and are protected through cyclic redundancy checks (CRC).

This section is based on (Hedenetz and Belschner 1998).

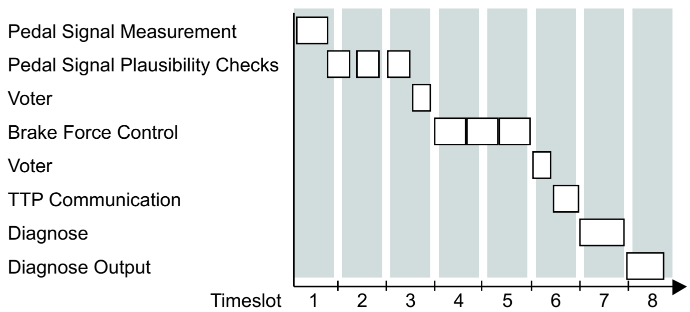

Figure 2.10: Local Task Schedule of the BBWM

Chapter 3

Wheel slip dynamics

This chapter will first discuss the slip dynamics which is used in the following chapter for controller design. In Section 3.1, a mathematical model of the wheel slip dynamics is reviewed, see also (Burckhardt 1993; Freeman 1995; Drakunov, Özgüner, Dix, and Ashrafi 1995). Second part of this chapter will look into friction models. The actual friction model used in this research was provided by DaimlerChrysler and due to its confidentiality, no description can be provided. Therefore, a section is provided as an introduction to friction modelling followed by a section on estimation of friction curves to be used on experimental data later in this thesis, where a friction curve is produced from each experiment. Finally, suspension dynamics are considered as it might affect the controller performance since it is not included in the controller design.

3.1 Wheel slip dynamics

The problem of wheel slip control is best explained by looking at a quarter car model as shown in Figure 3.1. The model consists of a single wheel attached to a mass m. As the wheel rotates, driven by the inertia of the mass m in the direction of the velocity v, a tyre reaction force F_x is generated by the friction between the tyre surface and the road surface. The tyre reaction force will generate a torque that results in a rolling motion of the wheel causing an angular velocity ω. A brake torque applied to the wheel will act against the spinning of the wheel causing a negative angular acceleration.

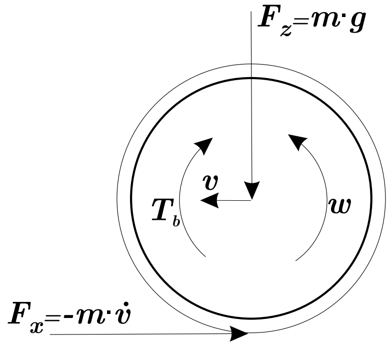

Figure 3.1: Quarter car forces and torques.

The equations of motion of the quarter car are

$$m\dot{v} = -F_x \tag{3.1}$$

$$J\dot{\omega} = r\,F_x - T_b\,\mathrm{sign}(\omega) \tag{3.2}$$

where

m	mass of the quarter vehicle
v	longitudinal speed at which the vehicle travels
ω	angular speed of the wheel
F_z	vertical force
F_x	tyre friction force
T_b	brake torque
r	wheel radius
J	wheel inertia

The tyre friction force F_x is given by

$$F_x = F_z\mu(\lambda, \mu_H, \alpha) \tag{3.3}$$

where the friction coefficient μ is a nonlinear function of

λ	longitudinal tyre slip
μ_H	maximum friction coefficient between tyre and road
α	slip angle of the wheel

The longitudinal slip is defined by

$$\lambda = \frac{v - \omega r}{v} \tag{3.4}$$

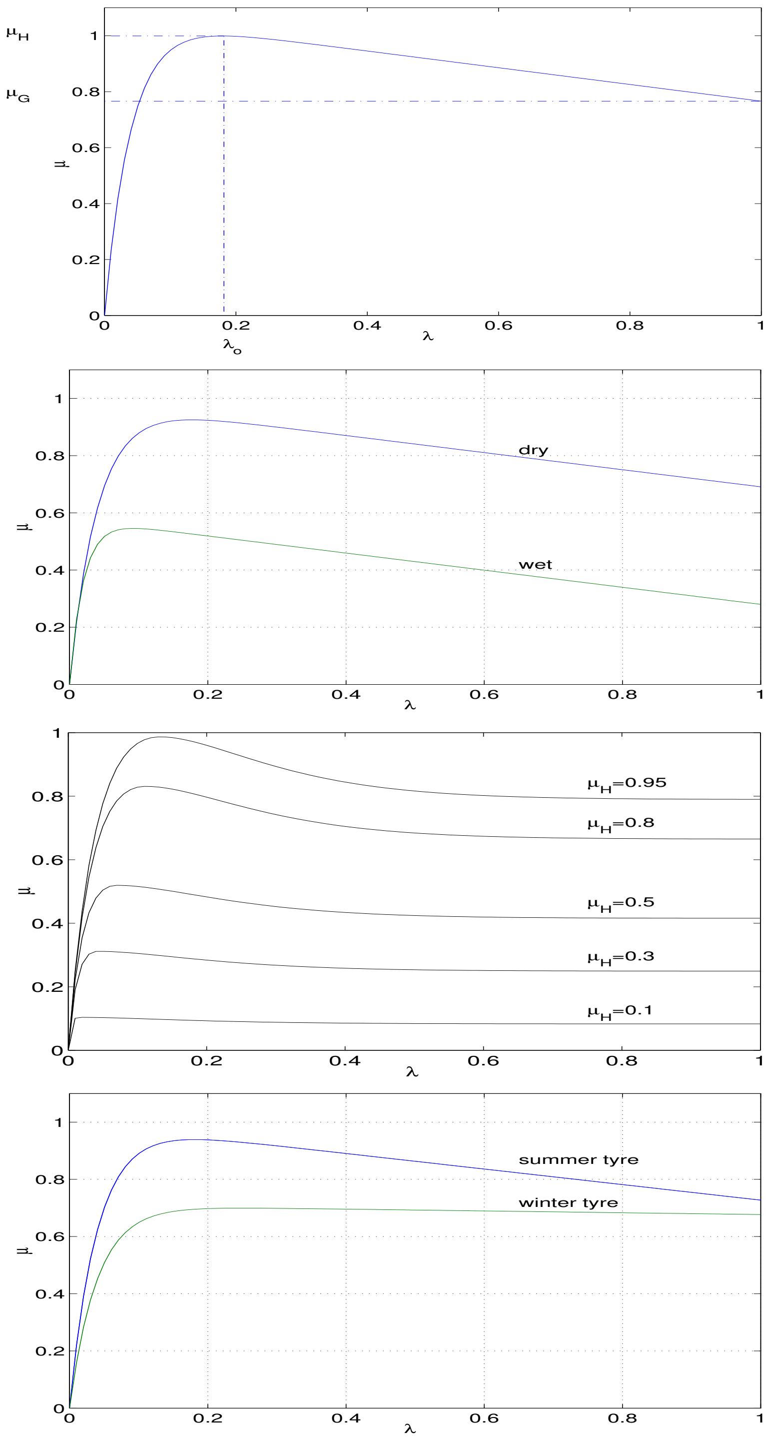

Figure 3.2: Typical friction curves.

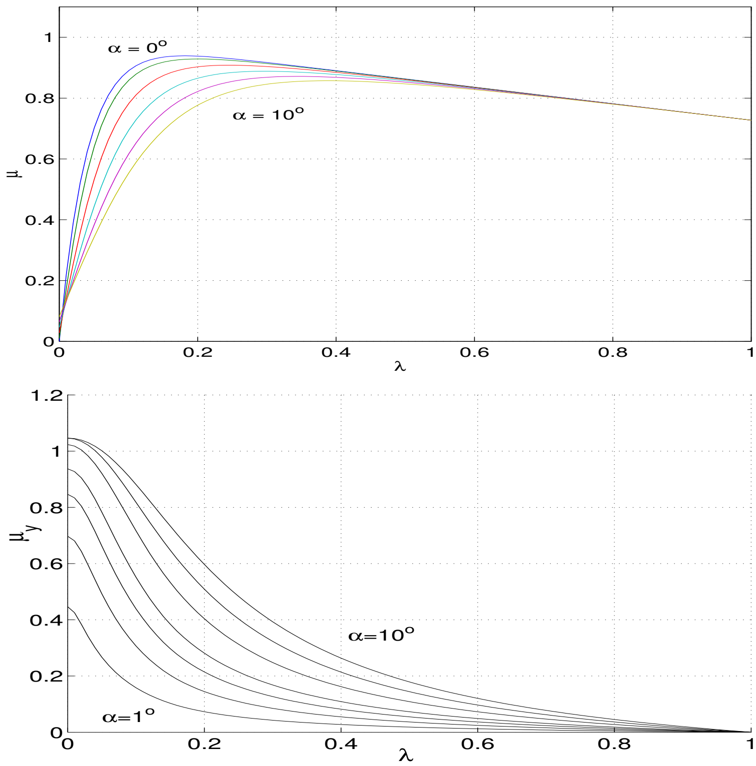

Figure 3.3: Tyre side slip/friction curves. In top figure, $\mu = \mu_x$.

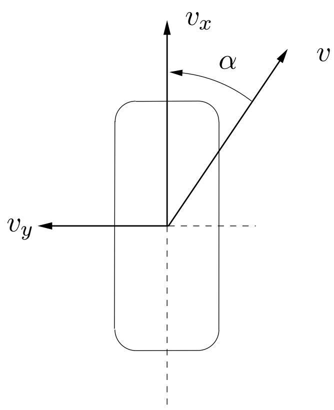

Figure 3.4: Definition of wheel slip angle.

Surface	μ_H
Asphalt and concrete (dry)	0.8-0.9
Concrete (wet)	0.8
Asphalt (wet)	0.5-0.6
Earth road (dry)	0.7
Earth road (wet)	0.5-0.6
Gravel	0.6
Snow (hard packed)	0.3
Ice	0.1

Table 3.1: Tyre/road friction peak

and describes the normalized difference between the vehicle speed v and the speed of the wheel perimeter ωr. The slip value of $\lambda = 0$ characterizes the free motion of the wheel where no friction force F_x is exerted. If the slip attains the value $\lambda = 1$, then the wheel is locked ($\omega = 0$).

The friction coefficient μ can span over a very wide range, but is generally a differentiable function with respect to all arguments and has the properties $\mu(0, \mu_H, \alpha) = 0$ and $\mu(\lambda, \mu_H, \alpha) > 0$ for $\lambda > 0$. Its typical qualitative dependence on longitudinal slip λ is shown in Figure 3.2. The upper part shows how the friction coefficient μ increases with slip λ up to a value λ_0, where it attains its maximum value μ_H. For higher slip values, the friction coefficient will decrease to a minimum μ_G where the wheel is locked and only the sliding friction will act on the wheel. The dependence of friction on the road condition is shown in the two figures in the middle of Figure 3.2. For wet or icy roads, the maximum friction μ_H is small and the right part of the curve is flatter. The tyre friction curve will also depend on the brand of the tyre, as illustrated in the lower part of Figure 3.2. In particular, for winter tyres, the curve will cease to have a pronounced peak. Typical friction peak values (Burckhardt 1993; Gustafsson 1997; Hunter 1998; Canudas de Wit, Horowitz, and P.Tsiotras 1999) for different surface conditions are given in Table 3.1.

If the motion of the wheel is extended to two dimensions, then the lateral slip of the tyre must also be considered. The slip angle α is the angle between the wheel bearing and the velocity vector of the vehicle, shown in Figure 3.4. In this case (Burckhardt 1993), the longitudinal slip

$$\lambda_x = \frac{v_x - \omega r}{v} \tag{3.5}$$

and the lateral slip

$$\lambda_y = \frac{\omega r \sin\alpha}{v} = (1 - \lambda_x)\sin\alpha \tag{3.6}$$

are distinguished as well as the longitudinal and lateral friction coefficients μ_x and μ_y. v_x is the wheel longitudinal speed in the wheel's longitudinal direction.

The upper part of Figure 3.3 shows the dependence of the friction coefficient μ_x on the side slip angle α. The lateral friction is dramatically reduced as the longitudinal slip increases. The lateral friction μ_y depends greatly on the side slip angle α and is shown in the lower part of Figure 3.3. The longitudinal force gets smaller as side slip angle is increased. This physical phenomenon is the main motivation for ABS brakes, since avoiding high longitudinal slip values will maintain high steerability and lateral stability of the vehicle during braking. Achieving this by manual control is difficult because the slip dynamics are fast and open loop unstable when operating at wheel slip values to the right of any peak of the friction curve. Observe that a reasonable tradeoff between high longitudinal friction μ_x and lateral friction μ_y is achieved under all road conditions for longitudinal slip λ_x close to its peak value on the longitudinal slip curve. Hereafter, for simplification purposes unless otherwise stated, the side slip angle will be considered to be zero with $\mu_x = \mu$ and $v_x = v$.

Using (3.1)-(3.4), for $v > 0$ and $\omega \geq 0$, the wheel slip dynamics is obtained by calculating the time derivative of (3.4) with respect to time

$$\begin{aligned}\dot{\lambda} &= \frac{\mathrm{d}}{\mathrm{d}t}\left(1 - \frac{\omega r}{v}\right)\\ &= -\frac{\dot{\omega} r}{v} + \underbrace{\frac{\omega r}{v}}_{1-\lambda} \cdot \frac{\dot{v}}{v}\\ &= -\frac{1}{v}\left(\frac{1}{m}(1-\lambda) + \frac{r^2}{J}\right) F_z \mu(\lambda, \mu_H, \alpha) + \frac{1}{v}\frac{r}{J} T_b\end{aligned} \tag{3.7}$$

and

$$\dot{v} = -\frac{1}{m} F_z \mu(\lambda, \mu_H, \alpha) \tag{3.8}$$

Notice that when $v \to 0$, the open loop slip dynamics (from T_b to λ) becomes infinitely fast with infinite high-frequency gain. Hence, the slip controller should be switched off for small v. The following result shows that the interval $[0, 1]$ is a positively invariant set for the wheel slip λ under the condition that $v > 0$ and $T_b \geq 0$ (i.e. there is braking and no traction):

Proposition 3.1 *Consider the system (3.7)-(3.8) with $T_b(t) \geq 0$ for all $t \geq 0$. If $v(0) > 0$ and $\lambda(0) \in [0, 1]$, then $\lambda(t) \in [0, 1]$ and $\dot{v}(t) \leq 0$ for all $t \geq 0$ where $v(t) > 0$.*

Proof 3.1 *Note that $\lambda(t)$ is a continuous trajectory since $v(t) > 0$. Hence, the possible escape points are $\lambda = 0$ and $\lambda = 1$. Consider first $\lambda = 0$. Since $\mu(0, \mu_H, \alpha) = 0$, it follows from (3.7) that $\dot{\lambda} = \frac{r}{vJ} T_b \geq 0$ due to $T_b \geq 0$. Hence, $\lambda(0) \geq 0$ implies $\lambda(t) \geq 0$ for all $t \geq 0$. Consider next $\lambda = 1$. Then, $\omega = 0$ and from (3.2) it follows that $\dot{\omega} \geq 0$ due to the discontinuity sign(ω) in (3.2). From (3.4), we conclude that $\dot{\lambda} = -r\dot{\omega}/v \leq 0$, which implies $\lambda(t) \leq 1$ for all $t \geq 0$. Finally, note that $\dot{v} \leq 0$ from (3.1) because $F_x \geq 0$ for $\lambda \in [0, 1]$.*

□

3.2 Friction modelling

The qualitative dependence of the tyre reaction forces on slip, type of tyre and road condition was explained in the previous section. Here, a background to tyre friction modelling will be given.

Several tyre friction models describing the nonlinear behaviour are reported in the literature. There are static models as well as dynamic models, models which are constructed based on heuristical data as well as others which have been derived from physical behaviour. The most reputed tyre model is by (Bakker, Nyborg, and Pacejka 1987), and by (Pacejka and Sharp 1991), also known as "magic formula" and it is derived heuristically from experimental data. It provides the tyre/road coefficient of friction μ as a function of the slip λ by using static maps. The "magic formula" has been shown to suitably match experimental data and is on the form:

$$F_x(\lambda_x) = D \sin(C \arctan(B\lambda_x - E(B\lambda_x - \arctan(B\lambda_x))))$$

The parameters, $B - E$, characterises the model and can be identified by comparing experimental data as shown in (Bakker, Nyborg, and Pacejka 1987). The model can also be used for modelling two other characteristics, the lateral force and the aligning torque. Effects due to either ply-steer or conicity effects are also taken into account (Pacejka and Sharp 1991).

Surface conditions	C_1	C_2	C_3
Asphalt, dry	1.2801	23.99	0.52
Asphalt, wet	0.857	33.822	0.347
Concrete, dry	1.1973	25.168	0.5373
Cobblestones, dry	1.3713	6.4565	0.6691
Cobblestones, wet	0.4004	33.7080	0.1204
Snow	0.1946	94.129	0.0646
Ice	0.05	306.39	0

Table 3.2: Friction parameters

The expression in (Burckhardt 1993) is derived with similar methodology where μ is expressed as a function of the wheel slip, λ, and the vehicle velocity, v. The vertical force on the tyre is assumed constant which gives

$$\mu_x(\lambda, v) = \left[C_1\left(1 - e^{-C_2\lambda}\right) - C_3\lambda\right] e^{-C_4\lambda v} \tag{3.9}$$

where the parameters are specified for different road surfaces, see Table 3.2 (Kiencke and Nielsen 2000). The parameters in (3.9) denote the following:

C_1	-	maximum value of friction curve
C_2	-	friction curve shape
C_3	-	friction curve difference between the maximum value and the value at $\lambda = 1$
C_4	-	wetness characteristic value and is in the range $0.02 - 0.04 s/m$.

(Daiß and Kiencke 1996) has simplified (Burckhardt 1993)'s model to make it linear in the parameters (a and b) with the model

$$\mu(\lambda) = \frac{k\lambda}{a\lambda^2 + b\lambda + 1}$$

where k is the initial slope value (at $\lambda = 0$).

The dynamical tyre friction models can be formulated as a lumped or distributed models, where a lumped friction model (Canudas de Wit, Olsson, Åström, and Lischinsky 1995) assumes punctual tyre/road friction contact and a distributed model (Canudas de Wit, Horowitz, and P.Tsiotras 1999) assumes the existence of an area of contact between tyre/road. The lumped model is written on the form

$$g(v_r) = \mu_C + (\mu_S - \mu_C)\, e^{-|v_r/v_s|^{1/2}}$$
$$\dot{z} = v_r - \frac{\sigma_0\,|v_r|}{g(v_r)} z$$
$$F_x = (\sigma_0 z + \sigma_1 \dot{z} + \sigma_2 v_r) F_z$$

where

F_x	-	the friction force
F_z	-	normal force
σ_0	-	rubber longitudinal lumped stiffness
σ_1	-	rubber longitudinal lumped damping
σ_2	-	viscous relative damping
μ_C	-	normalized Coulomb friction
μ_S	-	normalized static friction, $\mu_C \leq \mu_S \in [0, 1]$
v_S	-	Stribeck relative velocity
v_r	-	relative velocity = $(r\omega - v)$
z	-	internal friction state

Apart from the nonlinear behaviour of the slip, the tyre friction depends on other uncertainties like road condition, tyre pressure, brand of tyre, temperature etc.

3.2.1 Estimation of friction curves

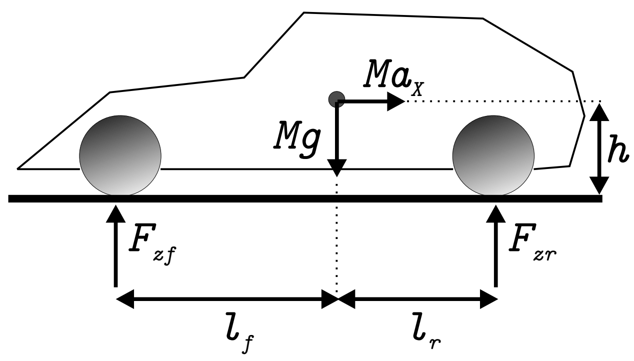

Figure 3.5: Axle torque balance.

As the previous section has described some friction modelling strategies and properties, it is of interest to be able to estimate a model of the surface conditions for different test scenarios based on the available experimental data.

Straight-line braking

The friction coefficient is defined as the ratio (3.3),

$$\mu = \frac{F_x}{F_z} \tag{3.10}$$

In order to estimate the friction coefficient μ, the values of F_x and F_z are needed. This can be carried out using the method described in (Kiencke and Nielsen 2000). Equation (3.2) gives the longitudinal friction force F_x, which gives the friction value μ:

$$\mu = \frac{J\dot{\omega} + T_b}{F_z r} \tag{3.11}$$

The friction value can be found by using a torque balancing about the wheel axis (single wheel model). In order to find an expression for F_z, a few assumptions can be made. The coupling between roll and pitch is neglected, thus the dependencies of the quarter vehicle forces on the longitudinal and lateral accelerations can be determined separately. By disregarding suspension dynamics, the quarter vehicle forces are identical to the wheel vertical forces F_z.

The force due to longitudinal deceleration (Ma_x) at the center of gravity (CoG), see Figure 3.5, causes a pitch torque which reduces the rear axle load and increases the front axle load. Constructing the torque balance at the rear axis contact point gives the front vertical force

$$\begin{aligned} lF_{zf} &= l_r Mg - hMa_x \\ &\Downarrow \\ F_{zf} &= \frac{M(l_r g - ha_x)}{l} \end{aligned} \tag{3.12}$$

where M is vehicle mass at CoG, a_x is the longitudinal acceleration of CoG, h is the height of CoG and $l = l_f + l_r$. This gives the vertical force for a single front wheel to be ($F_{z(f=front/r=rear,l=left/r=right)}$)

$$F_{zfl} = F_{zfr} = \frac{M(l_r g - ha_x)}{2l} \tag{3.13}$$

with the corresponding friction coefficient

$$\mu_f = \frac{(J\dot{\omega} + T_b)\,2l}{M(l_r g - h a_x) r} \tag{3.14}$$

Similarly, balancing the torque at the front axis contact point gives the vertical force (ground contact force) for a single rear wheel

$$F_{zrl} = F_{zrr} = \frac{M(l_f g + h a_x)}{2l} \tag{3.15}$$

with the corresponding friction coefficient

$$\mu_r = \frac{(J\dot{\omega} + T_b)\,2l}{M(l_f g + h a_x) r} \tag{3.16}$$

The same technique is applied to find the vertical force due to roll torques (assuming that the front and rear axles are decoupled). This gives the wheel force, F_Z, for the four wheel forces:

$$F_{zfl} = \frac{M(l_r g - h a_x)}{l}\left(\frac{1}{2} - \frac{h a_y}{b_f g}\right) \tag{3.17}$$

$$F_{zfr} = \frac{M(l_r g - h a_x)}{l}\left(\frac{1}{2} + \frac{h a_y}{b_f g}\right) \tag{3.18}$$

$$F_{zrl} = \frac{M(l_f g + h a_x)}{l}\left(\frac{1}{2} - \frac{h a_y}{b_r g}\right) \tag{3.19}$$

$$F_{zrr} = \frac{M(l_f g + h a_x)}{l}\left(\frac{1}{2} + \frac{h a_y}{b_r g}\right) \tag{3.20}$$

where a_y (leftwards positive) is the lateral acceleration of CoG and b_f and b_r are the distances between wheels on the front and rear axles respectively.

Measurements needed for estimation of friction curve

A friction curve can then be plotted for each wheel from experiments, where stationary wheel load is achieved, by post-calculating experimental data. This will yield friction curves (Section 6) which resemble what is shown in Section 3.1.

To obtain the friction value from equations (3.14,3.16,3.17-3.20), the wheel angular acceleration ($\dot{\omega}$), the brake torque (T_b), the longitudinal deceleration (a_x), lateral acceleration (a_y) and the position of the center of gravity are required. The brake torque, T_b, is derived from the measured clamping force.The wheel angular acceleration is calculated from the differences between two consecutive samples of the wheel angular speed:

$$\dot{\omega}(n) = \frac{\omega(n) - \omega(n-1)}{T_s} \tag{3.21}$$

3.3 Suspension dynamics

A suspension system can be best studied as a dynamic system by looking at the basic properties of the suspensions properties, i.e. the motions of the body and the axles. Due to the suspension dynamics, there may be resonance frequencies which will cause oscillations in the suspension system. Therefore, a wheel slip control design should, if possible, be tuned to avoid exciting the suspension system.

The inputs to the suspension system are the road displacement and the vertical force on the body, while the output is the vertical motion of the body when a quarter car model is considered, as shown in Figure 3.6, where the suspension can be seen to have stiffness and damping properties. The tyre is also represented with spring/damper, although the amount contributed by the viscoelastic damping can be neglected.

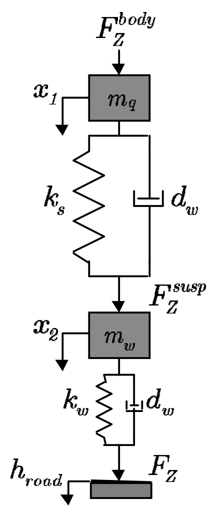

Figure 3.6: Quarter car model of suspension.

In Figure 3.6, x_1 is the vehicle body displacement, x_2 is the wheel displacement and h_{road} is the road profile (Gillespie 1992). F_z is the vertical

$m_w = 55kg$	Wheel/suspension mass
$m_q = 395kg$	1/4 of vehicle body mass (excluding wheels)
$k_s = 24kN/m$	Suspension spring stiffness
$k_w = 200kN/m$	Tyre stiffness
$d_s = 1350Ns/m$	Suspension damping constant
$d_w = 120Ns/m$	Tyre damping constant

Table 3.3: Suspension parameters

force on suspension as described in Section 3.1: F_z vertical force from tyre to road surface, which includes a vertical force component acting on the vehicle body due to the pitch moment when the vehicle is braking. Other parameters, typical values for a sporty sedan family car, are given in Table 3.3 (Mastinu 1988; Dixon 1996; Kiencke and Nielsen 2000).

The torque balance between the pitch torque around the centre of gravity gives (roll dynamics together with the constant gravity force are neglected):

$$h\left(F_{xf} + F_{xr}\right) = l_f F_{zf} - l_r F_{zr} \tag{3.22}$$

For illustration purposes let $l_f = l_r$, then (3.22) can be rewritten as

$$F_z^{body} = \frac{h}{l_f} F_x \tag{3.23}$$

where $F_x = F_{xf} + F_{xr}$, $F_z^{body} = F_{zf} - F_{zr}$ and h is the height of CoG. The horizontal distances from COG to the front and rear wheel axels are l_f and l_r respectively. This notation is also explained and used in Section 3.2.1 (see Figure 3.5).

Using Newton's Second Law, the vertical dynamics for a quarter vehicle can be written as follows:

$$m_q \ddot{x}_1 = F_z^{body} - d_s(\dot{x}_1 - \dot{x}_2) - k_s(x_1 - x_2) \tag{3.24}$$

$$m_w \ddot{x}_2 = d_s(\dot{x}_1 - \dot{x}_2) + k_s(x_1 - x_2) + d_w(\dot{h}_{road} - \dot{x}_2) + k_w(h_{road} - x_2) \tag{3.25}$$

Since the motion equations (3.24) and (3.25) represent a linear system, frequency domain analysis can be used by taking the Laplace transform of the above equations (all initial conditions are set to zero):

$$(m_q s^2 + d_s s + k_s)X_1(s) - (d_s s + k_s)X_2(s) = F_z^{body}(s) \tag{3.26}$$

$$-(d_s s + k_s)X_1(s) + (m_w s^2 + (d_s + d_w)s + (k_s + k_w))X_2(s) = (d_w s + k_w)H_{road}(s) \quad (3.27)$$

which can be written on the form

$$A(s)\begin{bmatrix} X_1(s) \\ X_2(s) \end{bmatrix} = \begin{bmatrix} F_z^{body}(s) \\ (d_w s + k_w)\, H_{road}(s) \end{bmatrix} \quad (3.28)$$

where

$$A(s) = \begin{bmatrix} m_q s^2 + d_s s + k_s & -(d_s s + k_s) \\ -(d_s s + k_s) & m_w s^2 + (d_s + d_w)s + (k_s + k_{w)} \end{bmatrix} \quad (3.29)$$

Undamped resonance frequencies found by solving $det(A(j\omega)) = 0$ with $d_s = d_w = 0$:

$$m_q m_w \omega^4 - (m_q (k_s + k_w) + k_s m_w)\, \omega^2 + k_s k_w = 0 \quad (3.30)$$

Equation (3.30) gives the undamped resonance frequencies $f_1^{und} = 0.6Hz$ and $f_2^{und} = 10.2Hz$. The f_1^{und} resonance is largely due to the movement of the vehicle body and the f_2^{und} resonance comprises mostly the movement of the wheel cf. Figure 3.7.

An analysis of a forced quarter vehicle model with damping and a harmonic input, is done by rewriting (3.28):

$$\begin{bmatrix} X_1(s) \\ X_2(s) \end{bmatrix} = A^{-1}(s)\begin{bmatrix} F_z^{body}(s) \\ (d_w s + k_w)\, H_{road}(s) \end{bmatrix} \quad (3.31)$$

$$A^{-1}(s) = \frac{1}{\Delta(s)}\begin{bmatrix} m_w s^2 + (d_s + d_w)s + (k_s + k_w) & d_s s + k_s \\ d_s s + k_s & m_q s^2 + d_s s + k_s \end{bmatrix} \quad (3.32)$$

where $(\Delta(s) = \det A(s))$

$$\begin{aligned} \Delta(s) = {} & m_q m_w s^4 + [m_q (d_s + d_w) + d_s m_w]\, s^3 \\ & + [m_q (k_s + k_w) + d_s d_w + k_s m_w]\, s^2 \\ & + [d_s k_w + k_s d_w]s + k_s k_w \end{aligned} \quad (3.33)$$

Further, (3.31) can then be rewritten as

$$\begin{bmatrix} X_1(s) \\ X_2(s) \end{bmatrix} = \frac{1}{\Delta(s)} A_1(s) \begin{bmatrix} F_z^{body}(s) \\ H_{road}(s) \end{bmatrix} \tag{3.34}$$

where elements of the $A_1(s)$ matrix are:

$$a_{1,1}(s) = m_w s^2 + (d_s + d_w)s + (k_s + k_w) \tag{3.35}$$

$$a_{1,2}(s) = d_s d_w s^2 + (d_s k_w + d_w k_s)\, s + k_s k_w \tag{3.36}$$

$$a_{2,1}(s) = d_s s + k_s \tag{3.37}$$

$$a_{2,2}(s) = m_q d_w s^3 + (m_q k_w + d_s d_w)s^2 + (d_s k_w + d_w k_s)\, s + k_s k_w \tag{3.38}$$

Using (3.34), the transfer function for the vertical body acceleration $\ddot{X}_1(s)$ with input $F_z^{body}(s)$ becomes:

$$\frac{\ddot{X}_1(s)}{F_z^{body}(s)} = \frac{s^2 X_1(s)}{F_z^{body}(s)} \tag{3.39}$$

$$\Downarrow$$

$$G_1(s) = \frac{\ddot{X}_1(s)}{F_z^{body}(s)} = \frac{m_w s^4 + (d_s + d_w)s^3 + (k_s + k_w)s^2}{\Delta(s)} \tag{3.40}$$

Similar, the transfer function for the vertical wheel acceleration $\ddot{X}_2(s)$ with input $F_z^{body}(s)$:

$$G_2(s) = \frac{\ddot{X}_2(s)}{F_z^{body}(s)} = \frac{d_s s^3 + k_s s^2}{\Delta(s)} \tag{3.41}$$

Figure 3.7 shows the frequency responses for the vehicle body (3.40) and the wheel (3.41). The vehicle body has a resonance frequency at $f_1^c \approx 1.3Hz$ and the wheel has a resonance frequency at $f_2^w \approx 10.1Hz$.

Another way to view the dynamics is to consider the distance $x_1 - x_2$, as the deformation $x_2 - h_{road}$ is negligible. For the situation where the vehicle under excitation by $H_{road}(s)$, with $F_z^{body}(s) = 0$, the transfer function for the chassis displacement becomes

$$\frac{X_1(s)}{H_{road}(s)} = \frac{d_s d_w s^2 + (d_s k_w + d_w k_s)\, s + k_s k_w}{\Delta(s)} \tag{3.42}$$

and the transfer function for the vertical wheel displacement:

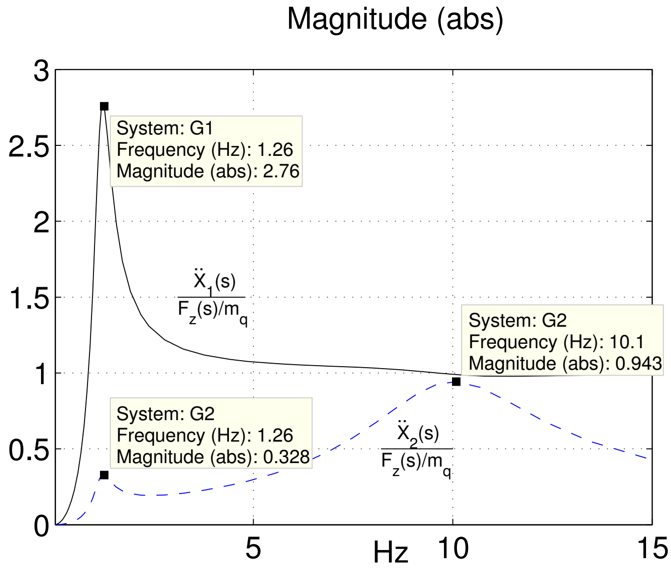

Figure 3.7: Frequency responses, $G_1(s)$ and $G_2(s)$, with F_z as input.

$$\frac{X_2(s)}{H_{road}(s)} = \frac{m_q d_w s^3 + (m_q k_w + d_s d_w)s^2 + (d_s k_w + d_w k_s)\, s + k_s k_w}{\Delta(s)} \tag{3.43}$$

The transfer function for the distance $X_1(s) - X_2(s)$ where the vehicle is under excitation by the $H_{road}(s)$ (and with $F_z^{body}(s) = 0$), is:

$$G_3(s) = \frac{X_2(s) - X_1(s)}{H_{road}(s)} = \frac{m_q d_w s^3 + m_q k_w s^2}{\Delta(s)} \tag{3.44}$$

Figure (3.8) shows the frequency response for (3.44), the vertical difference between the chassis and the undercarriage contact points with road as input. The resonance frequencies are $f_1^{x_{diff}} \approx 1.3Hz$ and $f_2^{x_{diff}} \approx 9.6Hz$. Similar methods and results are shown in (Gillespie 1992; Kiencke and Nielsen 2000).

As shown above, the suspension dynamics has consequences for the wheel slip control design. Figure 3.9 shows how the suspension dynamics interacts with the ABS system through the loop in which the friction force applied by the ABS controller causes a pitching moment, which again will affect the vertical force and back on the friction force. As a result of this suspension

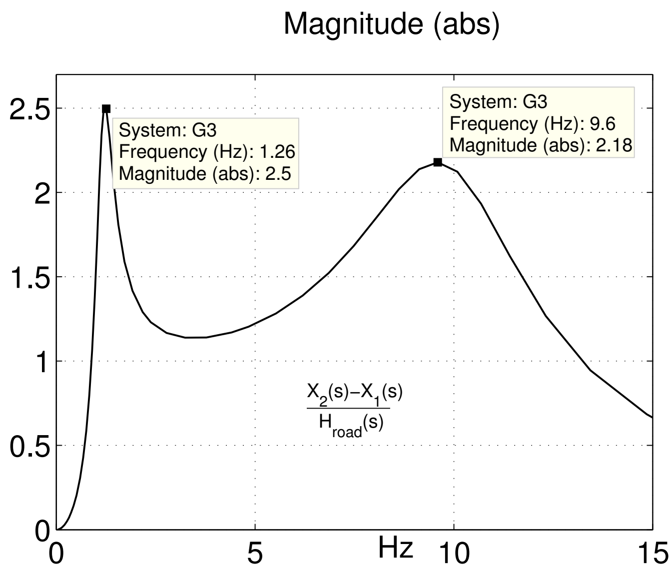

Figure 3.8: Frequency response, $G_3(s)$, with road position as input.

analysis, the tuning of the wheel slip controller should take into account the suspension dynamics and avoid the suspension resonance at $f_2^w \approx 10.1Hz$.

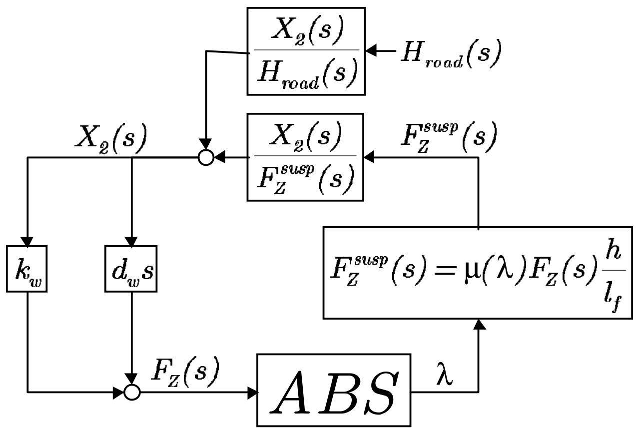

Figure 3.9: The interaction between suspension dynamics and ABS system.

Chapter 4

Gain scheduled wheel slip control

The wheel slip control problem is essentially to regulate the value of the longitudinal slip λ to a given setpoint λ^*, which is either constant or commanded from a higher-level control system such as ESP. The controller must be robust with respect to uncertainties in the tyre characteristic and the brake pads/discs, the variations in the road surface conditions, the load on the vehicle, etc. Integral action or adaptation must be incorporated to remove steady-state error due to model inaccuracies, in particular the unknown road/tyre friction coefficient μ_H.

This chapter explains the linearized slip dynamics and the wheel slip control design and analysis for i) system with just slip dynamics and no integral action ii) with integral action and iii) with actuator dynamics.

4.1 Motivation for gain scheduling

The dynamics of the wheel and car body are given by (3.7) and (3.8) respectively. Due to large differences in inertia, the wheel dynamics and car body dynamics will evolve on significantly different time scales. The speed v will change much more slowly than the wheel slip λ, and v is therefore a natural candidate for gain scheduling. Thus, for the control design, only (3.7) is considered and v is regarded as a slow time-varying parameter. A gain scheduled control design requires a set of nominal linearized models for design.

Model-based nonlinear wheel slip control design shown in (Lüdemann 2002) depends strongly on knowing the friction coefficient and the friction curve. The aim is to obtain (a robust) control design method which achieves robustness by avoiding using the uncertain friction model in the design.

4.2 Linearized slip dynamics

Let $(\hat{\lambda}, \hat{T}_b)$ be an equilibrium point for (3.7) defined by the nominal values $\hat{\alpha}$, $\hat{F}_z$ and $\hat{\mu}_H$

$$\hat{T}_b = \left(\frac{J}{mr}(1-\hat{\lambda}) + r\right)\hat{F}_z \mu(\hat{\lambda}, \hat{\mu}_H, \hat{\alpha}) \tag{4.1}$$

The speed-dependent nominal linearized slip dynamics are given by

$$\dot{\lambda} = \frac{\alpha_1}{v}(\lambda - \hat{\lambda}) + \frac{\beta_1}{v}(T_b - \hat{T}_b) + \text{h.o.t.} \tag{4.2}$$

where α_1 and β_1 are linearization constants given by

$$\alpha_1 = -\hat{F}_z\left(\frac{1}{m}(1-\hat{\lambda}) + \frac{r^2}{J}\right)\frac{\partial \mu}{\partial \lambda}(\hat{\lambda}, \hat{\mu}_H, \hat{\alpha}) + \hat{F}_z\frac{1}{m}\mu(\hat{\lambda}, \hat{\mu}_H, \hat{\alpha}) \tag{4.3}$$

$$\beta_1 = \frac{r}{J} \tag{4.4}$$

and "h.o.t" denotes "higher-order terms". Notice that for nominal wheel slip values $\hat{\lambda}$ to the right of any peak of the friction curve, $\alpha_1 > 0$, such that the open-loop dynamics becomes open-loop unstable. For nominal slip values $\hat{\lambda}$ sufficiently to the left of any peak, $\alpha_1 < 0$, and the dynamics are open-loop stable. Assuming arbitrary values of α, F_z and μ_H, the wheel slip dynamics (3.7) can be written in the form

$$\dot{x}_2 = \frac{\phi(x_2)}{v} + \frac{\beta_1}{v}(T_b - T_b^*) \tag{4.5}$$

where $x_2 = \lambda - \lambda^*$ and λ^* is the desired slip (setpoint). Furthermore, define

$$\phi(x_2) = -\left(\frac{1}{m}(1-\lambda^* - x_2) + \frac{r^2}{J}\right)F_z\mu(x_2 + \lambda^*, \mu_H, \alpha) + \frac{r}{J}T_b^* \tag{4.6}$$

and

$$T_b^* = \left(\frac{J}{mr}(1-\lambda^*) + r\right)F_z\mu(\lambda^*, \mu_H, \alpha) \tag{4.7}$$

It can be seen that (4.5) has an equilibrium point given by $x_2 = 0$, $T_b = T_b^*$ since $\phi(0) = 0$, and the linearized slip model (4.2) with a perturbation term is written as follows

$$\dot{x}_2 = \frac{\alpha_1}{v}x_2 + \frac{\beta_1}{v}(T_b - T_b^*) + \frac{\epsilon_\mu(x_2)}{v} \tag{4.8}$$

where $\epsilon_\mu(x_2) = \phi(x_2) - \alpha_1 x_2$. Eq. (4.8) will be used later on for control design and analysis.

4.3 Wheel slip control design and analysis

4.3.1 Without integral action

For simplicity, a design without integral action is studied first and where the infinite-horizon quadratic cost function is defined as:

$$J(x(t), u[t, \infty)) = \int_t^\infty (x^2(\tau)Q(v) + u^2(\tau)R)d\tau \tag{4.9}$$

with $R > 0$ and $Q(v) \geq 0$ for all $v > 0$. Assuming v is constant (due to the separation of time-scales) and neglecting the nonlinearity $\epsilon_\mu(x)$, the optimal control law (Anderson and Moore 1989) is uniquely given by the gain scheduled state feedback

$$\hat{u} = -R^{-1}\frac{\beta_1}{v}P(v)x = K(v)x, \text{ where } K(v) = -R^{-1}\frac{\beta_1}{v}P(v) \tag{4.10}$$

The algebraic Riccati equation is

$$\frac{2P(v)\alpha_1}{v} - \left(\frac{P(v)\beta_1}{v}\right)^2 R^{-1} + Q(v) = 0 \tag{4.11}$$

with the positive solution

$$P(v) = \frac{\alpha_1 + \left(\alpha_1^2 + \beta_1^2 R^{-1} Q(v)\right)^{1/2}}{\beta_1^2 R^{-1}} v = P^{'}(v)v \tag{4.12}$$

Due to actuator constraints, the saturated control is defined as

$$u = \begin{cases} T_b^{\max} - T_b^*, & \hat{u} > T_b^{\max} - T_b^* \\ T_b^{\min} - T_b^*, & \hat{u} < T_b^{\min} - T_b^* \\ \hat{u}, & \text{otherwise} \end{cases} \tag{4.13}$$

for some $T_b^{\max} > T_b^{\min} \geq 0$. Furthermore, the error (note that both u and $\hat{u}$ depend on v and x) is defined as

$$\epsilon_s(x, v) = \beta_1(u - \hat{u}) \tag{4.14}$$

With the definition $\epsilon(x, v) = \epsilon_s(x, v) + \epsilon_\mu(x)$, the closed loop dynamics can be written as

$$\dot{x} = \left(\frac{\alpha_1}{v} + \frac{\beta_1 K(v)}{v}\right)x + \frac{\epsilon(x, v)}{v} \tag{4.15}$$

It is easy to see that $\epsilon(0, v) = 0$ for all $v > 0$.

Proposition 4.1 *Consider the system (3.7) with controller (4.13), where* $R > 0$ *and the smooth function* Q *satisfies* $Q(v) \geq 0$ *and* $\frac{dQ(v)}{dv} \geq 0$ *for all* $v > 0$*. Suppose for some* $\delta \in (0,1)$

$$x\epsilon(x,v) \leq (1-\delta)\frac{Q(v)}{2P'(v)}x^2 \tag{4.16}$$

for all $v > 0$ *and* $x \in [-\lambda^*, 1-\lambda^*]$*. Then, for all* $v(0) > 0$ *and* $\lambda(0) \in [0,1]$*, the equilibrium* $x = 0$ *is uniformly exponentially stable.*

Proof 4.1 *Let a Lyapunov function candidate be defined as*

$$V(x) = x^2 P(v) \tag{4.17}$$

Along trajectories of (4.15), one has

$$\dot{V} = \frac{d}{dt}V(x) = x^2\left(\frac{dP(v)}{dv}\frac{dv}{dt}\right) + 2\dot{x}xP(v) \tag{4.18}$$

Substituting for (4.8), (4.10) and (4.11) in (4.18) gives

$$\dot{V} = x^2\left(P^{'}(v) + v\frac{dP^{'}(v)}{dv}\right)\dot{v} + 2\epsilon(x,v)P^{'}(v)x - x^2Q(v) \tag{4.19}$$

Note that $P^{'}(v) \geq 0$ *and* $\frac{dP^{'}(v)}{dv} \geq 0$ *for all* $v > 0$*. It follows from Proposition 3.1 that*

$$\dot{V} \leq 2\epsilon(x,v)P^{'}(v)x - x^2Q(v) \leq -\delta Q(v)x^2 \tag{4.20}$$

and the equilibrium is uniformly exponentially stable by Corollary 3.4, in (Khalil 1996), since $V(x)$ *and the right hand side in (4.20) are upper and lower bounded by a positive definite quadratic functions in* $\tilde{x}$ *for all* $v \geq v_{\min}$*. The region of attraction follows from Proposition 3.1 since* $[0,1]$ *is positively invariant for* λ*.*

□

Essentially, (4.16) requires that the error weight $Q(v)$ must be chosen sufficiently large, which means that the gain $K(v)$ must be sufficiently large in order to stabilize the system. Note that the system is open loop unstable when operating in a region where the friction curve has negative slope $\frac{\partial\mu}{\partial\lambda}$ (in this case $\alpha_1 > 0$). The controller is gain scheduled since K depends on v. From a practical point of view, it makes sense to choose $\frac{dQ(v)}{dv} > 0$ since this leads to $\frac{dK(v)}{dv} > 0$. Hence, the gain is reduced as $v \to 0$ and one avoids instability due to unmodelled dynamics that typically become dominant as $v \to 0$.

The above analysis shows that the heuristics of local linearization and gain scheduling do not lead to instability when $Q(v)$ is chosen sufficiently large. Unfortunately, it is not possible to implement this controller without significant loss of performance since the steady state brake torque T_b^* is unknown; recall that $T_b = T_b^* + u$ and T_b^* depends on μ_H which is highly uncertain and time-varying. Hence, all practical wheel slip controllers need some form of integral action or adaptation. Thus, the design and analysis is extended with integral action without further discussion.

4.3.2 With integral action

Let the system dynamics (4.8) be augmented with a slip error integrator $\dot{x}_1 = \lambda - \lambda^* = x_2$ such that

$$\begin{pmatrix} \dot{x}_1 \\ \dot{x}_2 \end{pmatrix} = A(v) \begin{pmatrix} x_1 \\ x_2 \end{pmatrix} + B(v)\,(u - T_b^*) + W(v)\epsilon_\mu(x_2) \tag{4.21}$$

where

$$A(v) = \begin{pmatrix} 0 & 1 \\ 0 & \frac{\alpha_1}{v} \end{pmatrix}, B(v) = \begin{pmatrix} 0 \\ \frac{\beta_1}{v} \end{pmatrix}, W(v) = \begin{pmatrix} 0 \\ \frac{1}{v} \end{pmatrix} \tag{4.22}$$

The steady-state brake torque T_b^* depends on road and tyre properties such as μ_H and must therefore be assumed unknown. Hence, the control input is defined as $u = T_b$, and the equilibrium point is

$$x^* = \begin{pmatrix} x_1^* \\ 0 \end{pmatrix}, \quad u^* = T_b^* \tag{4.23}$$

where the value x_1^* depends on the controller due to the integral action. This leads to

$$\dot{x} = A(v)\,(x - x^*) + B(v)\,(u - u^*) + W(v)\epsilon_\mu(x_2) \tag{4.24}$$

Next, the quadratic cost function for the purpose of local LQ design based on the nominal part of (4.24), is defined as follows:

$$\begin{aligned} J(x(t), u[t,\infty)) \quad &= \quad \int_t^\infty ((x(\tau) - x^*)^T\, Q(v)\,(x(\tau) - x^*) \\ &\qquad + (u(\tau) - u^*)^T\, R\,(u(\tau) - u^*))d\tau \end{aligned} \tag{4.25}$$

Assuming constant v, the optimal control law (Anderson and Moore 1989) is given by

$$u = K(v)x \tag{4.26}$$

where the gain matrix is $K(v) = -R^{-1}B^T(v)P(v)$. The unknowns x^* and u^* are neglected, which will be accounted for due to the integral action. The symmetric matrix $P(v) > 0$ is defined by the solution to the associated algebraic Riccati equation:

$$P(v)A(v) + A^T(v)P(v) - 2P(v)B(v)R^{-1}B^T(v)P(v) = -Q(v) \tag{4.27}$$

The elements of the matrix equation (4.27) are

$$\left(\frac{\beta_1}{v}\right)^2 \frac{P_{1,2}^2(v)}{R} = Q_{1,1}(v) \tag{4.28}$$

$$P_{1,1}(v) + P_{1,2}(v)\left(\frac{\alpha_1}{v} - \left(\frac{\beta_1}{v}\right)^2 \frac{P_{2,2}(v)}{R}\right) = 0 \tag{4.29}$$

$$2P_{1,2}(v) + P_{2,2}(v)\left(\frac{2\alpha_1}{v} - \left(\frac{\beta_1}{v}\right)^2 \frac{P_{2,2}(v)}{R}\right) = -Q_{2,2}(v) \tag{4.30}$$

This gives the following solution with $P(v) > 0$:

$$P_{1,1}(v) = \frac{\left(\alpha_1^2 + \beta_1^2 R^{-1}\left(Q_{2,2}(v) + \frac{2(Q_{1,1}(v)R)^{1/2}}{\beta_1}v\right)\right)^{1/2}}{(Q_{1,1}(v)R)^{-1/2}\beta_1} \tag{4.31}$$

$$P_{1,2}(v) = \frac{v}{\beta_1}(Q_{1,1}(v)R)^{1/2} \tag{4.32}$$

$$P_{2,2}(v) = \frac{\alpha_1 + \left(\alpha_1^2 + \beta_1^2 R^{-1}\left(Q_{2,2}(v) + \frac{2(Q_{1,1}(v)R)^{1/2}}{\beta_1}v\right)\right)^{1/2}}{\beta_1^2 R^{-1}} v \tag{4.33}$$

and the gains

$$K_1(v) = -\left(Q_{1,1}(v)R^{-1}\right)^{1/2} \tag{4.34}$$

$$K_2(v) = -\frac{\alpha_1 + \left(\alpha_1^2 + \beta_1^2 R^{-1}\left(Q_{2,2}(v) + \frac{2(Q_{1,1}(v)R)^{1/2}}{\beta_1}v\right)\right)^{1/2}}{\beta_1} \tag{4.35}$$

Setting $x_1^* = T_b^*/K_1(v)$ gives the closed loop error dynamics

$$\dot{\tilde{x}} = (A(v) + B(v)K(v))\,\tilde{x} + W(v)\epsilon_\mu(x_2) \tag{4.36}$$

with the controller error $\tilde{x} = x - x^*$.

Proposition 4.2 *Consider the system (3.7) with controller defined by (4.26) and (4.34)-(4.35). Assume $R > 0$ and the smooth matrix-valued function Q satisfies $Q_{1,2}(v) = Q_{2,1}(v) = 0$, $Q_{1,1}(v) > 0$, $Q_{2,2}(v) > 0$, $\frac{dQ_{1,1}(v)}{dv} \geq 0$, $\frac{dQ_{2,2}(v)}{dv} \geq 0$ for all $v \geq v_{min} > 0$. Moreover, suppose $T_b(t) \geq 0$ for all $t \geq 0$ and*

$$D(v) = P'_{1,1}(v)P'_{2,2}(v) - P'_{1,2}(v)P'_{2,1}(v) > 0 \tag{4.37}$$

$$Q_{1,1}(v)(1-\delta) > \frac{P_{2,1}(v)C}{v} \tag{4.38}$$

$$Q_{2,2}(v)\tilde{x}_2^2(1-\delta) > \left(\frac{2}{v}\epsilon_\mu(\tilde{x}_2)P_{2,2}(v)\tilde{x}_2 + \frac{P_{2,1}(v)\epsilon_\mu^2(\tilde{x}_2)}{vC}\right) \tag{4.39}$$

are satisfied for all $v \geq v_{min} > 0$, $\tilde{x}_2 \in [-\lambda^*, 1-\lambda^*]$ and some $C > 0$ and $\delta \in (0,1)$. Then, the equilibrium $\tilde{x} = 0$ is uniformly exponentially stable.

Proof 4.2 *Let a Lyapunov function candidate be*

$$V(\tilde{x}) = \tilde{x}^T P(v)\tilde{x} \tag{4.40}$$

Its time-derivative along trajectories of (4.36)

$$\dot{V} = \frac{d}{dt}V(\tilde{x}(t)) = \tilde{x}^T\left(\frac{dP(v)}{dv}\dot{v}\right)\tilde{x} + \dot{\tilde{x}}^T P\tilde{x} + \tilde{x}^T P\dot{\tilde{x}} \tag{4.41}$$

is found by substituting for (4.24), (4.26) and (4.27) in (4.41):

$$\dot{V} = \tilde{x}^T\frac{dP(v)}{dv}\dot{v}\tilde{x} + \epsilon_\mu(\tilde{x}_2)(W^T(v)P(v)\tilde{x} + \tilde{x}^T P(v)W(v)) - \tilde{x}^T Q(v)\tilde{x} \tag{4.42}$$

From Proposition 3.1, it is clear that $\dot{v} \leq 0$ since $T_b \geq 0$. Thus, the non-positivity of $\tilde{x}^T\left(\frac{dP(v)}{dv}\dot{v}\right)\tilde{x}$ requires $P'(v) = \frac{dP(v)}{dv} > 0$ for all $v > 0$. For $P'(v)$ to be positive definite, it is sufficient that $P'_{1,1}(v) > 0$ since $D(v) > 0$. Note that since $Q_{1,1}(v), Q_{2,2}(v), \beta_1 > 0$, it follows immediately that $P'_{1,1}(v) > 0$. Then, (4.42) becomes:

$$\begin{aligned}\dot{V} &\leq \epsilon_\mu(\tilde{x}_2)(W^T P(v)\tilde{x} + \tilde{x}^T P(v)W(v)) - \tilde{x}^T Q(v)\tilde{x} \\ &= -Q_{1,1}(v)\tilde{x}_1^2 - Q_{2,2}(v)\tilde{x}_2^2 + \frac{2}{v}\epsilon_\mu(\tilde{x}_2)(P_{2,2}(v)\tilde{x}_2 + P_{2,1}(v)\tilde{x}_1)\end{aligned} \tag{4.43}$$

To obtain all $\tilde{x}_1$-terms in (4.43) in a quadratic form, Young's inequality $2ab \leq a^2/C + Cb^2$ is applied. Hence,

$$\begin{aligned}\dot{V} \quad \leq \quad & -Q_{1,1}(v)\tilde{x}_1^2 + \frac{P_{2,1}(v)}{v}\tilde{x}_1^2 C - Q_{2,2}(v)\tilde{x}_2^2 \\ & + \frac{2}{v}\epsilon_\mu(\tilde{x}_2)P_{2,2}(v)\tilde{x}_2 + \frac{P_{2,1}(v)}{v}\frac{\epsilon_\mu^2(\tilde{x}_2)}{C}\end{aligned} \tag{4.44}$$

Due to (4.38) and (4.39) it follows that

$$\dot{V} \leq -\delta Q_{1,1}(v)\tilde{x}_1^2 - \delta Q_{2,2}(v)\tilde{x}_2^2 \tag{4.45}$$

and one concludes that the equilibrium is uniformly exponentially stable by Corollary 3.4, in (Khalil 1996), since $V(\tilde{x})$ and the right hand side in (4.38) are upper and lower bounded by a positive definite quadratic functions in $\tilde{x}$ for all $v \geq v_{\min}$.

□

Inequality (4.38) states that the error weight $Q_{1,1}(v)$ must be sufficiently large, leading to a sufficiently large controller gain. In this inequality, $P_{2,1}(v)$ depends on $Q_{1,1}(v)$, but it is evident that $P_{2,1}(v)$ increases with $\sqrt{Q_{1,1}(v)}$ such that (4.38) will indeed hold for a sufficiently large $Q_{1,1}(v)$, except when $v \to 0$.

Inequality (4.39) states that the error weight $Q_{2,2}(v)$ must also be sufficiently large, leading to a sufficiently high gain to stabilize the system. Note that $P_{2,2}(v)$ increases with $\sqrt{Q_{2,2}(v)}$ such that this is also possible, except for $v \to 0$. In (4.39), $Q_{2,2}(v)\,|\tilde{x}_2|$ is essentially chosen to dominate the perturbation $\epsilon(\tilde{x}_2)$. Inequality (4.39) must be checked with respect to the perturbations ϵ_μ that are generated by *all* possible friction curves $\mu(\cdot)$ to ensure robust stability.

Inequality (4.37) can be seen to be non-restrictive since it will always be satisfied for α_1 close to zero, see Appendix B. This corresponds to generating the nominal model by linearizing near the peak of the friction curve. Experience shows that high performance is indeed achieved this way. For $\alpha_1 = 0$, no information on the friction curves is actually utilized in the control design.

The constant $C > 0$ should be chosen to minimize conservativeness. However, the choice $Q_{1,2}(v) = Q_{2,1}(v) = 0$ and taking $P(v)$ from the solutions of the Riccati equation are possibly conservative.

The controller gain $K(v)$ depends on the speed (gain scheduling). From a practical point of view, a useful gain schedule is achieved by letting $\frac{dQ_{1,1}(v)}{dv} > 0$ and $\frac{dQ_{2,2}(v)}{dv} > 0$, as this reduces the gain as $v \to 0$. As mentioned earlier, this is necessary to avoid instability due to the unmodelled dynamics since these tend to dominate as $v \to 0$.

An important aspect is the initialization of the integrator state x_1. Note that x_1 is a controller state that can be initialized arbitrarily, while x_1^* is unknown since it depends on the road/tyre friction coefficient μ_H. Hence, an intelligent initialization of $x_1(0)$ based on any a priori information on μ_H and possibly on the known $\tilde{x}_2(0)$, may significantly improve the transient performance after the controller is activated (Johansen, Kalkkuhl, Lüdemann, and Petersen 2001).

An idealized design example

Consider a design example with the following parameters $m = 450\ kg$, $F_z = 4414\ N$, $r = 0.32\ m$, $J = 1.0\ kg\ m^2$ and the friction model in the third part of Figure 3.2. Assuming $\lambda^* = 0.14$ and the nominal friction parameters $\mu_H^* = 0.8$ and $\alpha^* = 0$, this give $\alpha_1 = 10.2$ and $\beta_1 = 0.32$. Choose $R = 1$ and $Q(v) = \tilde{Q}v^{3/2}$ with $\tilde{Q}_{1,1} = 6 \cdot 10^9$ and $\tilde{Q}_{2,2} = 40 \cdot 10^6$. Note the scaling due to the different magnitudes of T_b and λ. The choice for $Q(v)$ leads to a gain schedule with reduced gain as $v \to 0$, which is useful to avoid instability due to unmodelled dynamics as $v \to 0$.

Figures 4.1 and 4.2 show that the robust stability requirement (4.39) is satisfied for all $\tilde{x}_2 \in [-\lambda^*, 1-\lambda^*]$ for all the friction curves in the third figure of Figure 3.2. Although curves are shown only for $v = 1$ m/s and $v = 32$ m/s, (4.37) has been verified to be fulfilled for intermediate values of v. The control design also satisfies the stability requirements (4.38) and (4.37), and gives robust uniform exponential stability of the equilibrium.

4.3.3 With actuator dynamics

Next, a gain scheduled LQ approach is described for a wheel slip control design where the actuator dynamics are taken into account, the integral action is included and the rate of the clamping force is used as the control input. The latter is introduced partly to simplify the handling of rate constraints in the implementation and partly to get velocity-based gain scheduled control, the benefits of which are reported in (Kaminer, Pascoal, Khargonekar, and Coleman 1995; Leith and Leithead 1996). The dynamics of the augmented system are given by the following equations

$$\dot{x}_1 = x_2 \tag{4.46}$$

$$\dot{x}_2 = \frac{\alpha_1}{v}x_2 + \frac{\beta_1}{v}(x_3 - T_b^*) + \frac{1}{v}\epsilon_\mu(x_2) \tag{4.47}$$

$$\dot{x}_3 = -a(x_3 - T_b^*) + a(x_4 - T_b^*) \tag{4.48}$$

$$\dot{x}_4 = u \tag{4.49}$$

The state x_1 is the integrated slip error (giving integral action), x_2 is the slip error, x_3 is the clamping torque produced by the actuator, x_4 is the clamping torque commanded to the actuator and u is the commanded rate of change of the clamping torque. The parameter $a = 72$ rad/s is the bandwidth of the actuator, see Section 2.3.2. With

$$A(v) = \begin{pmatrix} 0 & 1 & 0 & 0 \\ 0 & \frac{\alpha_1}{v} & \frac{\beta_1}{v} & 0 \\ 0 & 0 & -a & a \\ 0 & 0 & 0 & 0 \end{pmatrix}$$

$$B = \begin{pmatrix} 0 \\ 0 \\ 0 \\ 1 \end{pmatrix}, \quad W(v) = \begin{pmatrix} 0 \\ \frac{1}{v} \\ 0 \\ 0 \end{pmatrix}$$

the system can be written as the following linear parameter-varying (LPV) system with a perturbation:

$$\dot{x} = A(v)(x - x_0) + Bu + W(v)\epsilon_\mu(x_2) \tag{4.50}$$

where $x_0 = (0, 0, T_b^*, T_b^*)$. Assuming a fixed v, the gain scheduled LQ controller (Anderson and Moore 1989) is given in the form

$$u = -K(v)x \tag{4.51}$$

where the matrix $K(v)$ is computed by solving the following standard linear quadratic optimal control problem

$$J(u, x(t), v) = \int_t^\infty \left(x^T(\tau)Q(v)x(\tau) + Ru^2(\tau)\right) d\tau \tag{4.52}$$

Note that x is known while x_0 is unknown as T_b^* depends on the tyre parameters, vertical load, wheel slip angle, road friction, etc.

An idealized design example

The design parameters given in Section 4.3.2 are used with the following modifications. For the control design, $\tilde{Q}_{1,1} = 8 \cdot 10^6$ and all other elements of $\tilde{Q}$ in $Q(v) = \tilde{Q}v^{3/2}$ are set to zero. The choice for $Q(v)$ leads to a gain schedule with reduced gain as $v \to 0$, see Figure 4.3 (for presentation purposes K_1 has been reduced by a factor of 10 and K_3 and K_4 have been increased by a factor of 1000).

Stability and robustness

The control design presented above is based on gain scheduling and linearized nominal models such that stability must be investigated separately. Moreover, there are numerous uncertain model parameters, the most important being the friction coefficient μ_H, which calls for a robustness analysis. A Lyapunov approach is taken based on the closed loop error dynamics

$$\dot{x} = (A(v) - B(v)K(v))\, x - A(v)x_0 + W(v)\epsilon_\mu(x_2) \tag{4.53}$$

The equilibrium point $x^* = (x_1^*, x_2^*, x_3^*, x_4^*)$ for the closed loop system (4.53) is now defined by

$$x_1^* = -\frac{K_3(v) + K_4(v)}{K_1(v)} T_b^* \tag{4.54}$$

$$x_2^* = 0, \quad x_3^* = T_b^*, \quad x_4^* = T_b^* \tag{4.55}$$

Observe that $x_2^* = 0$ because $x_2 = \lambda - \lambda^*$. Defining the error variable $\tilde{x} = x - x^*$, the closed loop system can be written in the following form

$$\dot{\tilde{x}} = (A(v) - B(v)K(v))\tilde{x} + W(v)\epsilon_\mu(\tilde{x}_2) \tag{4.56}$$

Note that $\epsilon_\mu(0) = 0$, i.e. it is a vanishing perturbation. In order to analyze the stability and robustness of the closed loop with respect to the uncertain road/tyre friction characteristics, a Lyapunov function is sought for the closed loop system (4.56). The approach is first to seek a Lyapunov function that proves uniform exponential stability of origin of the nominal LPV closed loop system

$$\dot{\tilde{x}} = A_0(v)\tilde{x} \tag{4.57}$$

with $A_0(v) = A(v) - B(v)K(v)$. The next step is to study if the stability margin provided by this Lyapunov function is sufficient to show robustness with respect to a large class of unknown tyre/road friction characteristics influencing the vanishing perturbation ϵ_μ. Standard methods for LPV systems will be utilized, namely a parameter-dependent quadratic Lyapunov-candidate, and the problems will be formulated in terms of LMIs. Let the Lyapunov function candidate be

$$V(\tilde{x}) = \tilde{x}^T P(v)\tilde{x} \tag{4.58}$$

where $P(v) > 0$ is symmetric and specified below. The following result shows conditions for uniform exponential stability of the nominal closed loop dynamics.

Proposition 4.3 *Assume there exist a constant* $\gamma > 0$ *and a smooth function* $P(v)$ *that satisfies for all* $v_{max} \geq v \geq v_{min} > 0$

$$P(v) > 0 \tag{4.59}$$

$$\frac{dP}{dv}(v) \geq 0 \tag{4.60}$$

$$P(v)A_0(v) + A_0^T(v)P(v) + \gamma P(v) \leq 0 \tag{4.61}$$

Then, the origin is a uniformly exponentially stable equilibrium for all trajectories of the nominal closed loop system (4.57) that satisfies $-\lambda^* \leq x_2(0) \leq 1 - \lambda^*$, $x_3(t) \geq 0$, $x_4(t) \geq 0$ *and* $v_{max} \geq v(t) \geq v_{min}$ *for all* $t \geq 0$.

Proof 4.3 V *is a suitable Lyapunov function candidate since (4.59) ensures that it is positive definite with upper and lower bounds. Along trajectories of the nominal closed loop (4.57), the time-derivative of* V *is*

$$\dot{V} = \tilde{x}^T(P(v)A_0(v) + A_0(v)^T P(v))\tilde{x} + \tilde{x}^T \frac{dP(v)}{dv}\tilde{x}\dot{v} \tag{4.62}$$

It is known from Proposition 3.1 that $\dot{v} \leq 0$ *during braking such that (4.60) ensures that the last term in (4.62) is not positive. Hence, (4.61) implies that*

$$\dot{V} \leq -\gamma\tilde{x}^T P(v)\tilde{x} = -\gamma V \tag{4.63}$$

It is then a standard result (Khalil 1996) that the origin is uniformly exponentially stable, i.e. $\tilde{x}(t)$ *tends to zero exponentially with rate bounded by* $\gamma/2$.

□

In order to transform these conditions to standard LMI conditions, introduce a smooth parameterization of $P(v)$ similar to (Gahinet, Apkarian, and Chilali 1996) and discretize a suitable interval for the parameter v:

$$P(v) = P_0 + P_1 v^{1/2} + P_2 v + P_3 v^{3/2} \tag{4.64}$$

with symmetric 4×4 matrices P_0, P_1, P_2 and P_3. The terms depending on v are motivated by the explicit expressions for $P(v)$ in Section 4.3.2. Of course, in this case, a more complex parameterization may lead to a less conservative Lyapunov function so that it may prove a larger stability margin. Conditions (4.59) - (4.60) are now given by

$$P(v) = P_0 + P_1 v^{1/2} + P_2 v + P_3 v^{3/2} \quad > \quad 0 \tag{4.65}$$

$$\frac{dP}{dv}(v) \quad = \quad \frac{P_1}{2v^{1/2}} + P_2 + \frac{3}{2}P_3 v^{1/2} \quad \geq \quad 0 \tag{4.66}$$

$$P(v)A_0(v) + A_0^T(v)P(v) + \gamma P(v) \quad \leq \quad 0 \tag{4.67}$$

Inequalities (4.65), (4.66) and (4.67) now define a standard LMI problem (Boyd, Balakrishnan, Feron, and Ghaoui 1993) with the objective of maximizing the scalar variable $\gamma > 0$, where the LMI conditions are imposed at a finite number of values v. A gridding approach is chosen because the parameterization of $P(v)$ is not convex. 12 values in the interval $0.75m/s \leq v \leq 33m/s$ have been chosen. This leads to a solution of the LMI conditions (4.65) - (4.67) with $\gamma = 26.9$. It follows that the given design makes the equilibrium point $\tilde{x} = 0$ locally exponentially stable when the setpoint is chosen $\lambda^* = 0.14$, even in the presence of uncertainty in the friction curve. The amount of uncertainty may, however, restrict the region of attraction.

Given the $\gamma > 0$ and matrices P_0, P_1, P_2, P_3 that solve the above mentioned LMI-problem, the Lyapunov function candidate may be examined to show that it proves a stability margin to account for the uncertainty in ϵ_μ. Along the trajectories of the perturbed closed loop (4.56), the time-derivative of the Lyapunov function V for the nominal closed loop satisfies

$$\dot{V} \leq -\gamma \tilde{x}^T P(v) \tilde{x} + 2\tilde{x}^T P(v) W(v) \epsilon_\mu(\tilde{x}_2) \tag{4.68}$$

In Figure 4.4, three figures are shown for $\dot{V}$; for $v = 0.75$, 8.5 and 24 m/s respectively. In the top figure, the side slip angle is $\alpha = 15$ degrees and zero in the other two figures. In each figure, three curves are shown for $\mu_H(= 0.1,\ 0.5,\ 0.9)$. $\tilde{x}_1, \tilde{x}_3$ and $\tilde{x}_4$ are set to their respective equilibrium values. Figure 4.4 shows that the robust stability requirement (4.68) is satisfied for all $\tilde{x}_2 \in [-\lambda^*, 1 - \lambda^*]$ for the selected friction curves. Although curves are shown only for $v = 0.75$, 8.5 and 24 m/s, it has been verified that (4.68) is fulfilled for intermediate values of v, λ and α. Unfortunately, this approach does not allow a rigorous conclusion, except local stability, since the Lyapunov-function candidate at hand appears to be conservative when $\tilde{x}_1$, $\tilde{x}_3$ and $\tilde{x}_4$ are taken sufficient far from their equilibrium values. However, the analysis indicates the following observations that agree well with the experience from simulations and experiments:

- The robustness margins are most difficult to fulfill at low speeds (less than say 5 m/s), high μ_H and high α. This is as expected, since the uncertainty scales with $1/v$ and at high μ_H and α, the slip dynamics have the highest degree of open loop instability.

- Largest robustness margins are achieved by placing the setpoint to the right of the friction curve peak. On the other hand, maximum friction is achieved at the peak value and maximum steerability suggests that the slip is as low as possible. In general, the slip value where the peak value is attained, is reduced as μ_H is reduced. Therefore, a reasonable compromise is to let the setpoint be close to the peak value and depend on an estimate of μ_H.

- A higher robustness margin and stronger theoretical robustness results could be achieved by choosing larger values in the $Q(v)$-matrix, such that the feedback gain is increased. However, due to other unmodelled phenomena such as tyre dynamics, computer system communication delay and suspension dynamics, this is not possible in a practical design.

4.4 Discussion

In this chapter, three theoretical results on wheel slip control design and analysis are presented. A design analysis for a first order system containing only wheel slip dynamics is shown. But, this controller design is cannot be implemented without a significant loss of performance since the steady-state brake torque is unknown. By incorporating integral action, steady-state errors due to model inaccuracies can be handled, it is shown to give uniform exponential stability. The actuator constraints are not considered in order to present the stability results in a comprehensible way as the problem otherwise becomes too complex to analyze. To extend the model even further to achieve the best possible approximation to the test vehicle, actuator dynamics and an integrator on the control input are included. Stability and robustness for variations in λ, μ_H, v and α are shown. But, for $\tilde{x}_1, \tilde{x}_3$ and $\tilde{x}_4$ taken sufficient far from their equilibria the analysis is non-conclusive.

None of the controller designs and analysis shown in this chapter are in discrete time and they don't incorporate saturation control. Still, they provide a starting point for the practical design and implementation using the LQRC method, as described in Chapter 5.

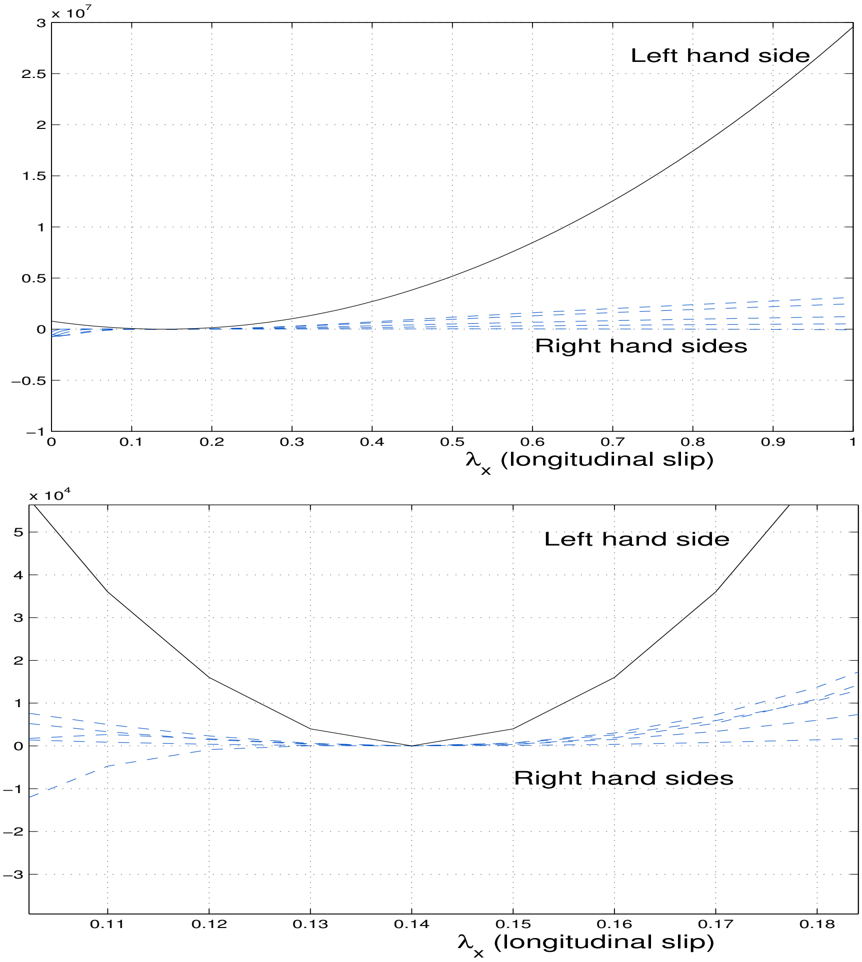

Figure 4.1: Illustration of the robust stability requirement, i.e. the left and right hand sides of equation (4.39) for $v = 1m/s$. The bottom plot shows an expanded view.

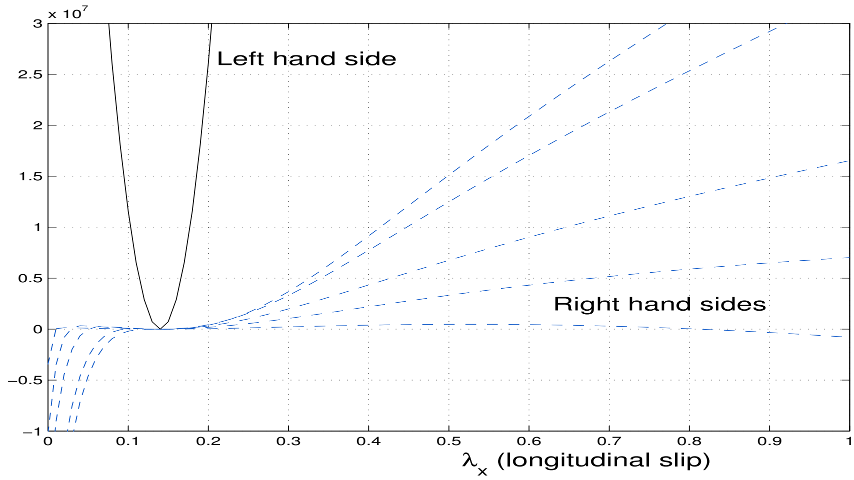

Figure 4.2: Illustration of the robust stability requirement, i.e. the left and right hand sides of equation (4.39) for $v = 32$ m/s.

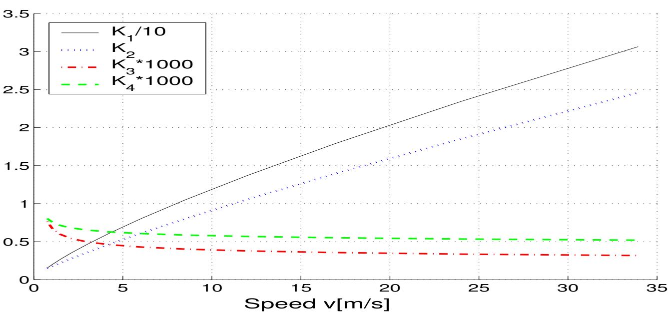

Figure 4.3: Gain $K(v)$, as a function of v.

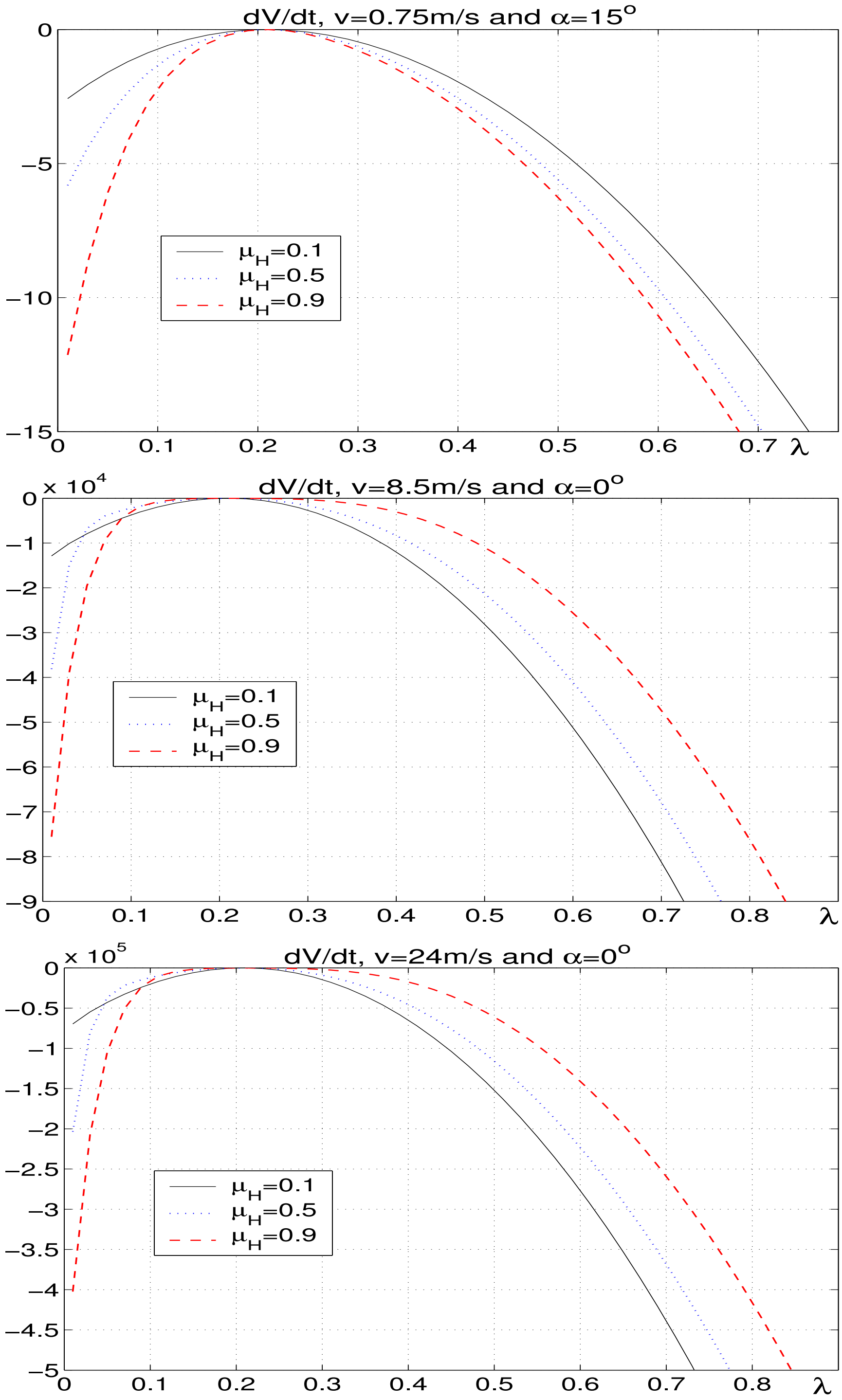

Figure 4.4: Time derivative of V.

Chapter 5

Implementation, redesign and tuning

An insight into the controller structure and states, and the ABS supervisory logic is given first to show the framework under which the controller was implemented. A brief description of the controller design method, LQRC, and how the system is specified for LQRC design are then given. The discrete time wheel slip control design and tuning shown in this chapter for implementation use the control design parameters from the control design and analysis developed in Chapter 4 in addition to the actuator constraints. Note that the stability analysis developed in Chapter 4 is based on a gain scheduled LQG design to simplify the analysis and to obtain comprehensible results. However, experiments showed that the actuator rate constraints did not have a significant impact on the experimental results. Then an analysis and a discussion are given on the choice of slip setpoint as the communications delay and actuator dynamics impose limitations. Two methods improving the initial transient response, controller initialization and off-equilibrium scheduling on slip are then described. Towards the end of this chapter, a description of the implementation of an anti-windup mechanism is provided.

5.1 Controller structure

The overall structure of the controller that has been implemented in the vehicle is shown in Figure 5.1. It consists of the slip controller (LQRC), the extended Kalman filter (EKF) and the vehicle equipped with electromechanical brakes operating on unknown road surfaces. The shaded boxes represent the controller and related elements implemented in software. The non-shaded boxes represents the physical system. The online estimated variables from the EKF (based on a nonlinear vehicle model) are:

- Tyre/road slip (λ)
- Vehicle velocity (v)
- Maxium friction coefficient (μ_H - not used for the LQRC design)

The measurements fed to the EKF are the four wheel speeds, the steering wheel angle, the longitudinal and lateral accelerations. In general, it can be said that the estimation error by the EKF leads to a loss in controller performance. For controller design, these variables are assumed as measurements and therefore, the dynamics of the estimator is not included in the design.

The brake-by-wire software is written in C and provides an interface for the wheel slip controller. The interface gives access to the sensor signals and reads the command signals for the brakes provided by the wheel slip controller. The wheel slip controller runs at a sampling period (T_s) of $7msec$ and with a delay of two time steps between the processing of a new control signal and until the sensor output has been received, see Figure 2.9 and 5.5.

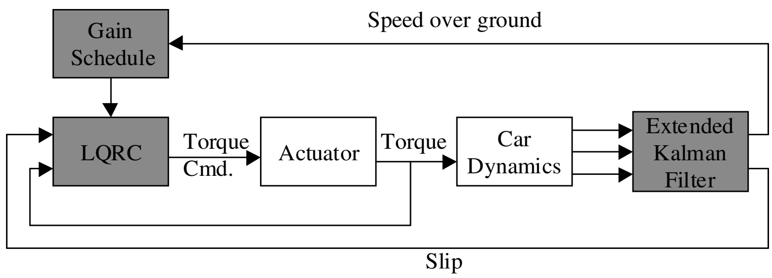

Figure 5.1: Wheel slip control - block diagram.

5.2 ABS supervisory logic

As a safety device, the ABS will only be activated when the driver commands a brake force resulting in higher slips than the setpoint of the controller, typical in critical or emergency situations. The maximal applied brake force is limited to the driver's commanded brake force. For safety reasons, the slip controller is only allowed to lower the brake force in order to prevent the wheel from locking. When the commanded brake force by the driver is lowered (by the brake pedal), the brake force should be decreased accordingly.

Figure 5.2 shows the on/off switching of the overall controller. An operation state f is achieved only when the controller is switched on manually (S), the gear g is set to forward (not reverse) and the reference speed v_r of the vehicle is higher than the minimum speed. Notice that the controller is switched off when the velocity drops below a minimum speed ($v_{min} = 1m/s$).

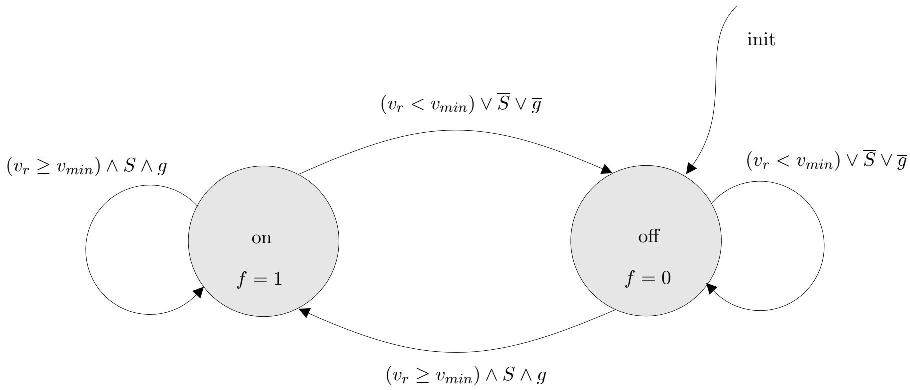

Figure 5.2: On/Off automaton

5.3 Controller states

Figure 5.3 shows the mode-switching automaton with three states. The controller remains in manual mode when f is off. The automaton enters the automatic state when f is on and the driver requests a brake force F_d that is higher than minimal brake force F_{min}, i.e. braking. If the brake pedal is released and f is off, the controller state is switched to manual state. If the brake pedal is not released and f is off, the controller state is switches to bumpless transfer. Normally, when ABS is activated, the brake demanded by the driver is higher than the brake torque applied by the controller. Therefore, to avoid a jerky transfer from the automatic state to the manual state with full brake force applied, a bumpless transfer is implemented. In the bumpless transfer state, the gradient of the brake force is limited until the output of the rate limiter has reached the desired clamping force F_d and thereby switched back to manual.

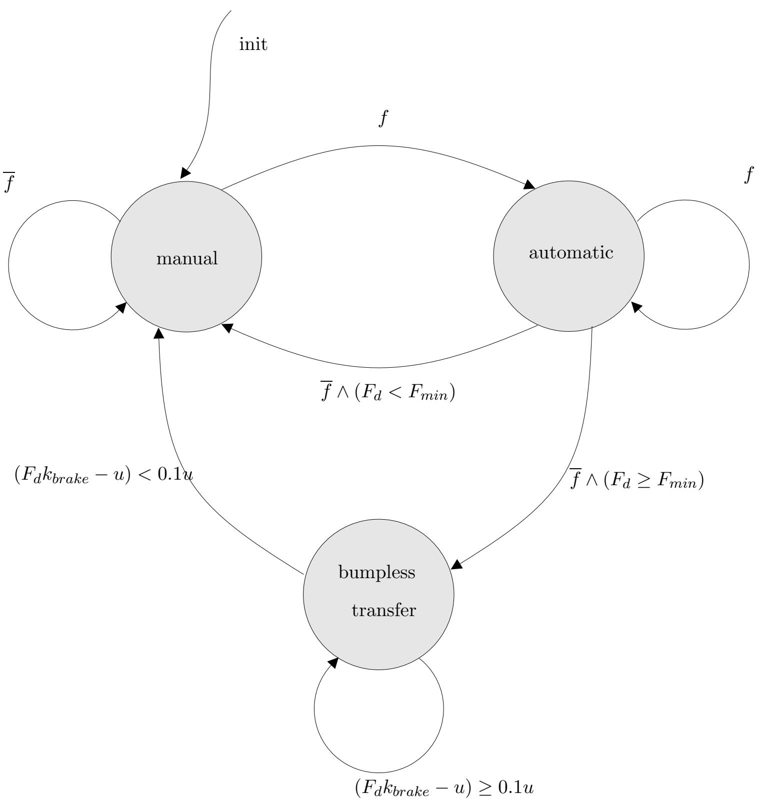

Figure 5.3: Mode change automaton

5.4 LQR with input and state constraints

5.4.1 Overview

The wheel slip controller design used in this research work is based on an explicit LQR design method (see Appendix A or (Johansen, Petersen, and Slupphaug 2002) and (Johansen, Petersen, and Slupphaug 2000a)) developed recently, which takes into account the input and state constraints, see also (Bemporad, Morari, Dua, and Pistikopoulos 2000) and (Tøndel, Johansen, and Bemporad 2003a) for related approaches.

This approach takes advantage of the piecewise linear (PWL) structure of the constrained LQR. For problems of sufficiently small dimensions, a combinatorial explosion is avoided and the PWL structure can be exploited both for design, analysis and in order to avoid the real-time optimization by explicitly implementing the PWL feedback controller. Hence, the main feature of this design method is that it allows computationally efficient implementation of constrained LQR, without relying on real-time optimization for problems of sufficiently small dimensions. Thus, it is a method suited for small embedded real-time applications with inherent constraints and sampling-rates in the range of microseconds to milliseconds, where conventional constrained optimal control implementations are not suited due to computational limitations or software complexity.

The software developed contains functions for controller design, analysis and implementation (including automatic generation of ANSI C code) using MATLAB. Several parameterized implementation strategies are available, allowing the code to be optimized to meet real-time target or simulator limitations in terms of processing capacity and computer memory as well as off-line processing time.

5.4.2 Brief introduction to LQRC design theory

The following describes briefly the constrained LQR method, for general linear systems subject to linear input and state constraints and a quadratic cost function. Consider the discrete-time linear time-invariant system

$$x(t+1) = Ax(t) + Bu(t) \tag{5.1}$$

where $x \in R^n$, and $u \in R^r$. The objective of the LQRC feedback controller is to minimize the infinite-horizon quadratic cost

$$J(u(t), u(t+1), u(t+2), ...; x(t)) = \sum_{\tau=t}^{\infty} \left(x^T(\tau)Qx(\tau) + u^T(\tau)Ru(\tau) \right) \tag{5.2}$$

subject to the linear constraints

$$Gx(\tau+1) \leq g \tag{5.3}$$

$$Hu(\tau) \leq h \tag{5.4}$$

for all $\tau \geq t$, where $R > 0$, $Q \geq 0$, $G \in R^{q\times n}$, and $H \in R^{p\times r}$. It is assumed that $g, h > 0$ to ensure that the equilibrium point ($x = 0$) is an interior point in the admissible region.

In order to reduce the computational complexity associated with the solution to the general problem stated above, the following additional assumptions are introduced:

- The infinite-horizon cost function (5.2) is approximated by the following finite-horizon cost function

$$\tilde{J}(u(t), u(t+1), u(t+2), ...; x(t)) = x^T(t+N)Px(t+N) + \sum_{\tau=t}^{t+N-1} \left(x^T(\tau)Qx(\tau) + u^T(\tau)Ru(\tau)\right) \tag{5.5}$$

where $N \geq 1$ is the prediction horizon and P is the solution to the algebraic Riccati equation (Anderson and Moore 1989) of the associated unconstrained LQR problem.

- The active constraint set is allowed to change only small number of times on the horizon N. In other words, the active constraint set can be different at the beginning and at the end of the horizon.

The Hamilton-Jacobi-Bellman equation of dynamic programming optimally balances the instantaneous cost with the cost-to-go, where $V(x)$ is the optimal cost-to-go (from state x to origin):

$$V(x(t)) = \min_{\substack{Gx(\tau+1)\leq g, Hu(\tau)\leq h \\ \tau\in\{t,t+1,t+2,...,t+N-1\}}} \left(V(x(t+N)) + \sum_{\tau=t}^{t+N-1} l_{QR}(x(\tau), u(\tau)) \right) \tag{5.6}$$

Reformulate (5.6) by replacing the inequality constraints by a set of equality constraint sets which constitutes all possible active constraint sets C (where C is an index set enumerating all (sub-)optimal combinations of active constraints), which gives:

$$V(x(t)) = \min_{\substack{k\in C, Gx_k^*(\tau+1)\leq g, Hu_k^*(\tau)\leq h \\ \tau\in\{t,t+1,t+2,...,t+N-1\}}} \left(\min_{H_k u = G_k x + h_k} \left(V(x(t+N)) + \sum_{\tau=t}^{t+N-1} l_{QR}(x(\tau), u(\tau)) \right) \right) \tag{5.7}$$

where x_k^* and u_k^* are the solutions of the inner optimization. The outer optimization is either executed online or pre-computed offline and the inner optimization is pre-computed offline.

5.4.3 Structure of the LQRC solution

The PWL control structure resulting from the LQRC specification and design may be summarized by the block diagram in Figure 5.4. There is a bank of affine state feedbacks of the form

$$u_k^*(t) = K_{k,2}x(t) + K_{k,1}^g g + K_{k,1}^h h \tag{5.8}$$

where each affine state feedback is designed with the objective of minimizing the LQ cost function subject to the state and input trajectories moving on a specific active constraint set. In other words, each affine feedback controller will force selected state and input constraints to be active on the horizon and use the additional available degrees of freedoms (if any) to minimize the LQ objective or the constraint violations if this cannot be avoided. The affine state feedbacks are designed off-line. So the real-time computations amount to selecting which affine state feedback to apply at a given state $x(t)$ and constraint limits g and h, and computing the control input using the associated pre-computed gain matrices $K_{k,1}^g, K_{k,1}^h$ and $K_{k,2}$. The control structure in Figure 5.4 corresponds to a switching controller since it switches between a number of affine feedbacks.

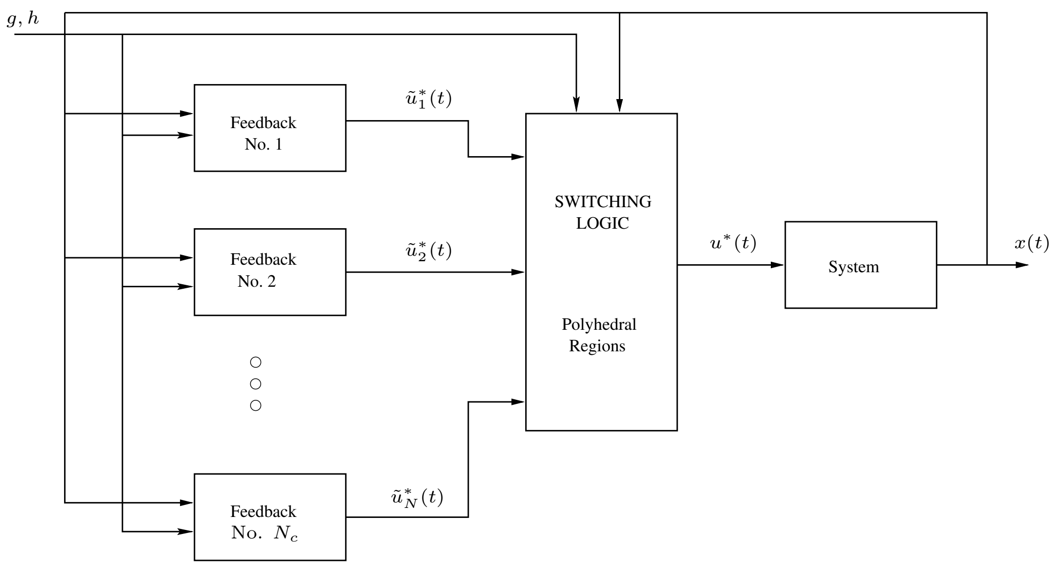

Figure 5.4: PWL constrained LQR control structure.

5.4.4 State space partitioning

As described above, the LQRC controller is a PWL function of the state x and constraint limits g and h. For any combination of active constraints it is straight forward to compute its constituent affine state feedback parameters and their associated cost functions. In order to fully explore and exploit the PWL structure, a characterization of the activity regions where each affine function is optimal (and feasible) is required. Note that due to the combinatorial nature of the problem, computation of such characterizations is computationally prohibitive for problems of a higher dimension.

The partitioning algorithm will first determine all candidate hyperplanes the partition may consist of. Then, a user-specified region of attention will be split recursively by considering optimality of the set of affine state feedbacks within each region of the partition. The algorithm will terminate when the number of candidate optimal affine state feedbacks within each region are less than a user-specified number, or when it is not possible to split any further. Note that in the latter case, the algorithm may fail to find the user-specified number of candidate affine state feedbacks within each region.

5.4.5 Computational strategies

In order to compute a control input u for a given state x and constraint limits g and h, the following two tasks must be accomplished:

i. Determine which affine state feedback is optimal.

ii. Compute the control input according to the affine state feedback law

While the second task is simple to implement, the first task is considerably more complex and can be implemented in several ways:

- If no state-space partitioning exists, the costs associated with each of the affine state feedbacks must be compared at each sample. This may be done in a sequential fashion by computing the cost associated with each of them. However, in most cases one can rely on a branch-and-bound approach that takes advantage of the structural relationship between the active constraint sets associated with each affine state feedback in order to reduce the computational complexity considerably.

- If a state-space partitioning exists, it can be utilized to speed up the computations since the number of candidate optimal affine state feedbacks within a given polyhedral region is typically small. Determining which polyhedral region the state belongs to is essentially to keep account of the side of the constituent hyperplanes of the partition the given state is.

More efficient methods for state space partitioning has recently been developed (Tøndel, Johansen, and Bemporad 2003a; Bemporad, Morari, Dua, and Pistikopoulos 2000) as well as data structures supporting efficient evaluation of PWL control laws (Tøndel, Johansen, and Bemporad 2003b).

5.5 ABS specifications for LQRC design

This section describes in detail how the LQRC wheel slip controller was specified, designed and implemented.

5.5.1 Gain scheduling control

The controller is a gain scheduled constrained LQR on the form:

$$u(t) = u_{LQRC}(i_e(t), \hat{\lambda}(t) - \lambda^*, T_b(t), \tilde{T}_b(t), \hat{v}(t), \hat{\lambda}(t)) \tag{5.9}$$

where $\hat{v}(t)$ and $\hat{\lambda}(t)$ are estimates for speed-over-ground and wheel slip respectively (both from the extended Kalman-filter). The last two variables are used as gain scheduling parameters. The design method is an explicit constrained LQR that gives an explicit piecewise linear controller that incorporates constraints. Thus, if no constraints are active, the controller is of the form

$$u(t) = K(\hat{v}(t))x(t) \tag{5.10}$$

with state $x(t) = (i_e(t), \hat{\lambda}(t) - \lambda^*, T_b(t), \tilde{T}_b(t))$.

Gain scheduling is implemented by switching gain matrices, where the gain matrices (5.8) are computed for a finite number of operating points for v:

$$v = 0.75 - 32m/s, \text{ 12 velocities, logarithmically spaced} \tag{5.11}$$

This leads to an implemented controller of the form

$$u(t) = K_{i(\hat{v}(t))}x(t) \tag{5.12}$$

where the index $i(\hat{v}(t))$ is selected based on $\hat{v}$. As switching might lead to undesired transients in the controller (partially due to the equilibrium point x_1^* depends on the elements of the gain matrix K_i), bumpless transfer is implemented to avoid this undesired effect (see Section 5.8). The selected number of operating points and switching do not lead to significant loss of performance compared to continuous gain schedule (verified through simulation).

For the controller design, the nominal model parameters used are taken from Section 5.6 together with the performance specification and constraint parameters taken from the following two sections.

5.5.2 System and cost function specifications

A 4th order discrete-time LPV state space model form, based on the 4th order continuous-time model given in Section 4.3.3, is written as:

$$x(t+1) = \Phi(v, \lambda)x(t) + \Gamma u(t) \tag{5.13}$$

where x_1 is the integrated slip error, $x_2 = \lambda - \lambda^*$ is the slip error, x_3 is the brake torque produced by the actuator and x_4 is the brake torque commanded to the actuator. All states are available for feedback for the slip dynamic model: $\hat{v}(t)$ and $\hat{\lambda}(t)$ are estimated online, $T_b(t)$ is measured and $i_e(t)$ and T_b are states of the controller. The speed and slip dependent model matrices are given by

$$\Phi(v, \lambda) = \begin{pmatrix} 1 & T_s & 0 & 0 \\ 0 & a_1(v, \lambda) & b_1(v, \lambda) & 0 \\ 0 & 0 & a_{act} & b_{act} \\ 0 & 0 & 0 & 1 \end{pmatrix}, \Gamma = \begin{pmatrix} 0 \\ 0 \\ 0 \\ 1 \end{pmatrix} \tag{5.14}$$

with the following discretization (Åström and Wittenmark 1997)

$$a_1(v, \lambda) = e^{T_s \alpha_1 / v}, \quad b_1(v, \lambda) = \beta_1(a_1(v, \lambda) - 1)/\alpha_1 \tag{5.15}$$

where T_s is the sampling time ($7ms$), α_1 and β_1 are parameters calculated using equations (4.3) and (4.4) respectively. The parameters a_{act} and b_{act} (with values 0.6 and 0.4 respectively) are from the first order discrete-time linear model of the actuator dynamics, see Section 2.3.2.

The corresponding cost function parameters for the LQRC design (including actuator dynamics in the model and scaled with respect to T_b and λ):

$$R = 1, \quad Q(v) = \tilde{Q} v^{3/2} \tag{5.16}$$

with $\tilde{Q}_{1,1} = 8 \cdot 10^6$ and all other elements of $\tilde{Q}$ equal to zero. This corresponds to the design studied in Section 4.3.3. The simulator was extensively used for tuning and as a verification check of the wheel slip controller before it was decided to be implemented into the test vehicle.

Note that including the actuator model allows the weight on the control error to be increased (with respect to the other elements in $\tilde{Q}$) which effectively increases the gain and the performance without introducing oscillations in the closed loop.

5.5.3 Constraint specifications

The controller design uses only input constraints where the actuator rate constraint leads to the following input constraint (soft):

$$-\dot{T}_b^{max} T_s \leq u_{LQRC}(t) \ \leq \dot{T}_b^{max} T_s \tag{5.17}$$

The maximum brake torque applied to the rear wheel is half of the maximum front wheel brake torque (5.6). This is essential for the stability of the vehicle. Otherwise the vehicle might start to rotate because the rear wheels would lose their lateral traction. The LQRC control design incorporates the saturation of the maximum brake rate change, $\dot{T}_b^{max}$, whereas the saturated brake torques T_b^{min} and T_b^{max}, are limits handled by a simple software function (limiter) independent of the LQRC.

5.5.4 Constraint handling

The PWL structure of the controller consists of three regions as shown in (5.17), the lower/upper constrained regions and an unconstrained region. The prediction horizon was set to $N = 1$ and it is assumed to be sufficient as there are only input constraints. With $N = 1$, the resulting four wheel slip controllers occupied in total $1.7msec$ of the available $7msec$ (sampling time) which gave the individual wheel slip controller processing time of 425 microseconds. This time-limitation for controller processing is mainly due to the extended Kalman filter, which required most of the CPU's processing capacity, and other supervisory tasks. A more efficient method to improve the online controller processing is suggested in (Tøndel, Johansen, and Bemporad 2003b).

5.6 Frequency response analysis

For unstable operating points (with setpoint λ^* to the right of the friction curve peak), it is well known that a minimum gain is necessary to stabilize the open-loop unstable dynamics. Since the communications delay and actuator dynamics impose fundamental limitations on the maximum gain, it is of interest to investigate if all operating points, i.e. all values of λ^* for all possible friction curves, can be stabilized with acceptable performance. This analysis is carried out most conveniently using a classical frequency analysis based on a linearized model (see Section 5.5) or the equivalent block diagram for the linearized dynamics shown in Figure 5.5 where $K(v)$ is designed using LQRC.

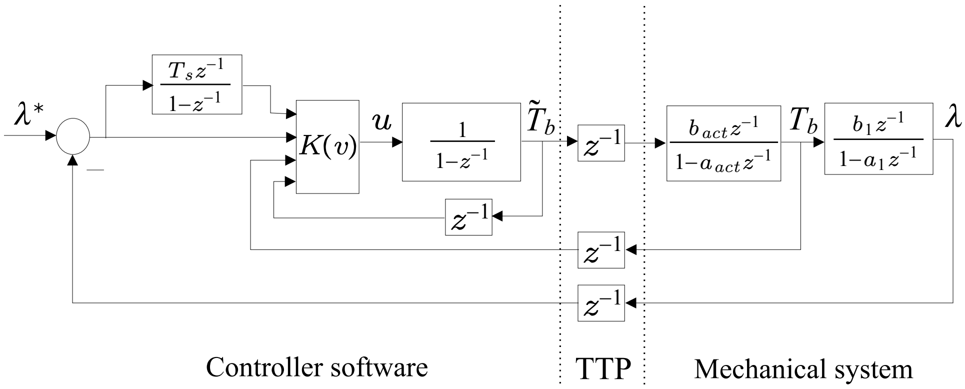

Figure 5.5: Block diagram including actuator dynamics and communication delays.

Assume for a moment the setpoint $\lambda^*(= 0.14)$ corresponds to a slip value near the peak of the friction curve. The family of frequency responses (from slip setpoint to slip, computed based on the block diagram in Figure 5.5) corresponding to values of v between $0.75m/s$ and $32m/s$ are given in Figure 5.6. It can be observed that the bandwidth (-3 dB frequency) is between 44 rad/s and 73 rad/s (depending on v). It can also be observed that the suspension resonance found in Section 3.3 is slightly larger than the bandwidth of the controller and the controller bandwidth cannot be increased any further without encountering interaction with the suspension system. If the setpoint is moved sufficiently far to the right of the peak of the friction curve, the closed loop becomes unstable since the gain is not sufficiently large to stabilize the open-loop unstable system. On the other

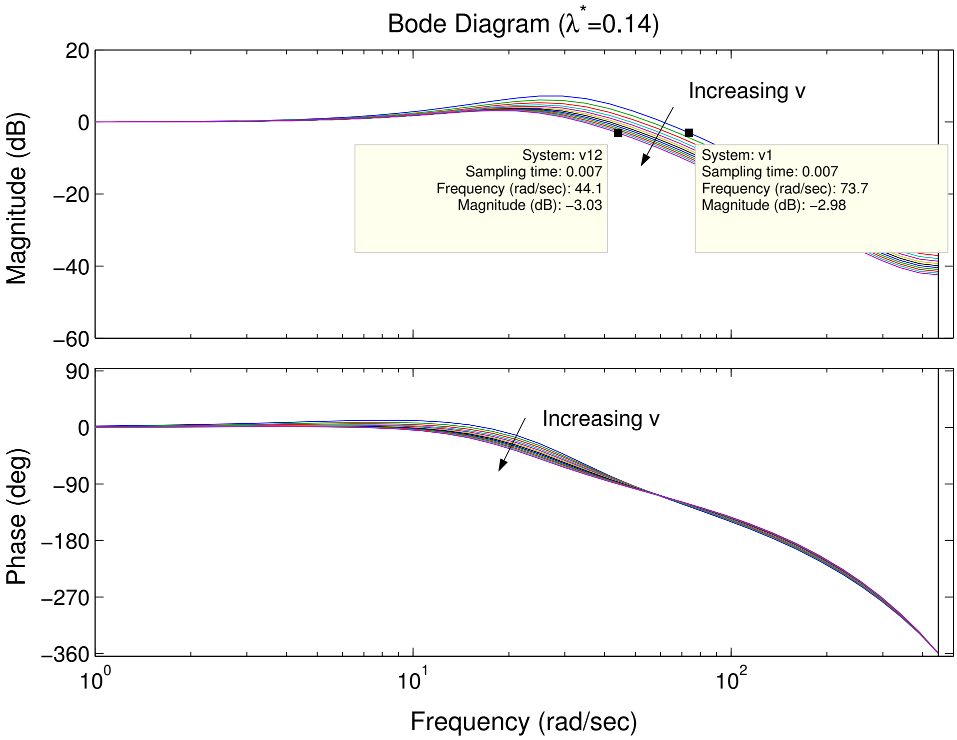

Figure 5.6: Transfer function from reference to output, when the setpoint is near the peak of the friction curve.

hand, if the setpoint is moved slightly to the left of the peak (say $\lambda^* = 0.1$) of the friction curve, the family of frequency responses changes to Figure 5.7. It is observed that the bandwidth decreases significantly, especially for small v, indicating a loss of performance. If the setpoint is moved even further left of the peak, a further loss of performance is experienced. Thus, high performance is achieved only if the setpoint is chosen near the peak of the friction curve. At low friction, the peak is less pronounced and the performance and the robustness are not expected to be very sensitive to the choice of setpoint. At high friction, however, the peak is significant and loss of stability will occur if the setpoint is chosen too high, and loss of performance may occur if the setpoint is chosen too low. It must be stressed that this analysis is based on a linearized model and is therefore not valid for transients that are far from the equilibrium. However, it still correctly points out fundamental limitations in performance and robustness,

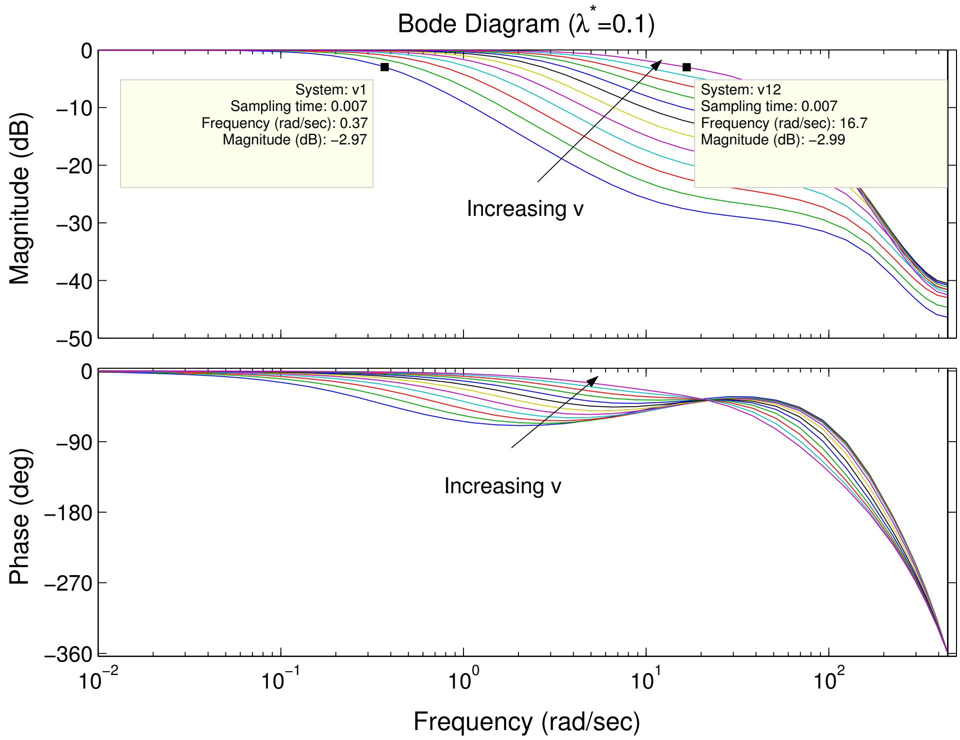

Figure 5.7: Transfer function from reference to output, when the setpoint is slightly to the left of the peak of the friction curve.

and suggests useful guidelines for selecting the slip setpoint λ^*, consistent with underestimation results in (Yi, Alvarez, and Horowitz 2002).

5.7 Improvement of initial transient response

As a result of a slow initial transient response which was discovered in an experiment on a high friction surface (see Section 6.4), two methods have been developed to improve the initial transient response. The first redesign approach focuses on the initial state of the controller. The second approach is based on the concept of off-equilibrium linearization and design in gain scheduled control.

5.7.1 Controller initialization

In the first method, the initial value of the integrator $x_1(0)$ is set to a value corresponding to a nominal steady-state value of the clamping torque T_b which typically is experienced on a given surface. This gives, for the nominal state (with $x_2 = 0$ and $x_3 = x_4 = T_b^*$), a steady-state consideration leads to

$$u_{LQRC} = K(\hat{v})x = 0 \tag{5.18}$$
$$\Downarrow$$
$$x_1(0) = -T_b^*(k_3 + k_4)/k_1 \tag{5.19}$$

Because the load is unevenly distributed during braking, it is a need to differentiate between initialization of front wheels and rear wheels. For the front wheels

$$x_1(0) = -\sqrt{2}T_b^*(k_3 + k_4)/k_1 \tag{5.20}$$

and for the rear wheels

$$x_1(0) = \frac{-1}{\sqrt{2}}T_b^*(k_3 + k_4)/k_1 \tag{5.21}$$

Other controller initialization methods are reported in (Kalkkuhl, Johansen, and Lüdemann 2002; Lüdemann 2002) using a multiple model adaptive control approach with an estimator resetting rule or by using a μ_H-estimator such as (Gustafsson 1997; Canudas de Wit, Horowitz, and P.Tsiotras 1999) for initialization.

5.7.2 Off-equilibrium scheduling on slip

A second redesign method to improve the initial transient response when braking on high μ_H, off-equilibrium linearization (Johansen, Hunt, Gawthrop, and H.Fritz 1998) with respect to the slip has been applied. The gain matrices (5.8) are computed for a finite number of operating points for both v (5.11) and $\lambda = 0.09, 0.14$. In particular, the controller is modified during transients at low wheel slip values such that slip setpoint is reached more rapidly. Thus, the controller switches to new gain matrices when the wheel slip is lower than a given threshold, $0.6\lambda^*$. The switching is implemented similar to that for bumpless transfer, described in Section 5.8, in order to avoid undesired transients. However, the nominal $\hat{\lambda}$ is now on the steep part on the left side of the friction curve peak and, therefore, leads to a higher gain near equilibria. Consequently, the transients are speeded up and the overall performance is improved as shown in the experiment described in Section 6.10. It is remarked that this method has the advantage that it does not require an estimate of the equilibrium torque T_b^* (or μ_H). Note that the operating point $\lambda = 0.09$ and the wheel slip threshold $0.6\lambda^*$ were selected by trial and error using the vehicle simulator.

5.8 Bumpless transfer due to controller switching (gain scheduling)

The gain scheduling implemented includes bumpless transfer which is achieved by resetting the integrator, x_1, at the switching instants, thereby obtaining a control signal without any discontinuities. At the switching instant, the commanded clamping torque signal ($\tilde{T}_b$, the integral value of the control input signal u) to the actuator must be constant. This is obtained with the control input signal u set to zero (recall that u is the change in commanded brake torque, so this essentially requires no jump in the brake torque).

$$0 = u_{LQRC}(x_1(t), x_2(t), x_3(t), x_4(t), \hat{v}(t), \hat{\lambda}(t)) = K(v, \lambda)x \tag{5.22}$$

$$\Downarrow$$

$$x_1^{new}(t) = -\left(k_2 x_2(t) + k_3 x_3(t) + k_4 x_4(t)\right)/k_1 \tag{5.23}$$

Bumpless transfer becomes more important the lower the μ_H is; e.g. on snow or ice, as the effect of the wheel inertia is more influential.

5.9 Anti-windup

The aim of an anti-windup compensation is to modify the dynamics of the control loop when the control signals saturate. Thus, a good transient behaviour is attained after de-saturation, while avoiding limit cycle oscillations and repeated saturations. The technique used here for model-based anti-windup reset is a standard dead-beat anti-windup mechanism (Åström and Wittenmark 1997), where the internal controller states are consistent with the saturated control input $u(t)$ and the saturated brake torque $T_b(t)$. Since there are both a rate and a saturation limit for the brake torque, one way to incorporate this saturation is through the control input u. The anti-windup for integral of the slip error, x_1:

$$x_1^{new}(t) = x_1^{'}(t) + \Big(T_b(t) - T_b^{'}(t) + u_{LQRC}(t) - u_{LQ}(t)\Big)/k_1 \tag{5.24}$$

where $u_{LQRC}(t)$ is the rate control input computed by the LQRC, $u_{LQ}(t)$ is the corresponding unconstrained control and

$$x_1^{'}(t) = \lambda(t) - \lambda(t-1) \tag{5.25}$$

$$T_b^{'}(t) = T_b(t-1) + u_{LQRC}(t) \tag{5.26}$$

$$T_b(t) = T_b^{\max} \geq T_b^{'}(t) \geq T_b^{\min} \tag{5.27}$$

For the case where no saturation occurs, it can be seen that the nominal dynamics is unchanged as $x_1 = x_1^{'}$ due to $T_b = T_b^{'}$ and $u_{LQ} = u_{LQRC}$. It should be noticed that this mechanism is also used in the case of controller initialization (see Section 5.7.1).

Chapter 6

Experimental Results

This section gives a description of the experimental results obtained with the controller described in Section 5. Procedures for testing of an ABS system's braking performance in a motor vehicle can be found in publications such as International Organization for Standardization (ISO) (ISO 1991; ISO 1995; ISO 1996; ISO 1999) and in publications of the Society of Automotive Engineers (SAE) (SAE 1973). Since this project was aimed at developing an ABS controller for a prototype electro-mechanical wheel brake and not for a production vehicle, a reduced and simplified test procedure was chosen.

The following subsections describe a series of successful experiments carried out for straight-line braking manoeuvre on different road surfaces (ice, snow, dry asphalt, wet asphalt and inhomogeneous asphalt/plastic coated surface) and a single experiment carried out for braking in a turn on dry asphalt.

6.1 Experimental scenarios

Table 6.1 gives an overview of the experiments and their order of appearance in this chapter with surface condition, controller configuration and steering action for the respective experiment.

For the experiments when braking on ice and snow, the vehicle was equipped with winter tyres, Conti TS790 215/55R16. All other experiments were carried out using summer tyres, ContiEcoContact CP 215/55R16. Both tyre types are produced by Continental.

Test no.	Surface condition	λ^*, Slip setpoint	Comments
1	Wet inhomogeneous	0.09	Straight
2	Dry asphalt	0.09	Straight
3	Wet asphalt	0.09	Straight
4	Snow	0.07	Straight
5	Ice	0.05	Straight
6	Dry asphalt	0.14	Turning
7	Dry asphalt	0.11	Straight, Controller initialization
8	Dry asphalt	0.11	Straight, Off-equilibrium design

Table 6.1: Experimental tests of EMB ABS

6.2 Presentation of experimental results

The following performance criteria are included in the evaluation:

- slip performance w.r.t. slip setpoint (peak, variability, stead-state error)
- lateral stability of vehicle (wheel lock avoided, lateral acceleration)
- deceleration of vehicle

To evaluate the controller performance, mainly the slip behaviour and clamping force are used. From the experimental vehicle, during the experiments, the following information was logged for each sample:

- The vehicle speed over ground estimated by the extended Kalman filter (EKF) and measured by an optical correlation sensor.
- The wheel speed for each wheel.
- The estimated wheel slip value for each wheel estimated by the extended Kalman filter.
- Clamping force, desired and measured values.
- Weather condition on the braking surface.
- Slip setpoint.
- Lateral and longitudinal acceleration.

Other sensor data like the steering wheel angle and the brake pedal position were also logged, but are omitted for presentation purposes.

For each experiment, there are four plots for each wheel and one plot for the vehicle.

i. The first plot shows the wheel slip λ (solid line) and the setpoint slip λ^* (dashed line).

ii. The second plot shows the measured clamping force by the electromechanical actuator (solid line) and the desired clamping force from the driver (dashed line).

iii. The third plot shows the measured wheel speed (solid line) and the measured vehicle speed (dashed line).

iv. The fourth plot shows the friction curve calculated (see Section 3.2.1) based on the wheel experimental data for the wheel.

v. The fifth plot shows the longitudinal (solid line) and lateral (dashed line) acceleration of the vehicle.

All plots (except the friction curve plot) are plotted with the time on the x-axis and for vehicle speed $v \geq 1m/s$. If the wheel speed $v < 1m/s$, then the controller is switched off. In the friction curve plot (iv), μ versus λ is plotted, and the figure is therefore limited to the slip values that are experienced by the wheel during a braking manoeuvre. The analysis of the friction curve plot is done with reference to (Burckhardt 1993; Canudas de Wit, Horowitz, and P.Tsiotras 1999; Gustafsson 1997; Hunter 1998) and Section 3.2.1.

6.3 Wet inhomogeneous surface

Figures 6.1 and 6.2 show braking without any steering manoeuvres on a wet asphalt partially covered with a plastic coating. The initial speed is $v(0) = 22\ m/s$ and the slip setpoint is $\lambda^* = 0.09$.

6.3.1 Slip

Observe that there is significant variability in the slip for $t \leq 6s$, whereas for $t > 6s$, the regulation is satisfactory. The variability is expected to be mainly due to the inhomogeneous road surface that provides external disturbances to the system. The peak slip value $\lambda \approx 0.45$ for $t = 3.7s$.

6.3.2 Lateral stability

The lateral acceleration shown in Figure 6.2 is negligible.

6.3.3 Deceleration of vehicle

A deceleration of $3m/s^2$ is reached very quickly and maintained during braking.

6.3.4 Friction estimate

The friction curve plot in Figure 6.1 shows a friction peak value $\mu_H \approx 0.5$ for $\lambda = 0.07 - 0.1$. Its shape, limited to a maximum slip of $\lambda < 0.45$, resembles the friction curve for $\mu_H = 0.5$ shown in Figure 3.2.

6.3.5 Controller performance

The transient performance is fast and the overall controller performance is satisfactory considering the road surface.

6.4 Dry asphalt

Figures 6.3-6.5 show experimental results with braking on dry asphalt. The initial speed is $v(0) = 21\ m/s$, the slip setpoint is $\lambda^* = 0.09$.

6.4.1 Slip

As the speed approaches zero, some variability in the slip emerges. The clamping force does not oscillate, this is probably due to the sensor noise that is known to increase as the speed approaches zero (see Section 3.1). The slip is too low and the resulting friction force is too low in the intervals $0.2 \leq t \leq 0.7$ and $0.2 \leq t \leq 0.4$ for the front and rear wheels respectively, leading to an unnecessarily large braking distance. This is due to the significant model inaccuracy in the low-slip region due to the friction curve being linearized in the control design, cf. Figure 3.2. The peak slip value (front wheel) $\lambda \approx 0.2$ for $t = 2.5s$.

6.4.2 Lateral stability

The lateral acceleration shown in Figure 6.5 is negligible.

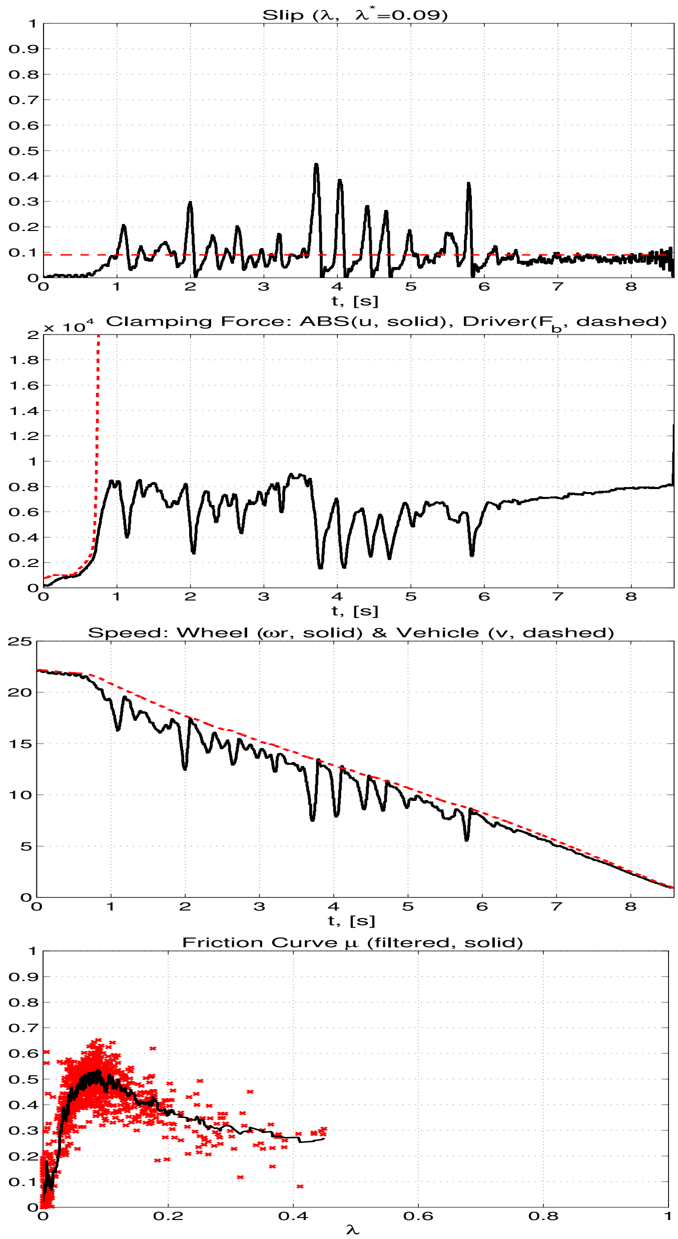

Figure 6.1: Wet inhomogeneous surface, front left wheel

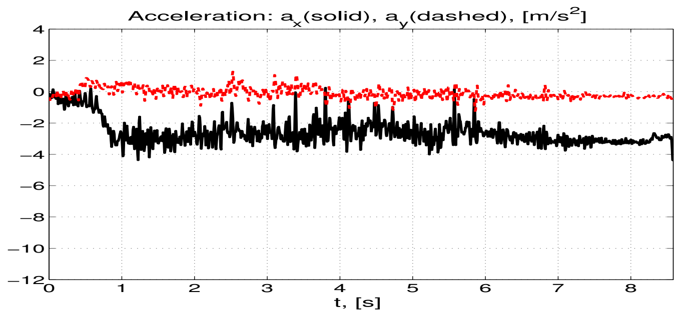

Figure 6.2: Wet inhomogeneous surface, car

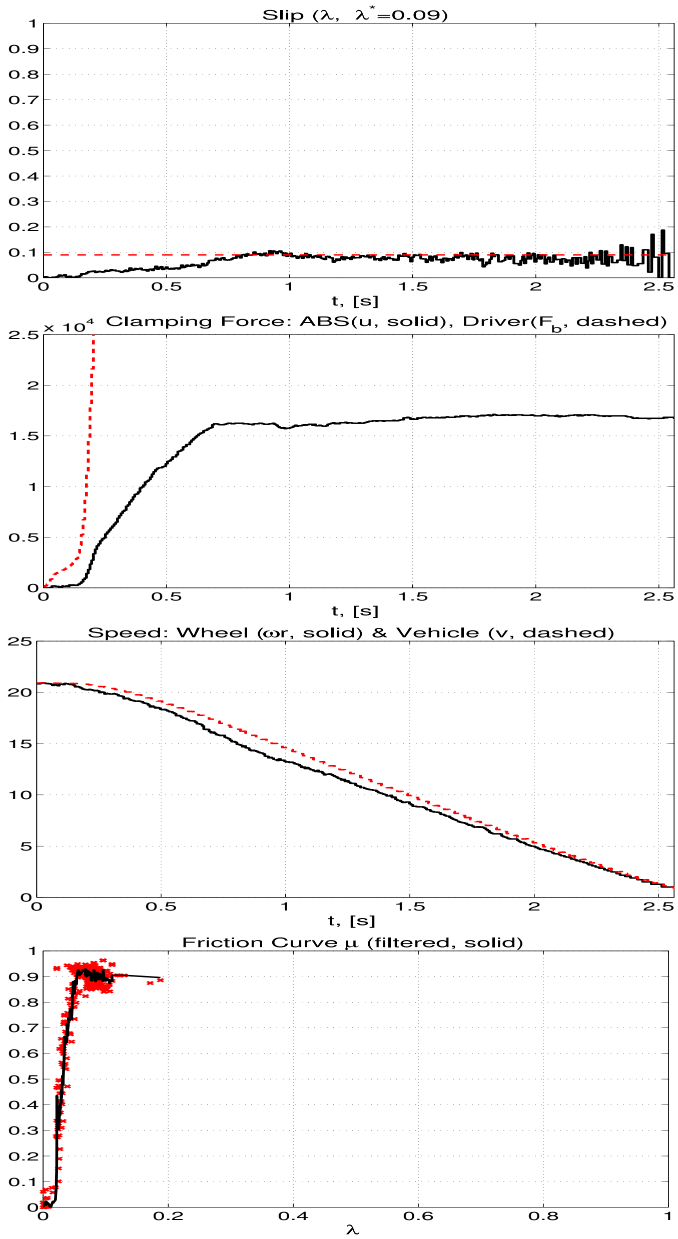

Figure 6.3: Dry asphalt, front left wheel

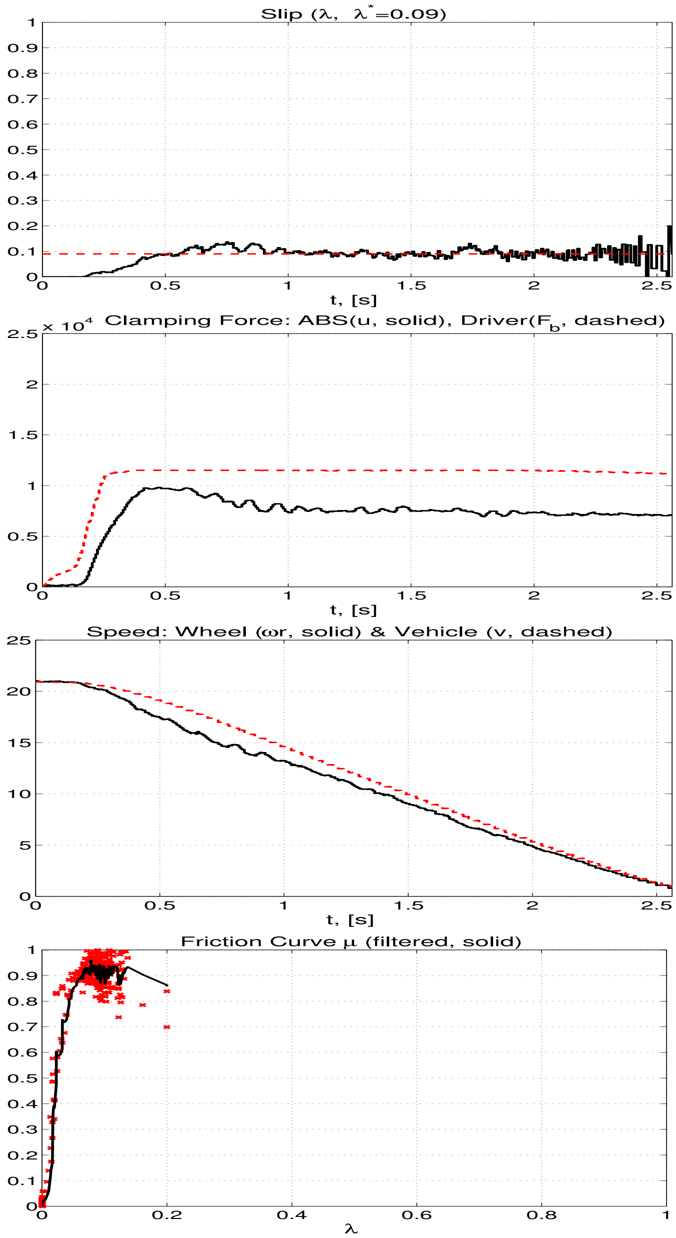

Figure 6.4: Dry asphalt, rear right wheel

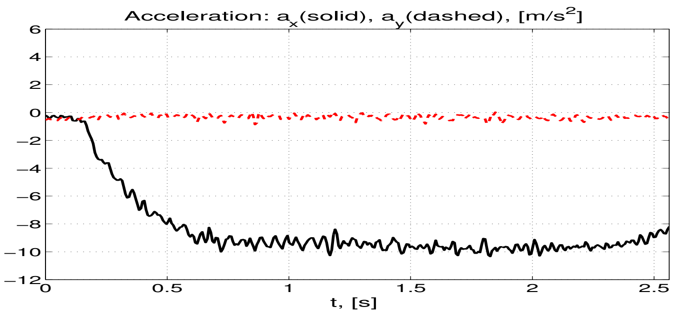

Figure 6.5: Dry asphalt, car

6.4.3 Deceleration of vehicle

Figure 6.5 shows that a high deceleration value, $a_x = 9 - 10m/s^2$, is reached and maintained for $t > 0.6s$, approximately $0.4s$ after braking commences.

6.4.4 Friction estimate

The friction curve plots for both the front and the rear wheels are shown in Figures 6.3 and 6.4, respectively. The figures resemble the dry asphalt friction plot in Figure 3.2 for $\mu_H \approx 0.9$. The friction peak occurs for $\lambda = 0.05 - 0.2$ and with a value of $\mu = 0.9$. The friction curves's complete shape cannot be produced as slip $\lambda < 0.2$, but they indicate that the brake force used corresponds to braking on dry asphalt.

6.4.5 Controller performance

It is important to note that the regulation is highly accurate and satisfactory. Observe that the transient performance is not as fast as experienced in Section 6.4 mainly because the steady-state value of the clamping force is further away from its initial state. Consequently, the initial transient response is not satisfactory as the clamping force does not increase fast enough. A redesign of the slip controller is necessary and two approaches were presented in Sections 5.7.1 and 5.7.2, and their experimental results are presented in Sections 6.9 and 6.10.

6.5 Wet asphalt

Figures 6.6-6.7 show experimental results with braking on wet asphalt. The initial speed is $v(0) = 23$ m/s and the slip setpoint is $\lambda^* = 0.09$.

6.5.1 Slip

Significantly less variability in the slip is observed than for the wet inhomogeneous case (see Section 6.3). The peak slip value $\lambda \approx 0.4$ for $t = 3.1s$ except when the velocity becomes very small. The initial slip variability is mainly due to an inhomogeneous road surface that provides external disturbances to the system.

6.5.2 Lateral stability

The lateral acceleration shown in Figure 6.7 is negligible.

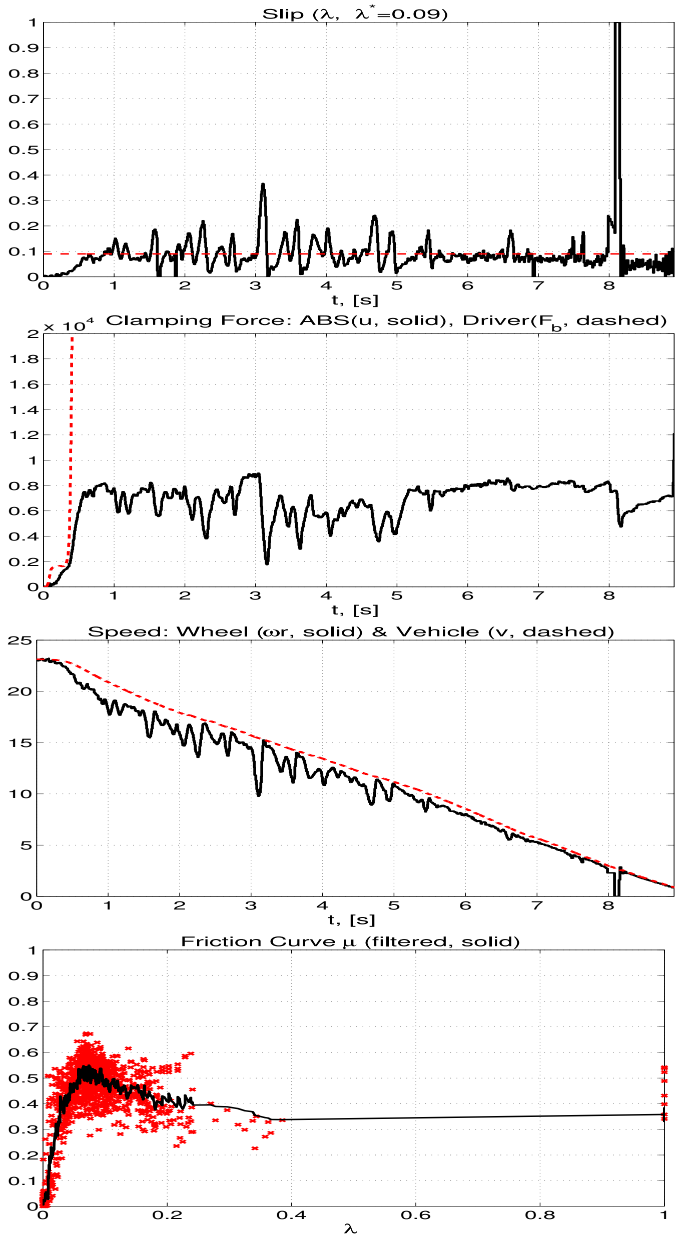

Figure 6.6: Wet asphalt, front left wheel

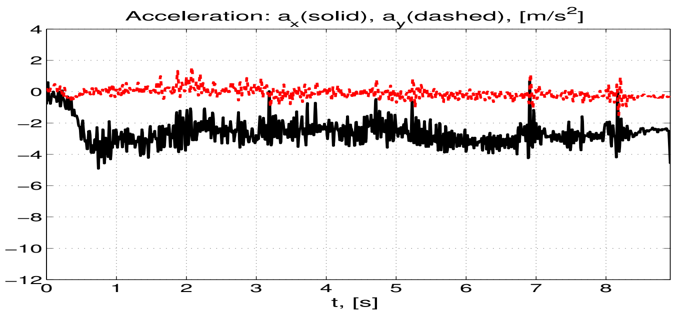

Figure 6.7: Wet asphalt, car

6.5.3 Deceleration of vehicle

Figure 6.7 shows that deceleration stays between $2 - 4m/s^2$ and reaches $4m/s^2$ approximately $0.25s$ after braking commences.

6.5.4 Friction estimate

The friction curve plots for the front wheel is shown in Figure 6.6. It is similar to the friction curve found for the wet, inhomogeneous surface in Figure 6.1. The friction peak occurs for $\lambda = 0.05 - 0.1$ and with a value of $\mu_H \approx 0.5$. Its shape resembles the wet, asphalt friction curve seen in Figure 3.2 for $\mu_H = 0.5$ and thus, the brake force used in this case corresponds to braking on wet asphalt.

6.5.5 Controller performance

Observe that the transient performance is again much better than on dry asphalt (see Section 6.4), mainly because the steady-state value of the clamping force is closer to its initial state. Overall, the controller performs satisfactorily.

6.6 Snow

Figures 6.8-6.10 show a straight-line braking manoeuvre on a road covered with 3 cm of fresh snow. The vehicle speed is $v = 22m/s$ when braking is commenced and without any steering manoeuvres. The slip set point is $\lambda^* = 0.07$.

6.6.1 Slip

The rear wheel slip, Figure 6.9, is slightly more oscillatory than the front wheel slip in Figure 6.8. The slip peak (rear) is approximately 0.25 and occurs at low speed (three places) for $5.8s < t < 7.2s$. The front slip peak is 0.6, but happens at low speed ($< 2.5m/s$) for $t = 7.2s$.

6.6.2 Lateral stability

The lateral acceleration and velocity shown in Figure 6.10 are negligible.

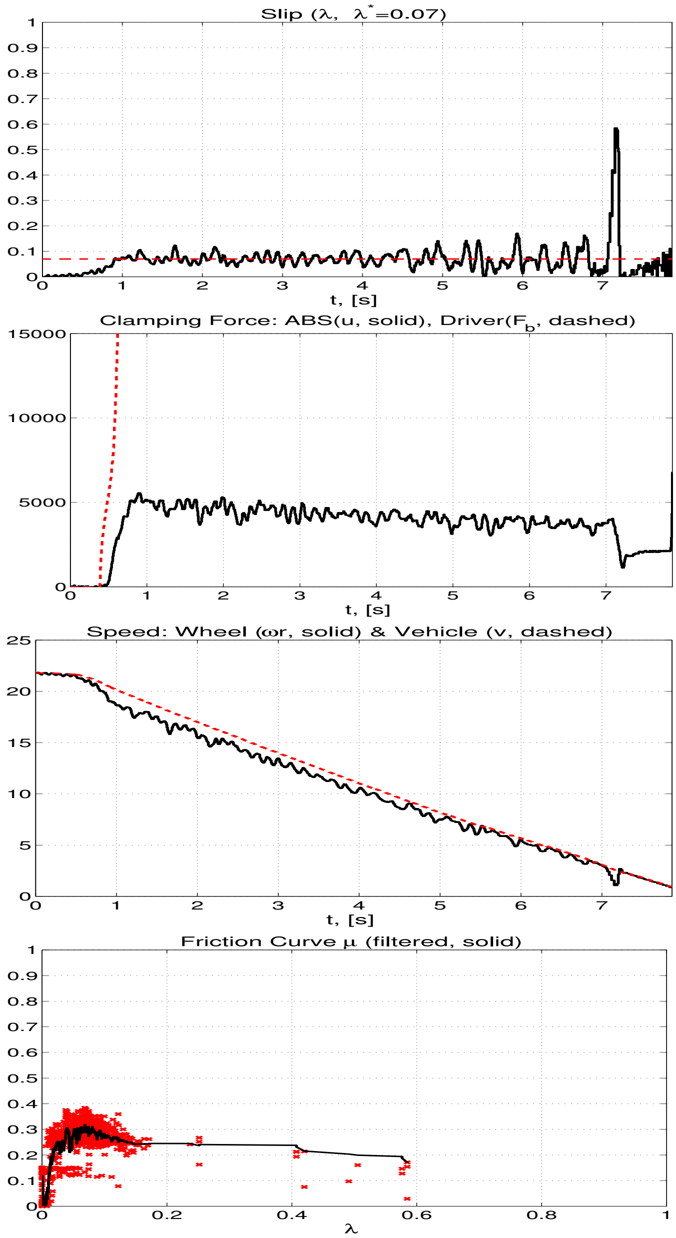

Figure 6.8: Snow, front left wheel

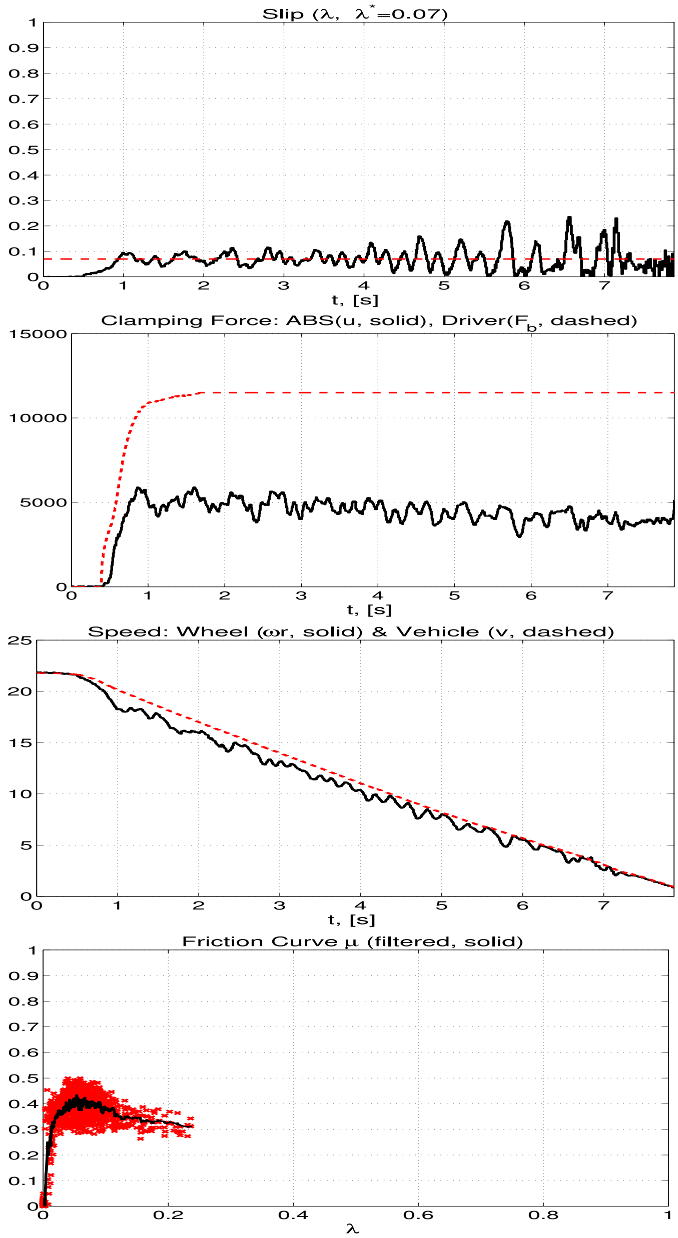

Figure 6.9: Snow, rear right wheel

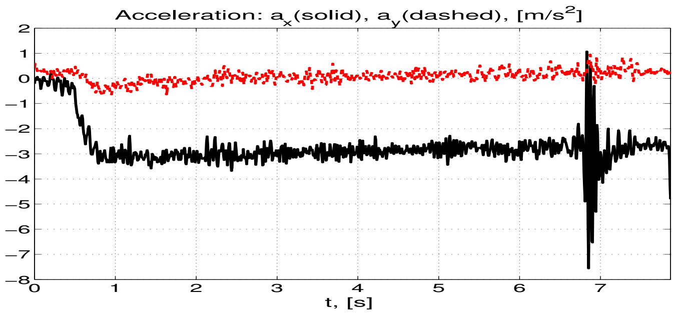

Figure 6.10: Snow, car

6.6.3 Deceleration of vehicle

A deceleration of $3m/s^2$ is reached and maintained $0.3s$ after braking commences.

6.6.4 Friction estimate

The maximum friction coefficient is $\mu_H \approx 0.3$ cf. Figure 6.8. A slightly higher friction value is obtained for the rear wheel than for the front wheel. Both wheels achieve maximum friction at $\lambda \approx 0.05 - 0.10$.

6.6.5 Controller performance

The transient performance is satisfactory and the regulation is excellent.

6.7 Ice

Figures 6.11-6.13 show a straight-line braking manoeuvre on an icy road. The vehicle speed is $v(0) = 16m/s$ when braking commences. The slip set point is $\lambda^* = 0.05$.

6.7.1 Slip

The front wheel slip peak, $\lambda = 0.3$, is at $t = 8.3s$ and for the rear wheel, $\lambda = 0.45$, at $t = 9.2s$. This occurs at low velocity, where the slip dynamics are more sensitive.

6.7.2 Lateral stability

In Figure 6.13, a_y changes suddenly by $2m/s^2$ at around $t = 4s$, from $-1m/s^2$ to $1m/s^2$. The lateral acceleration $a_y = 2m/s^2$ is maintained for $2s$.

6.7.3 Deceleration of vehicle

A deceleration of $2 - 3m/s^2$ is reached and maintained $0.5s$ after braking commences.

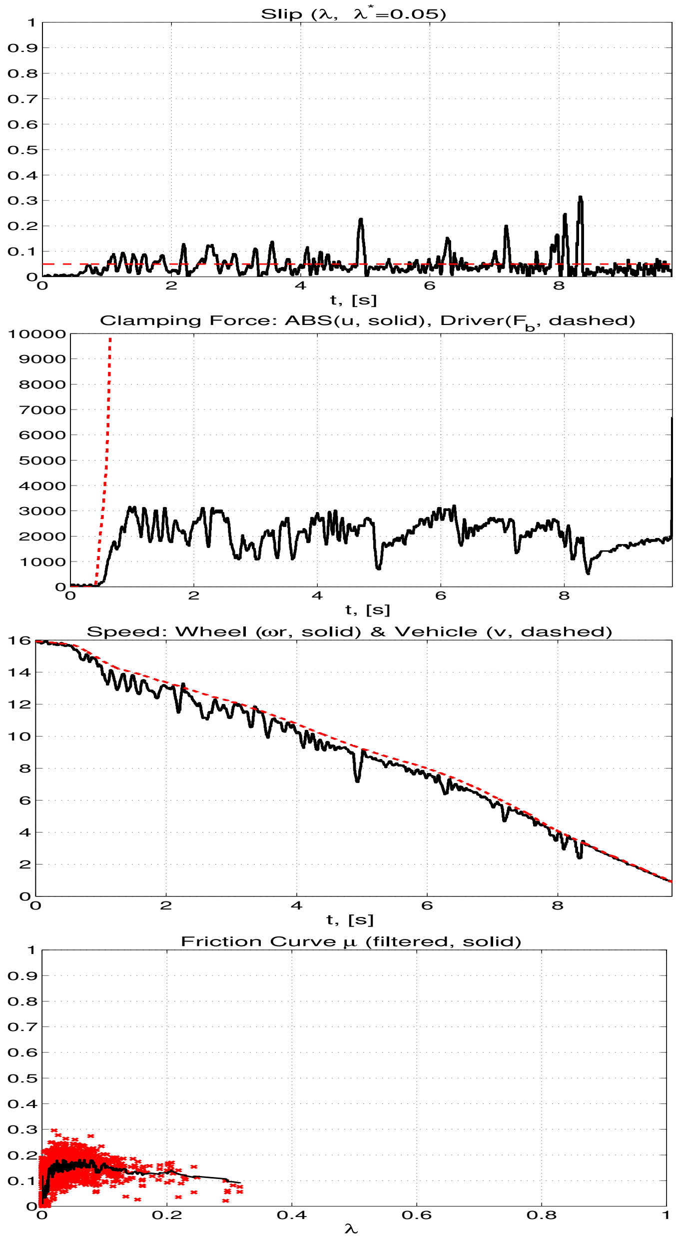

Figure 6.11: Ice, front left wheel

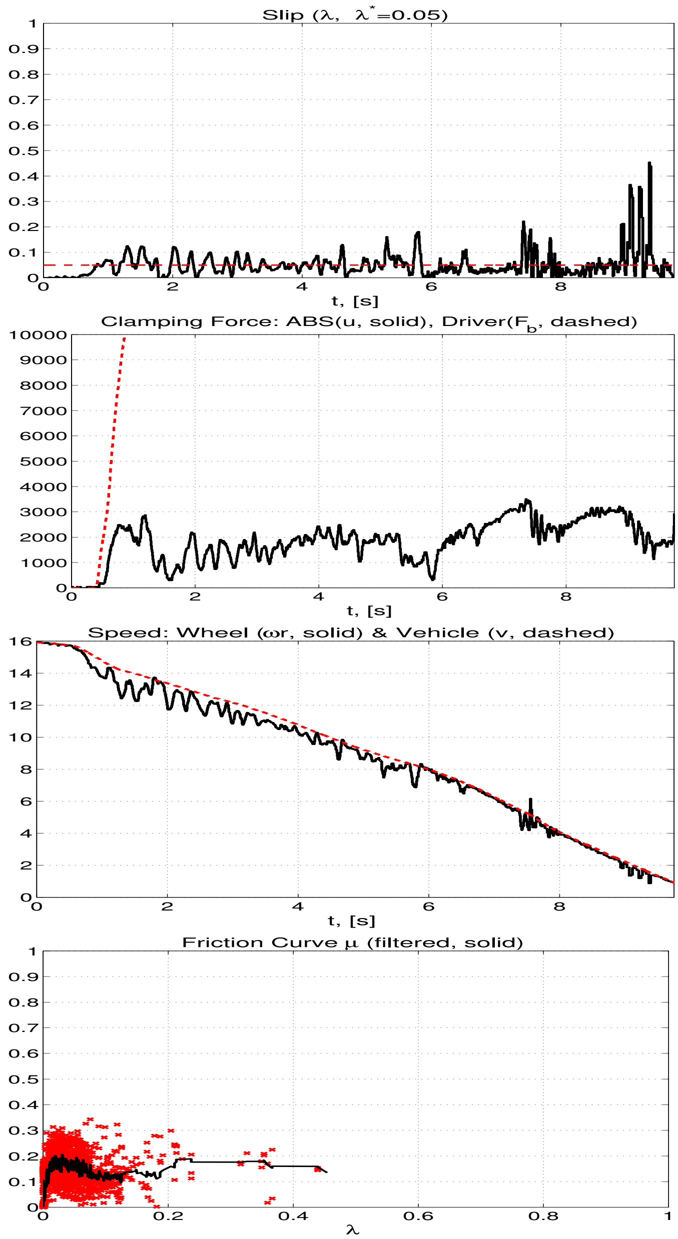

Figure 6.12: Ice, rear right wheel

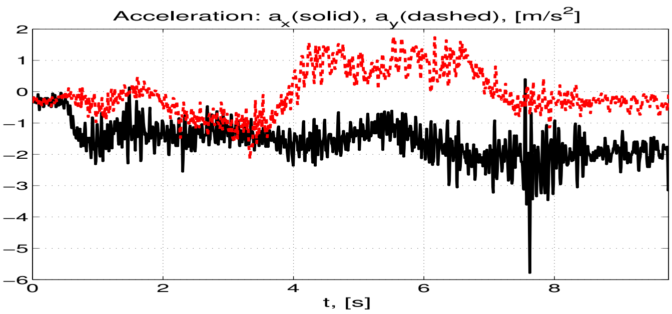

Figure 6.13: Ice, car

6.7.4 Friction estimate

The maximum friction coefficient is approximately $\mu_H \approx 0.15-0.20$. This is seen in the friction curve plots 6.11 and 6.12, with a slightly higher friction value obtained for the rear wheel. Both wheels reach maximum friction at $\lambda \approx 0.02$.

6.7.5 Controller performance

Braking on ice gives similar performance to that of braking on snow. At such low friction levels for both the wheel slip and the clamping force, the control system becomes very sensitive specially to disturbances due to an inhomogeneous road surface which is more likely to happen on ice. This can be seen as slip disturbances or with a split friction surface, a side acceleration of the vehicle. At such low wheel slip and clamping force levels, the control system is also sensitive towards disturbances in sensor noise, actuator inaccuracies, nonlinearities due to internal friction and other phenomena. The transient performance is satisfactory and the regulation is excellent.

6.8 Turning on dry asphalt

Figures 6.14-6.18 show a braking manoeuvre in a turn where the vehicle is driven clockwise in a circle with a radius of approximately $15m$. The initial speed $v(0) = 15m/s$ and the initial lateral acceleration $a_y \approx 8m/s^2$.In the speed figures for Figure 6.14-6.17, it can be seen that the estimation by the extended Kalman-filter of the vehicle speed is either $0.5m/s$ higher or lower compared to the wheel perimeter speed, when the vehicle is not braking. This is due to the fact that the outer wheels rotate faster than the inner wheels.

6.8.1 Slip

The outer front left wheel is locked for $2.05s < t < 2.2s$, see Figure 6.14. A similar situation occurs for the outer rear left wheel, but the slip peak reaches 0.8. The slip for the inner wheels $\lambda < 0.25$ throughout the manoeuvre.

6.8.2 Lateral stability

Figure 6.18 shows that the lateral acceleration decreases steadily during the braking manoeuvre, while the oscillations in a_x and also in a_y, indicate pitching and rolling movements of the vehicle. The approximately constant

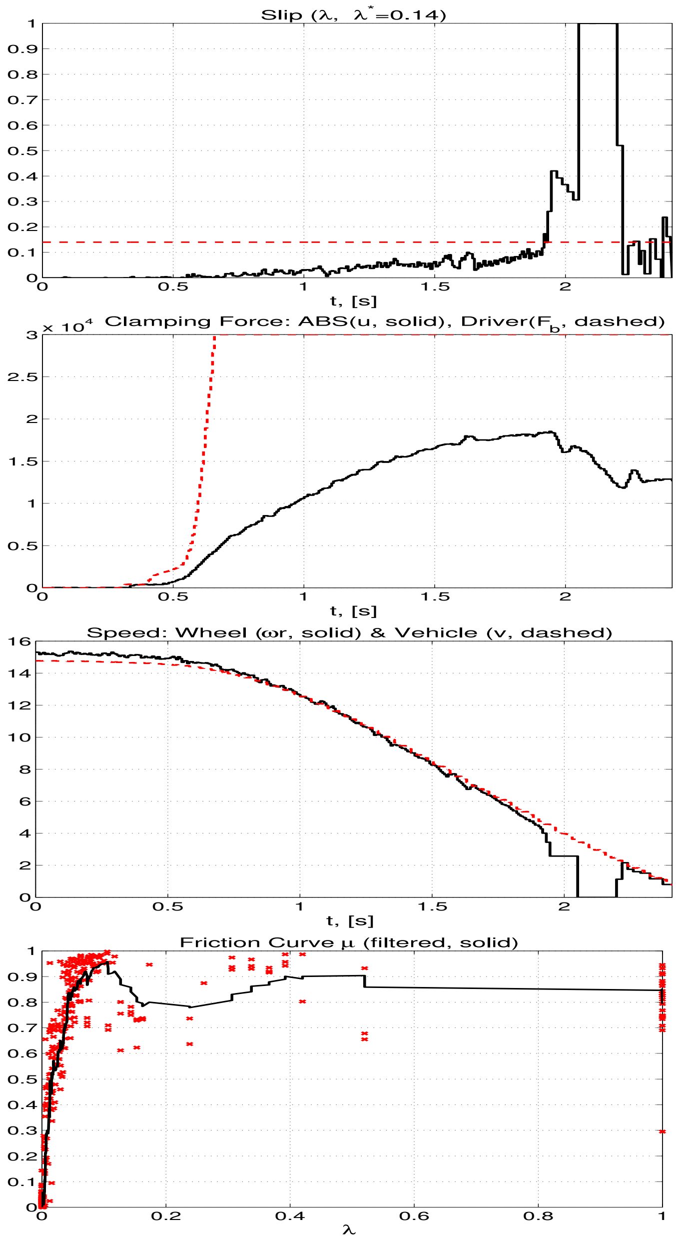

Figure 6.14: Turning, front left wheel

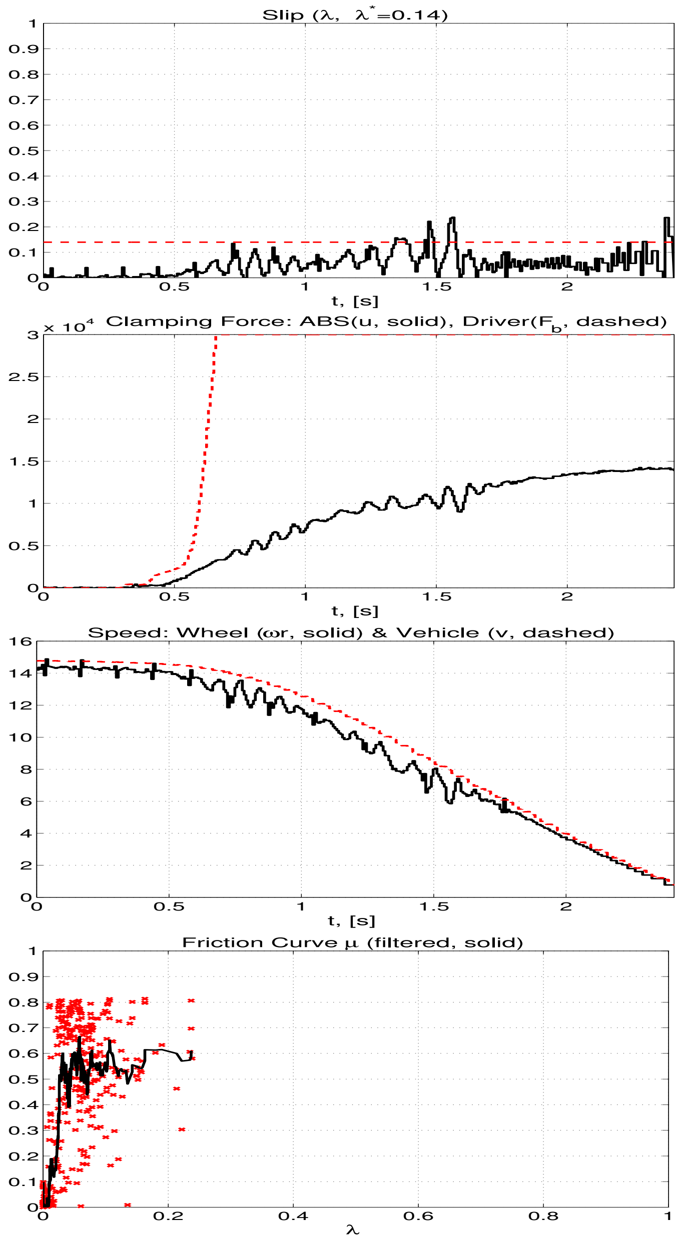

Figure 6.15: Turning, front right wheel

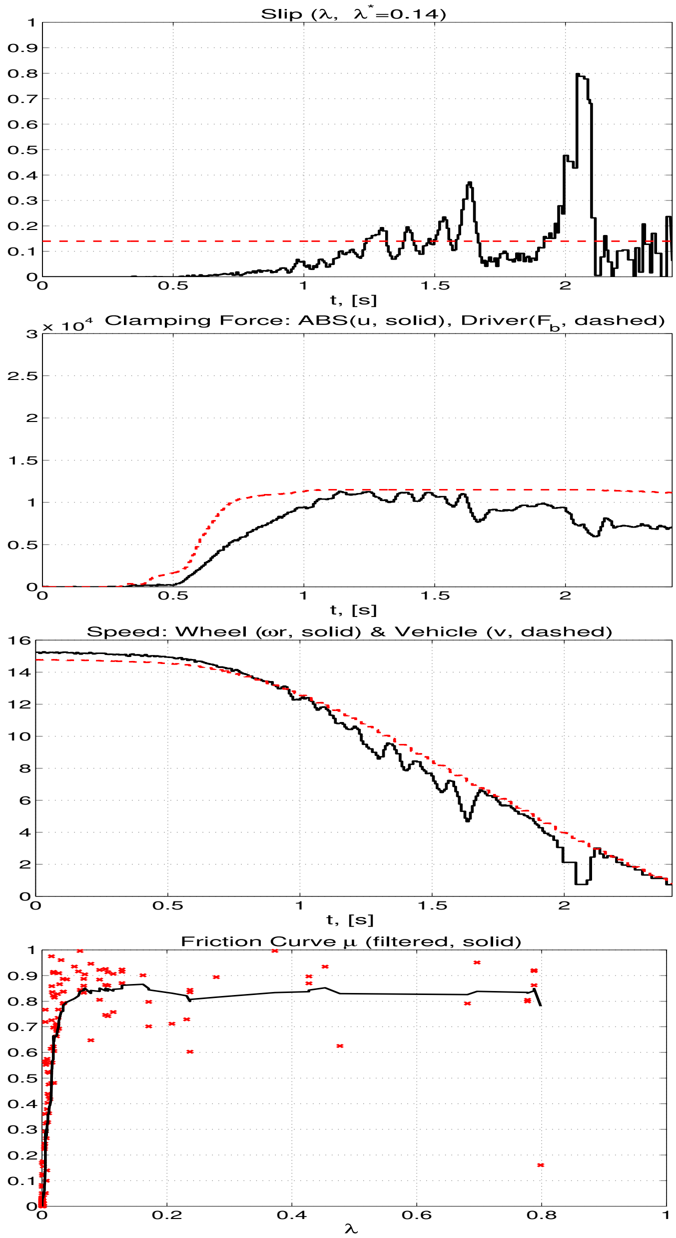

Figure 6.16: Turning, rear left wheel

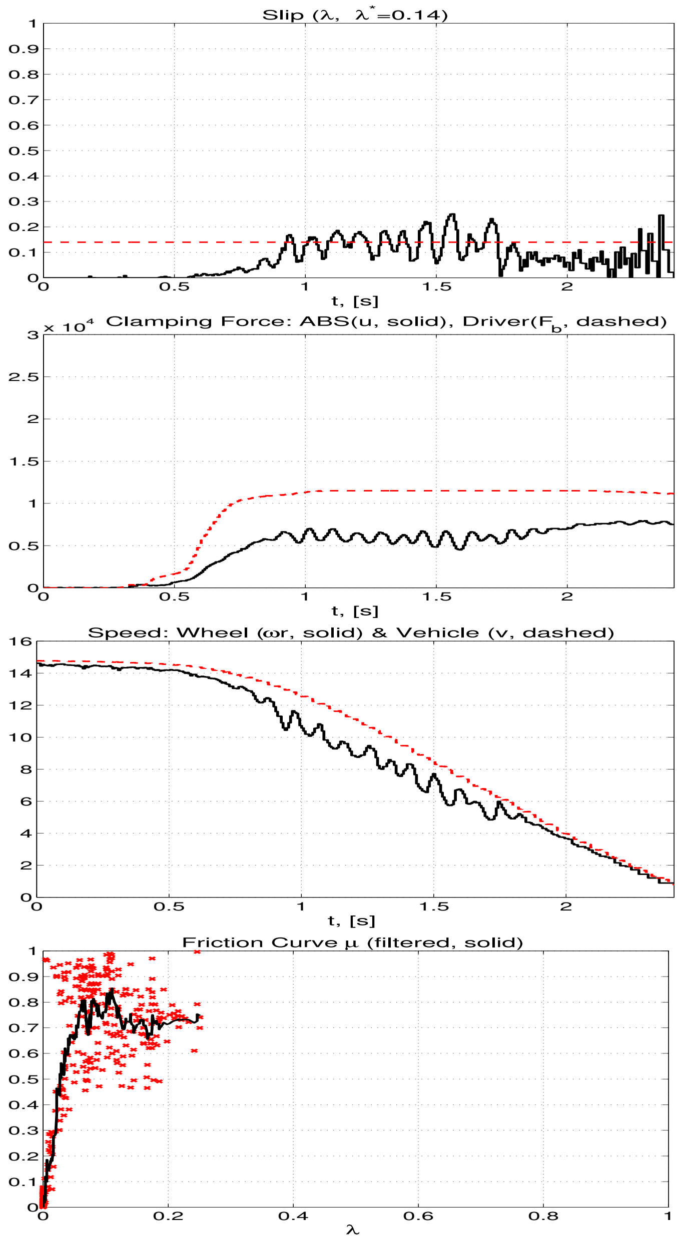

Figure 6.17: Turning, rear right wheel

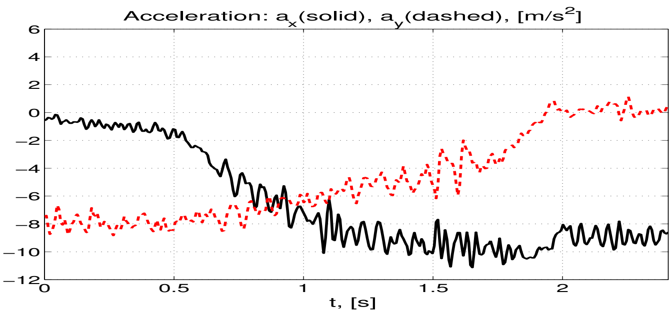

Figure 6.18: Turning, car

lateral acceleration confirms together with the slip that the vehicle is steerable during the manoeuvre. The lateral acceleration a_y decreases steadily until it reaches zero at $t = 1.9s$ and remains at zero until the vehicle comes to a standstill at approximately $t \approx 2.5s$.

6.8.3 Deceleration of vehicle

Figure 6.18 shows the vehicle reaching a deceleration of $8 - 10m/s^2$ and is maintained $0.5s$ after braking commences.

6.8.4 Friction estimate

The friction curve plots for the two front and the two rear wheels are shown in Figures 6.14-6.17, respectively. The theory for calculating the friction curve (see Section 3.2.1) for braking while turning requires that the vehicle side slip angle, the wheel turn angle and the vehicle yaw rate are known. As the vehicle side slip angle is not known, only the longitudinal friction can be calculated and the friction curve is therefore only an approximation. The friction peak, $\mu_H = 0.9$, occurs for $\lambda = 0.05 - 0.2$.

6.8.5 Controller performance

The controller transient response is very slow as the clamping force does not increase fast enough (for all the wheels). Consequently, the slip is too low and the resulting friction force is too low for the whole braking period leading to an unnecessarily large braking distance. This is principally due to the significant model inaccuracy occurring for side slips where $\alpha > 0$ and small λ. Notice that the linearization underlying the control design is done with the side slip $\alpha = 0$, cf. Figure 3.2.

6.9 Dry asphalt, controller initialization

This first redesign idea is based on the fact that the initial state of the controller will play an important role in the initial transient, see Section 5.7.1. For the dry asphalt experiment shown in Figures 6.19-6.21, the slip setpoint is $\lambda^* = 0.11$ and the initial speed is $v(0) = 30m/s$.

6.9.1 Slip

The front wheel slip peak, $\lambda = 0.7$, is at $t = 1.2s$ when the wheel slip controller is activated. For the rear wheel, the slip peak value $\lambda \approx 0.2$

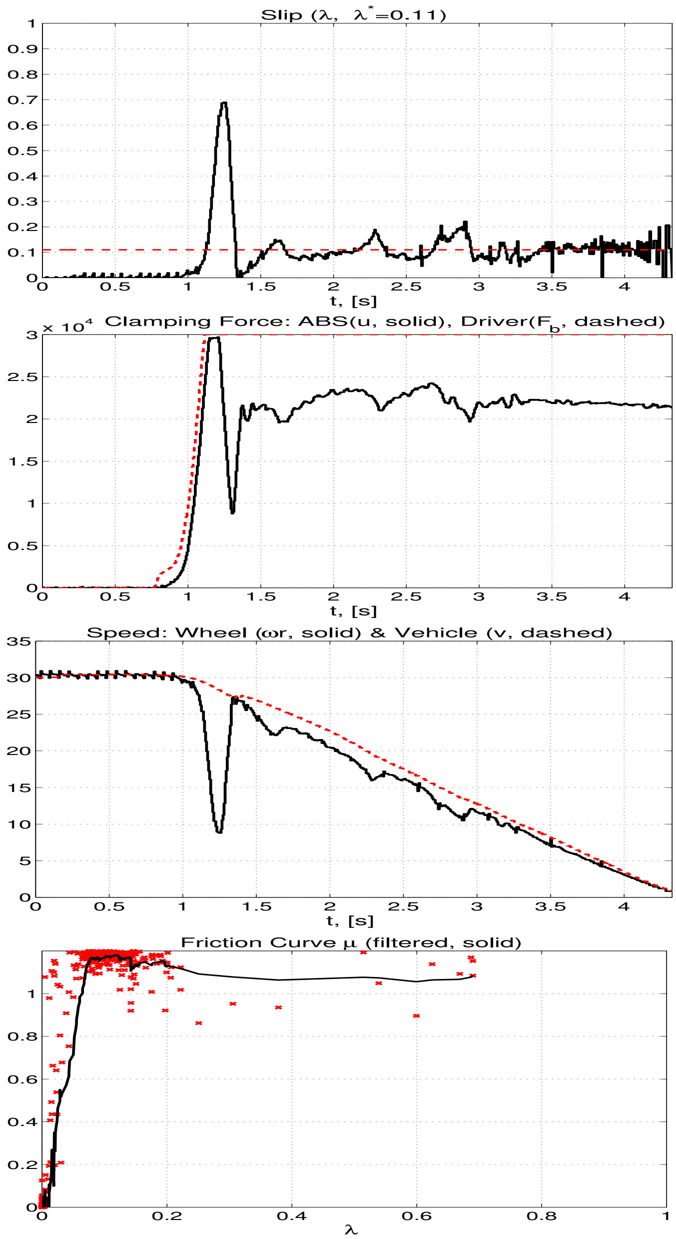

Figure 6.19: Controller initialization, front right wheel

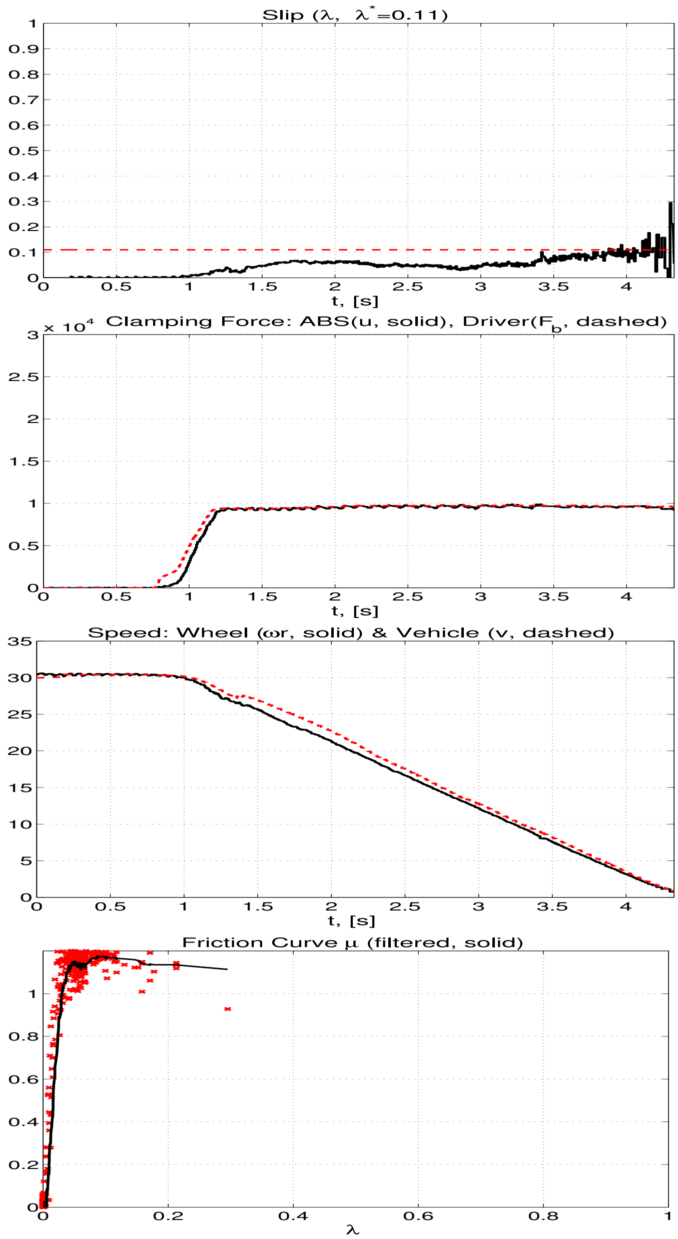

Figure 6.20: Controller initialization, rear right wheel

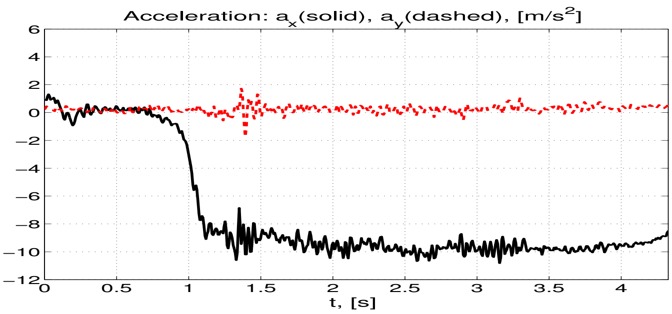

Figure 6.21: Controller initialization, car

occurs at low velocity, where the slip dynamics are more sensitive.

6.9.2 Lateral stability

The lateral acceleration shown in Figure 6.21 is negligible.

6.9.3 Deceleration of vehicle

Deceleration is between $8 - 10m/s^2$, see Figure 6.21, and is maintained $0.5s$ after braking commences.

6.9.4 Friction estimate

The friction curve plots for both the front and the rear wheels are shown in Figures 6.19 and 6.20, respectively. The figures's shape resemble the dry asphalt friction plot in Figure 3.2 for $\mu_H \approx 0.9$. The friction peak occurs for $\lambda = 0.1$ and with a value of $\mu \approx 1.2$.

6.9.5 Controller performance

When the wheel slip controller is activated, the initial state of the integrator $x_1(0)$ is set to a value that corresponds to the nominal steady-state clamping torque typically experienced on dry asphalt. Notice that the initial transient is significantly improved, but with an overshoot that might be eliminated by more accurate initialization (along the ideas in (Kalkkuhl, Johansen, Lüdemann, and Queda 2001; Kalkkuhl, Johansen, and Lüdemann 2002)). Note that since the experiment was conducted on dry asphalt with a high slip setpoint, the rear wheel brake torques saturate throughout the braking period without achieving the specified slip setpoint. Thus, the performance of the controller for the rear wheel cannot be evaluated.

6.10 Dry asphalt, off-equilibrium design

The second redesign idea is based on the concept of off-equilibrium linearization and design in gain scheduled control (see Section 5.7.2).

Figures 6.22-6.24 show experimental results with braking on dry asphalt with a modified controller to improve the initial response. The initial speed is $v(0) = 30m/s$ and the slip setpoint is $\lambda^* = 0.11$.

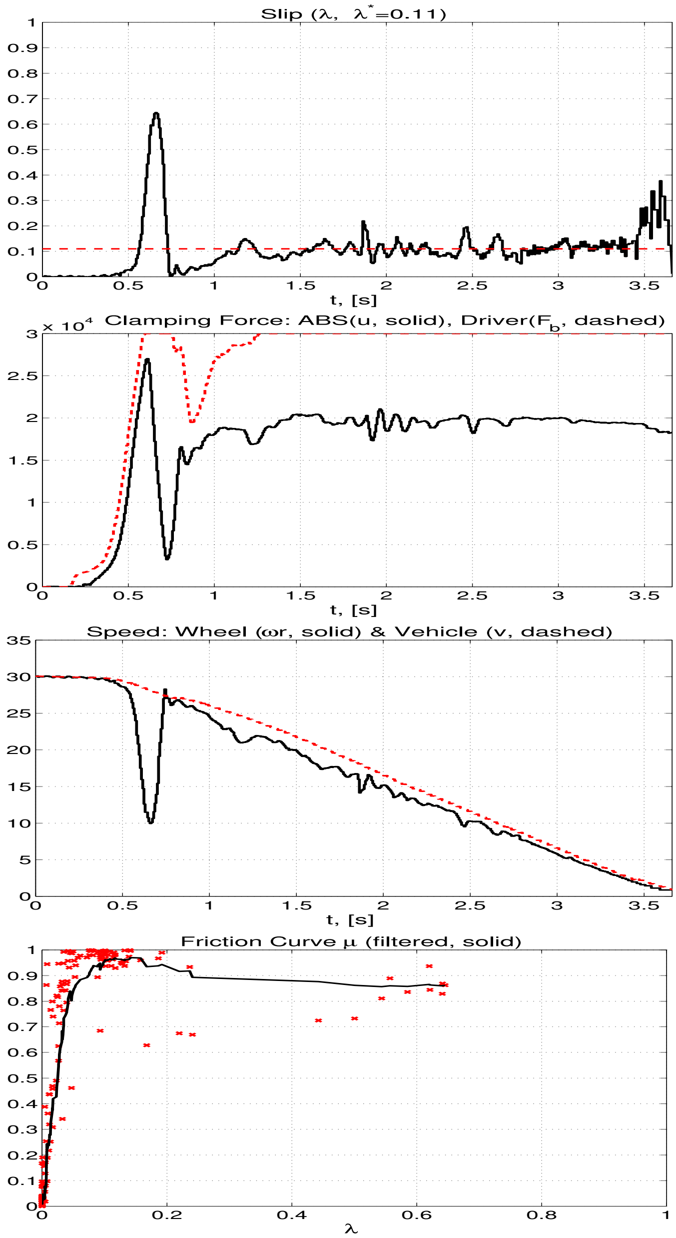

Figure 6.22: Off-equilibrium design, front left wheel

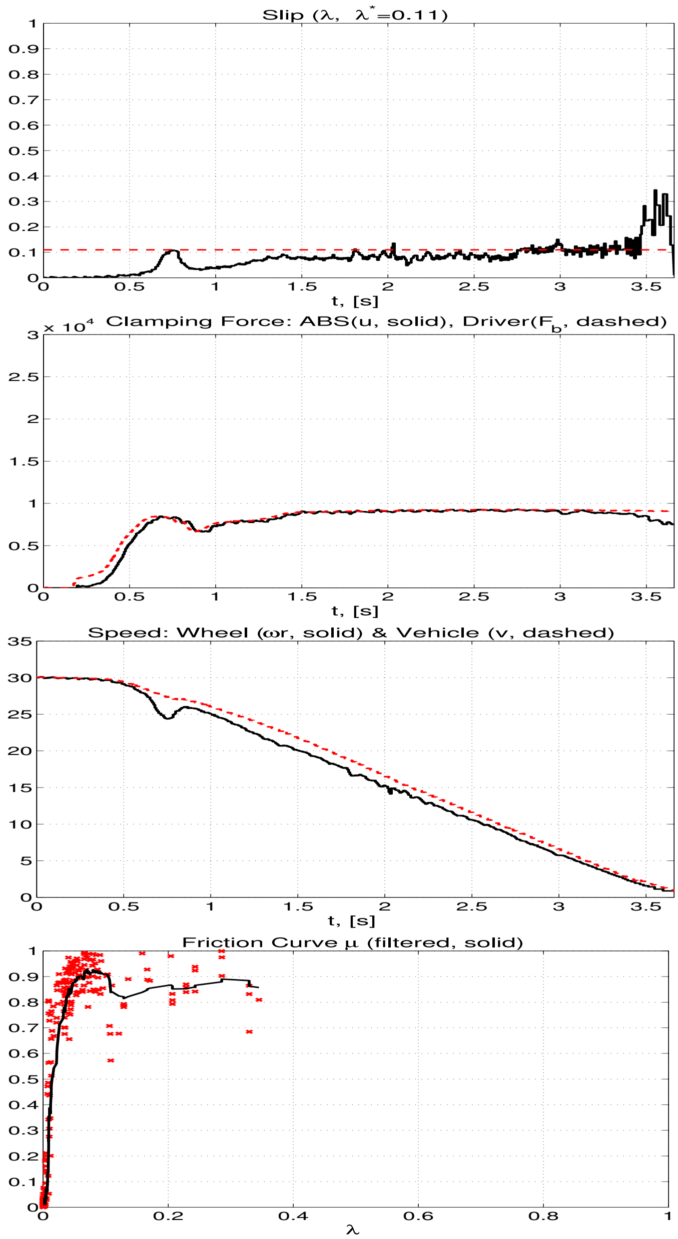

Figure 6.23: Off-equilibrium design, rear right wheel

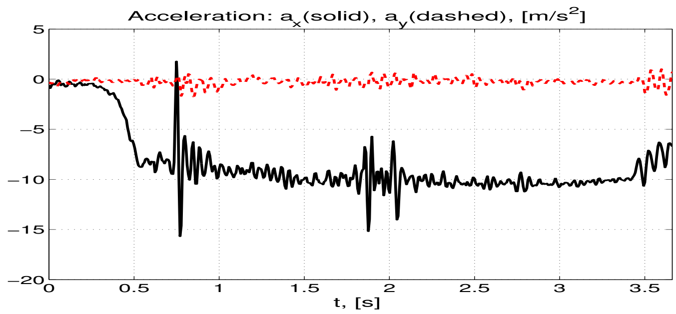

Figure 6.24: Off-equilibrium design, car

6.10.1 Slip

The front wheel slip peak, $\lambda = 0.65$, is at $t = 0.7s$. For the rear wheel, the slip peak value $\lambda \approx 0.35$ occurs at low velocity, where the slip dynamics are more sensitive.

6.10.2 Lateral stability

The lateral acceleration shown in Figure 6.24 is negligible.

6.10.3 Deceleration of vehicle

Deceleration reaches $8 - 10m/s^2$ $0.3s$ after braking commences, see Figure 6.24, and this is then maintained.

6.10.4 Friction estimate

The friction curve plots for the front and the rear wheels are shown respectively in Figures 6.22 and 6.23. The figures resemble the dry asphalt friction plot in Figure 3.2 for $\mu_H \approx 0.9$. The friction peak occurs for $\lambda = 0.1$ and with a value of $\mu = 0.95$.

6.10.5 Controller performance

As a result of the modification of the controller during transients at low wheel slip values, it appears that the setpoint is reached more rapidly. The controller switches to new gain matrices when the wheel slip λ is lower than a given threshold, namely $0.6\lambda^*$. Since the nominal $\hat{\lambda}$ is now on the steep part on the left side of the friction curve peak, this leads to a higher gain than near equilibria. As a result, the transients are speeded up and the overall performance is improved. Again, there is some initial overshoot, which could be reduced by fine-tuning the switching thresholds and the off-equilibrium control design.

It should be noticed that the driver eases the brake pedal at $t = 0.9s$. This affects only the performance of the rear wheel, see Figure 6.23.

6.11 Experimental problems

Rear wheel hardware problems occurred in experiments 1 and 3 (Sections 6.3 and 6.5), and no log-data was produced. Thus, for the experiments no.1 and 3, there are no figures showing the performance of the rear wheel controllers. In general, the performances achieved for the rear wheel slip controllers were better than those achieved for the front.

In experiment no.6 (Section 6.8) the speed figure for the front right wheel (see Figure 6.15), has a wheel speed noise (spikes) equivalent to 6% of the vehicle speed for $t < 0.6s$.

In experiment no.7 (Section 6.9), the friction curve plots shown in Figures 6.19 and 6.20, indicate an error in the logged values (or in the model) as the estimated friction curves have a positive offset of ≈ 0.3 versus the values experienced on other dry asphalt tests.

Chapter 7

Conclusions

In this thesis, several topics within control design and robustness, and stability analysis of a model-based wheel slip controller, together with a detailed experimental evaluation using a test vehicle have been addressed. The overall goal has been to investigate robustness through analysis and experiments using a recently developed controller design theory - explicit sub-optimal linear quadratic regulation with state and input constraints. Using Lyapunov theory, frequency analysis and experimental verifications, performance and robustness of a gain scheduled nonlinear wheel slip controller for a vehicle equipped with electromechanical brakes has been studied.

Despite the fact that the wheel slip dynamics are highly nonlinear, the control design relies on local linearization and gain scheduling. A control system containing just the slip dynamics is shown to be uniformly exponentially stable with a large region of attraction using Lyapunov theory. Since this controller cannot be implemented without significant loss of performance due to the dependency of the knowledge of the friction coefficient, a second control system including integral action (to eliminate steady-state friction uncertainties) is shown to be locally uniformly exponentially stable using Lyapunov theory and robust to the uncertain road/tyre friction. A third control system is then studied, also including an actuator model. A parameter-dependent Lyapunov function for the nominal linear parameter varying closed loop system is found by solving a linear matrix inequality (LMI) problem. This function is investigated for robustness with respect to uncertainty in the road/tyre friction characteristic. Unfortunately, the LMI approach does not allow a rigorous conclusion, except local stability, since the Lyapunov-function candidate at hand appears to be conservative. However, the analysis indicates that the observations agree well with the experience from simulations and experiments.

The fundamental limitations of performance are the TTP communication delay, the actuator dynamics (both which introduce phase losses) and the choice of open loop unstable slip setpoints. These limitations are analyzed using classical frequency analysis based on a linearized model. It is shown that high performance is obtained if the slip setpoint is chosen near the friction peak. For high friction, loss of stability will occur if slip setpoint is chosen too high or loss of performance if the slip setpoint is chosen too low. The communication delay will be reduced in the future as future systems may be using FlexRay, a communication protocol with a higher sampling rate than the TTP used in the test vehicle in this project. It should also be noted that the extended Kalman filter introduces estimator errors that may strongly influence the performance.

The experiments using a test vehicle show an accurate regulation of the wheel slip is feasible for a range of desired setpoints under a wide range of road conditions. A test scenario where braking in a turn is performed yields unsatisfactory performance as the model is linearized for straight-line braking. Although the design and experiments have been carried out for a vehicle with drive-by-wire system, the main ideas are believed to be suitable for conventional hydraulic and electro-hydraulic brakes actuators, and their sensory systems. Slip peaking, which occurs in production cars equipped with conventional ABS systems, reduces the driving comfort significantly. The model-based approach presented in this thesis, is more comfortable, yields better performance and does not rely on strong knowledge of the tyre/road friction curve. Moreover, a highly beneficial feature of this model-based design approach is the modest time taken to design and tune the wheel slip controller. The approach is also modular as the wheel slip controller can be combined with different estimation algorithms, actuators and supervisory control systems. Nevertheless, do note that conventional ABS systems are very robust.

Results from (Lüdemann 2002) for the controller designs used in the H_2C project show that the controller performances converge. This again indicates that the LQRC control design used in this thesis yields similar performance as the PI controller used by (Lüdemann 2002; Solyom and Rantzer 2002; Wang, Schmitt-Hartmann, Schinkel, and Hunt 2001).

The experimental results and the respective test scenarios presented in this thesis were not duplicated so as to analyze repeatability, due to limited access to the test vehicle, as the LQRC wheel slip controller therefore could not be optimally tuned. But, there are no foreseen problems causing non-repeatability.

As there is room for further improvements and extensions of the wheel slip control approach, a summary for future works is given in the following section.

7.1 Future works

The issues of interest listed for future works below contain both theoretical and practical aspects. The model used in this thesis for controller design is implemented and tested in a test vehicle. Since the H_2C project was aimed at developing an ABS controller for a prototype electro-mechanical wheel brake, a reduced and simplified test procedure was chosen as the controllers were not intended for production vehicles. To fully validate the proposed controllers, a more extended test program is needed, with both sufficient access to the test vehicle and more test scenarios as specified in some ISO and SAE documents (see Chapter 6). A list of topics for further research is listed below.

i. The control design presented in this thesis is only focused on longitudinal slip. It is the belief of the author that the slip control design can easily be extended for control problems such as lateral (side-slip) and yaw control cases, e.g. ESP. A similar problem that should be addressed is split-friction-coefficient surfaces.

ii. Unmodelled dynamics such as pitching and suspension should be taken more directly into account in the control design to improve the controller performance. Further, unmodelled dynamics such as brake interaction through the chassis should also be considered.

iii. An analytical analysis of a gain scheduled LQ using Lyapunov/LMI for the slip model including the actuator dynamics should be sought, although this has been tried unsuccessfully by the author due to the complex solution.

iv. Performance improvements expected when braking in a turn, with gain scheduling applied on side-slip α. Further, gain scheduling on the friction coefficient (μ_H) between tyre and road should yield significant reductions in the slip and clamping force transients on inhomogeneous surfaces.

v. To improve the initial controller performance for high friction surfaces (i.e. dry asphalt), a more accurate initialization strategy similar to what was done in (Kalkkuhl, Johansen, Lüdemann, and Queda 2001; Kalkkuhl, Johansen, and Lüdemann 2002; Lüdemann 2002) should be implemented.

vi. There is room for improved performance with tuning, especially for the off-equilibrium design.

vii. With faster CPU (BBWM) and more memory, a more refined gain scheduling should be possible.

Bibliography

Anderson, B. D. O. and J. B. Moore (1989). *Optimal control : linear quadratic methods*. Prentice-Hall.

Åström, K. J. and B. Wittenmark (1997). *Computer Controlled Systems: theory and design* (Third ed.). Prentice-Hall.

Bakker, E., L. Nyborg, and H. B. Pacejka (1987). Tyre modelling for Use in Vehicle Dynamic Studies. Technical Report 870421, Society of Automotive Engineers, Warrendale PA.

Bemporad, A., K. Fukuda, and F. D. Torrisi (2001). Convexity recognition of the union of polyhedra. *Computational Gemometry 18*, 141–154.

Bemporad, A., M. Morari, V. Dua, and E. Pistikopoulos (2000). The explicit solution of model predictive control via multiparametric quadratic programming. In *Proc. American Contr. Conf., Chicago*, Volume 2, pp. 872–876.

Bemporad, A., M. Morari, V. Dua, and E. N. Pistikopoulos (2002). The explicit linear quadratic regulator for constrained systems. *Automatica 38*, 3–20.

Boyd, S., V. Balakrishnan, E. Feron, and L. E. Ghaoui (1993). Control system analysis and synthesis via linear matrix inequalities. In *American Autom. Control Council*, Volume 2, Evanston, pp. 2147–2154.

Branicky, M. S., T. A. Johansen, I. Petersen, and E. Frazzoli (2000). Online techniques for behavioral programming. In *Proc. 39th IEEE Conf. on Decision and Control, Sydney*, Volume 2, pp. 1840–5.

Burckhardt, M. (1993). *Fahrwerktechnik: Radschlupf-Regelsysteme*. Würzburg: Vogel Verlag.

Canudas de Wit, C., R. Horowitz, and P.Tsiotras (1999). Model-based observers for Tire/Road contact friction prediction. In H. Nijmeijer and T. Fossen (Eds.), *New Directions in Nonlinear Observer Design*, pp. 23–42. Springer-Verlag.

Canudas de Wit, C., H. Olsson, K. J. Åström, and P. Lischinsky (1995). A new model for control of systems with friction. *IEEE Trans. Automatic Control 40*, 419–425.

Chisci, L. (1999). Fast algorithm for constrained infinte horizon LQ problem. *International Journal Control 72*, 1020–1026.

Chmielewski, D. and V. Manousiouthakis (1996). On constrained infinite-time linear quadratic optimal control. *System and Control Letters 29*, 121–129.

Choi, S. and D.-W. Cho (1998). Control of wheel slip ratio using sliding mode controller with pulse width modulation. In *Proceedings of the 4th International Symposium on Advanced Vehicle Control*, Nagoja, Japan, pp. 629–635. Society of Automotive Engineers.

Council (1971). On the approximation of the laws of the member states relating to the braking devices of certain categories of motor vehicles and of their trailers. Council Directive 1971/320/EEC, EEC.

Daiß, A. and U. Kiencke (1996). Estimation of tyre slip during combined cornering and braking observer supported fuzzy estimation. In *13th Triennal World Congress*, San Francisco, pp. 41–46.

Delphi (2002). X-by-wire. Technical report. http://www.delphi.com/automotive/nextech/products/xbywire.

Dixon, J. C. (1996). *Tires, Suspension and Handling.* Würzburg: Arnold.

Drakunov, S., Ü. Özgüner, P. Dix, and B. Ashrafi (1995). ABS control using optimum search via sliding modes. *IEEE Trans. Control Systems Technology 3*(1), 79–85.

Fajdiga, M. and N. Janičijevič (1992). A hybrid driving and braking system with wheel slip control. In *24th FISITA Congress, Total Vehicle Dynamics*, Volume 2, London, UK., pp. 1–6. The Institution of Mechanical Engineeres.

Flemming, W. J. (2001). Overview of Automotive Sensors. *IEEE Sensors Journal 1*(4), 296–308.

FlexRay (2002). Requirements specification v.2.0.2. Technical report. http://www.flexray.com/htm/pdfs/FlexRay_ReqSpec_2_0_2-final-web.pdf.

Freeman, R. (1995). Robust slip control for a single wheel. Research Report CCEC 95-0403, University of California, Santa Barbara.

Gahinet, P., P. Apkarian, and M. Chilali (1996). Affine parameter-dependent Lyapunov function and real parametric uncertainty. *IEEE Trans. Automatic Control 41*, 436–442.

Gillespie, T. D. (1992). *Fundamentals of vehicle dynamics.* Society of Automotive Engineers.

Gustafsson, F. (1997). Slip-based tire-road friction estimation. *Automatica 33*, 1087–1099.

Hattwig, P. (1993). Synthesis of abs hydraulic systems. Technical Report 930509, Society of Automotive Engineers, Warrendale PA.

Hedenetz, B. and R. Belschner (1998). Brake-by-wire without mechanical backup using a TTP communication network. In *SAE International Congress and Exhibition, Detroit.* SAE 981109.

Hedlund, S. and M. Johansson (1999, March). Pwltool - A MATLAB toolbox for analysis of piecewise linear systems. Technical Report LUTFD2/TFRT-7582-SE, Automatic Control Department, Lund Institute of Technology, Sweden.

Hunter, J. E. (1998). Reconstructing collisions involving ice and slippery surfaces. *The Source, The Society of Accident Reconstructionists* (Winter).

Isermann, R., R. Schwarz, and S. Stölzl (2002). Fault-tolerant drive-by-wire systems. *IEEE Control Systems Magazine 22*, 64–81.

ISO (1991). Road vehicles - hydraulic braking systems - measurement of braking performance. Technical Report 6597, International Organization for Standardization.

ISO (1995). Road vehicles - motor vehicles with anti-lock braking system - measurement of braking performance. Technical Report 11835, International Organization for Standardization.

ISO (1996). Passenger cars - braking in turn - open-loop test procedure. Technical Report 7975, International Organization for Standardization.

ISO (1999). Passenger cars - test track for a severe land-change manoeuvre. Technical Report 3888-1, International Organization for Standardization.

Jiang, F. (2000). *A novel approach to a class of antilock brake problems.* Ph. D. thesis, Cleveland State University.

Johansen, T. A., K. J. Hunt, P. J. Gawthrop, and H.Fritz (1998). Off-equilibrium linearisation and design of gain scheduled control with application to vehicle speed control. *Control Engineering Practice 6*, 167–180.

Johansen, T. A., J. Kalkkuhl, J. Lüdemann, and I. Petersen (2001). Hybrid control strategies in ABS. In *Proc. American Contr. Conf., Arlington*, Volume 2, pp. 1704–1705.

Johansen, T. A. and I. Petersen (2001). LQRC software user's guide. Technical Report STF72 F01309, SINTEF Electronics and Cybernetics, Trondheim, Norway.

Johansen, T. A., I. Petersen, J. Kalkkuhl, and J. Lüdemann (2003). Gain-scheduled wheel slip control in automotive brake systems. *Accepted for publication: IEEE Trans. on Control System Technology*.

Johansen, T. A., I. Petersen, and O. Slupphaug (2000a). Explicit suboptimal linear quadratic regulation with state and input constraints. In *Proc. 39th IEEE Conf. on Decision and Control, Sydney*, Volume 1, pp. 662–667.

Johansen, T. A., I. Petersen, and O. Slupphaug (2000b). Explicit suboptimal linear quadratic regulation with state and input constraints. Technical Report STF72-A00303, SINTEF.

Johansen, T. A., I. Petersen, and O. Slupphaug (2002). Explicit subopitmal linear quadratic regulation with input and state constraints. *Automatica* (38), 1099–1111.

Johansson, M. and A. Rantzer (1998). Computation of piecewise quadratic lyapunov functions for hybrid systems. *IEEE Trans. Automatic Control 4*, 555–559.

Jun, C. (1998). The study of ABS control system with different control methods. In *Proceedings of the 4th International Symposium on Advanced Vehicle Control*, Nagoja, Japan, pp. 623–628.

Kalkkuhl, J., T. A. Johansen, and J. Lüdemann (2002). Improved transient performance of nonlinear adaptive backstepping using estimator resetting based on multiple models. *IEEE Trans. Automatic Control 47*, 136–140.

Kalkkuhl, J., T. A. Johansen, J. Lüdemann, and A. Queda (2001). Nonlinear adaptive backstepping with estimator resetting using multiple observers. In *Proc. of the Hybrid Systems, Computation and Control, Rome*, pp. 319–332.

Kaminer, I., A. M. Pascoal, P. P. Khargonekar, and E. E. Coleman (1995). A velocity algorithm for the implementation of gain-scheduled controllers. *Automatica 31*, 1185–1191.

Kawabe, T., M. Nakazawa, I. Notsu, and Y. Watanabe (1997). A sliding mode controller for wheel slip ratio control system. *Vehicle system dynamic* (27), 393–408.

Khalil, H. K. (1996). *Nonlinear Systems*. Prentice Hall.

Kiencke, U. and L. Nielsen (2000). *Automotive Control Systems*. Springer-Verlag.

Kopetz, H. and G. Grünsteidl (1994). TTP - A protocol for fault-tolerant real-time systems. *IEEE Computer* (27(1)), 14–23.

Korf, R. E. (1990). Real-time heuristic search. *Artificial Intelligence*, 189–211.

Krstić, M., I. Kanellakopoulos, and P. Kokotović (1995). *Nonlinear Adaptive Control Design*. John Wiley & Sons Inc.

Laprie, J. C. (1995). *Predictably Dependable Computing Systems*, Chapter II, Dependability - Its Attributes, Impairments and Means, pp. 27–40. New York: Springer-Verlag.

Leen, G. and D. Heffernan (2002). Expanding automotive electronic systems. *Computer* (1), 88–93.

Leith, D. J. and W. E. Leithead (1996). Appropriate realization of gain-scheduled controllers with application to wind turbine regulation. *Int. J. Control 65*, 223–248.

Liu, Y. and J. Sun (1995). Target slip tracking using gain-scheduling for braking systems. In *American Control Conference*, Seatle, pp. 1178–82.

Lüdemann, J. (2002). *Heterogeneous and Hybrid Control with Application in Automotive Systems*. Ph. D. thesis, Glasgow University.

Maier, M. and K. Müller (1995). ABS5.3: The new and compact ABS5 unit for passenger cars. Technical Report 930757, Society of Automotive Engineers, Warrendale PA.

Maisch, W., W.-D. Mergenthaler, and A. Sigi (1993). ABS5 and ASR5: The new abs/asr family to optimize directional stability and traction.

Technical Report 930505, Society of Automotive Engineers, Warrendale PA.

Mastinu, G. (1988). Passive automobile suspension parameter adaptation. In *Advanced suspensions : international conference, London*, pp. 51–55.

Pacejka, H. B. and R. S. Sharp (1991). Shear force developments by pneumatic tyres in steady-state conditions: A review of modeling aspects. *Vehicle Systems Dynamics 29*, 409–422.

Petersen, I., T. A. Johansen, J. Kalkkuhl, and J. Lüdemann (2001). Wheel slip control in ABS brakes using gain scheduled constrained LQR. In *Proc. European Contr. Conf., Porto*, pp. 606–611.

Petersen, I., T. A. Johansen, J. Kalkkuhl, and J. Lüdemann (2002). Wheel slip control in ABS brakes using gain scheduled constrained LQR. In R. Johansson and A. Rantzer (Eds.), *Nonlinear and Hybrid Control in Automotive Applications*, pp. 125–146. Springer-Verlag.

Petersen, I., T. A. Johansen, J. Kalkkuhl, and J. Lüdemann (2003). Wheel slip control using gain-scheduled LQ - LPV/LMI analysis and experimental results. In *Proc. European Contr. Conf., Cambridge*. Accepted for publication.

Rantzer, A. and M. Johansson (2000). Piecewise linear quadratic optimal control. *IEEE Trans. Automatic Control 45*, 629–637.

Rawlings, J. B. and K. Muske (1993). The stability of constrained receding horizon control. *IEEE Trans. Automatic Control 38*, 1512–1516.

SAE (1992). Anti-lock brake system review. Technical Report J2246, Society of Automotive Engineers, Warrendale PA.

SAE (1993). Class c application requirement considerations. Technical Report J2056/1, Society of Automotive Engineers, Warrendale PA.

SAE (1993 (1973)). Wheel-slip brake-control system road test code. Technical Report J46, Society of Automotive Engineers, Warrendale PA.

Schinkel, M. and K. Hunt (2002). Anti-lock braking control using a sliding mode like approach. In *Proc. American Contr. Conf., Anchorage*, Volume 3, pp. 2386–2391.

Schwarz, R. (1999). *Rekonstruktion der Bremskraft Bei Fahrzeugen mit Elektromechanisch Betätigten Radbremsen*. Ph. D. thesis, Institut für Automatisierungstechnik der TU Darmstadt.

Seron, M., J. A. D. Dona, and G. C. Goodwin (2000). Global analytical model predictive control with input constraints. In *Proc. IEEE Conf. Decision and Control, Sydney*, pp. TuA05–2.

Slotine, J.-J. E. (1984). Sliding controller design for non-linear systems. *Int. J. Control 40*, 421–434.

Solyom, S. and A. Rantzer (2002). Nonlinear and Hybrid Control in Automotive Applications. Chapter ABS Control - A Design Model and Control Structure, pp. 85–96. Springer-Verlag.

Sontag, E. D. (1989). A "universal" construction of Artstein's theorem on nonlinear stabilization. *Systems and Control Letters 13*, 117–123.

Sontag, E. D. (1998). *Mathematical Control Theory.* Springer-Verlag.

Sznaier, M. and M. J. Damborg (1987). Suboptimal control of linear systems with state and control inequality constraints. In *Proc. 26th IEEE Conf. on Decision and Control, Los Angles*, pp. 761–762.

Sznaier, M. and M. J. Damborg (1990). Heuristically enhanced feedback control of constrained discrete-time linear systems. *Automatica 26*, 521–532.

Taheri, S. and E. Law (1991). Slip control braking of an automobile during combined braking and steering manoeuvres. In *Advanced Automotive Technologies*, Volume 40, pp. 209–227. ASME.

Tøndel, P., T. A. Johansen, and A. Bemporad (2001). An algorithm for multi-parametric quadratic programming and explicit MPC solutions. In *Proc. IEEE Conf. Decision and Control, Orlando*, pp. TuP11–4.

Tøndel, P., T. A. Johansen, and A. Bemporad (2003a). An algorithm for multi-parametric quadratic programming and explicit MPC solutions. *39*(3), 489–497.

Tøndel, P., T. A. Johansen, and A. Bemporad (2003b). Computation of piecewise affine control via binary search tree. *39*, 945–950.

Tsiotras, P. and C. Canudas de Wit (2000). On the optimal braking of wheeled vehicles. In *Proc. American Contr. Conf., Chicago*, Volume 1, pp. 569–573.

Wang, Y., T. Schmitt-Hartmann, M. Schinkel, and K. J. Hunt (2001). A new approach to simultanious stabilisation and strong simultanious stabilisation with d stability and its application to abs control systems design. In *Proc. European Contr. Conf., Porto*, pp. 612–617.

Wellstead, P. E. and N. Pettit (1997). Analysis and redesign of an antilock brake system controller. In *IEE Proceedings of Control Theory Application*, Volume 144, pp. 413–426. IEE.

Wredenhagen, G. F. and P. R. Belanger (1994). Piecewise-linear LQ control for systems with input constraints. *Automatica 30*, 403–416.

Wu, M. C. and M. C. Shih (2001). Hydraulic anti-lock braking control using the hybrid sliding-mode pulse width modulation pressure control method. *Proc. Instn. Mech. Engrs. 215*, 177–187.

Yi, J., L. Alvarez, and R. Horowitz (2002). Adaptive emergency braking control with underestimation of friction coefficient. *IEEE Trans. Control Systems Technology 10*, 381–392.

Yi, J., L. Alvarez, R. Horowitz, and C. Canudas de Wit (2000). Adaptive emergency braking control using a dynamical Tire/Road friction model. In *Proc. 39th IEEE Conf. on Decision and Control, Sydney*, Volume 1, pp. 456–461.

Yu, J. S. (1997). A robust adaptive wheel-slip controller for antilock brake system. In *Proc. 36th IEEE Conf. on Decision and Control, San Diego*, Volume 3, pp. 2545–2546.

Zheng, A. and M. Morari (1995). Stability of model predictive control with mixed constraints. *IEEE Trans. Automatic Control 60*, 1818–1823.

Appendix A

Explicit Sub-optimal Linear Quadratic Regulation with State and Input Constraints

This appendix is a reprint of the paper (Johansen, Petersen, and Slupphaug 2002).

A.1 Introduction

Consider the linear time-invariant system

$$x(t+1) = Ax(t) + Bu(t) \tag{A.1}$$

where $x \in R^n$, and $u \in R^r$. The constrained LQ feedback controller minimizes the infinite horizon quadratic cost

$$J(u(t), u(t+1), ...; x(t)) = \sum_{\tau=t}^{\infty} l_{QR}(x(\tau), u(\tau)) \tag{A.2}$$

$$l_{QR}(x, u) = x^T Q x + u^T R u \tag{A.3}$$

subject to the linear constraints

$$Gx(\tau+1) \leq g \tag{A.4}$$

$$Hu(\tau) \leq h \tag{A.5}$$

for all $\tau \geq t$, where $R > 0$, $Q \geq 0$, $G \in R^{q \times n}$, and $H \in R^{p \times r}$. It is assumed that $g > 0$ and $h > 0$ (where the inequalities are elementwise since g and h

are vectors) to ensure that the origin is an interior point in the admissible region. The *optimal cost function* is defined as

$$V(x(t)) \quad = \min_{u(t),u(t+1),...} J(u(t), u(t+1), ...; x(t)) \tag{A.6}$$

where the minimization is subject to the dynamics of the system (A.1), and the constraints (A.4)-(A.5) are imposed at every time instant $\tau \in \{t, t+1, t+2, ...\}$ on the trajectory. The cost of moving from the state $x(t)$ to the origin in an optimal manner is given by $V(x(t))$. Consider the following Hamilton-Jacobi-Bellman (HJB) equation

$$\begin{aligned} 0 \quad = \min_{\substack{u(\tau)\in R^r, Gx(\tau+1)\leq g, Hu(\tau)\leq h \\ \tau\in\{t,t+1,t+2,...,t+N-1\}}} & \Big(V(x(t+N)) - V(x(t)) \\ & + \sum_{\tau=t}^{t+N-1} l_{QR}(x(\tau), u(\tau)) \Big) \end{aligned} \tag{A.7}$$

where $N \geq 1$ is some horizon, and $V(0) = 0$. This equation characterizes the optimal cost function and optimal control action for the problem when N is so large that there are no active or violated constraints beyond this horizon, since the unconstrained LQ solution is optimal beyond the horizon, (Sznaier and Damborg 1987; Chmielewski and Manousiouthakis 1996). Under the assumptions of feasibility, non-explicit optimal solutions to the HJB (A.7) can be computed using real-time quadratic programming, where a finite-dimensional optimization problem is achieved since $V(x(t+N)) = x^T(t+N)Px(t+N)$, where P is the solution to the algebraic Riccati equation associated with the unconstrained LQR. This is an optimal approach, in contrast to common suboptimal (approximate) approaches used in model predictive control with a finite horizon cost function approximation or a finite input move horizon, e.g. (Rawlings and Muske 1993). In any case, the real-time quadratic programming imposes severe limitations on the achievable sample rate that may discourage the use of this approach in many applications.

Recently, (Bemporad, Morari, Dua, and Pistikopoulos 2000) (see also (Bemporad, Morari, Dua, and Pistikopoulos 2002) for further details) derived an optimal explicit solution to the constrained LQR problem, in the sense that no real-time quadratic program needs to be solved. The explicit controller is computed offline using multi-parametric quadratic programming. The constrained LQR problem is viewed as a quadratic program parameterized by the state x, and the multi-parametric quadratic programming approach essentially finds an explicit solution for all x within an arbitrary subset of the state space. The resulting optimal controller was proved to be a continuous piecewise linear function defined on a polyhedral partitioning of the state-space. Recently, a computationally more efficient approach to multi-parametric programming is proposed in (Tøndel, Johansen, and Bemporad 2001). Related characterizations of the piecewise linear nature of constrained LQ control are derived for some cases in (Seron, Dona, and Goodwin 2000), and other efficient but non-explicit variants of constrained LQR were suggested in (Chisci 1999; Sznaier and Damborg 1990; Wredenhagen and Belanger 1994).

In this paper (see also (Johansen, Petersen, and Slupphaug 2000a)) we also seek an explicit solution to this problem in order to reduce the demand for real-time computations. However, in order to address the restrictions imposed by real-time applications on both computer memory and processing capacity, a (possibly) suboptimal strategy is developed. Hence, we introduce a mechanism to trade performance for computational advantages. The main differences compared to (Bemporad, Morari, Dua, and Pistikopoulos 2002) are:

- Here we consider a suboptimal strategy where an approximation to the optimal cost function is utilized and we impose restrictions on the allowed switching between the active constraint sets during the prediction horizon. As a limiting case, the presented approach is equivalent to the optimal explicit LQR of (Bemporad, Morari, Dua, and Pistikopoulos 2002).

- Due to the sub-optimality of the controller, its performance is not known a priori, so one may rely on computational analysis tools which can be used to compute upper and lower bounds on suboptimal performance as well as assess stability.

- The solution strategies are different; the present approach is not based on multi-parametric quadratic programming. Both strategies leads to a piecewise linear (PWL) controller. While the exact approach leads to a continuous PWL function on a polyhedral partitioning, the suboptimal approach will not do so in all cases.

- The present approach explicitly addresses the possibility of infeasibility in the design by minimizing the constraint violation, while in the approach of (Bemporad, Morari, Dua, and Pistikopoulos 2002) a method based on slack variables is used (Zheng and Morari 1995).

- The present design approach includes practical modifications to relax high gain feedback at the boundary of the state constraints due to the choice of a short horizon.

This paper is organized as follows: In section A.2 it is shown that the HJB equation can be decomposed into two nested parts by considering the finite number of combinations of active constraint sets. It is shown in section A.3 that the solution of the innermost part of the HJB equation is an affine state feedback, when the active constraint set is given. The outer part of the HJB equation, addressed in section A.4, is to determine which constraints should be active at any current state $x(t)$. Some aspects of sub-optimality, computational complexity and real-time implementation are discussed in section A.5.

A.2 Controller decomposition

The main idea is to introduce active constraint set sequences as a formalism to decompose the HJB equation. This decomposition is discussed in this section.

A.2.1 Active constraint set sequences

A single inequality constraint $d_i^T z \geq e_i$ is said to be an *active constraint* if $d_i^T z = e_i$, where d_i is a vector, e_i is a scalar and the vector z is the design variable. Let $D^T = (d_1, d_2, ..., d_m)$ and $e^T = (e_1, e_2, ..., e_n)$. An *active constraint set* associated with some set of inequality constraints $Dz \leq e$ is the set of indices to those constraints that are active. At each sample one may impose a number of equality constraints (selected from the inequality constraints (A.4) and (A.5)) on the states and inputs that, except for degenerate cases, is less than or equal to the number of inputs r. This selection of constraints is the *active constraint set* associated with that sample. A sequence of active constraint sets imposed at each sample on the horizon finite N is called an *active constraint set sequence.*

A naive solution strategy to the optimal explicit LQR problem is simply to evaluate all feasible active constraint set sequences on a sufficiently large horizon N. This naive solution strategy to the optimal explicit LQR will indeed have offline computational disadvantages compared to the multiparametric quadratic programming approach of (Bemporad, Morari, Dua, and Pistikopoulos 2002) since the number of candidate active constraint set sequences increases very rapidly with the horizon N and the number of inputs r and states n. However, it has the advantage that it can be easily modified to determine suboptimal explicit LQR solutions with reduced offline and real-time computational demands. The main idea in the present work is to use a smaller horizon N than optimal, and in addition to reduce the flexibility in the active constraint set sequence by allowing changes in the active constraint set to be made only at a limited number of predetermined samples.

Suppose the set of indices α is associated with the active input constraints in (A.5) at some sample, and the set of indices β is associated with the active state constraints (A.4) at the same sample. Then (α, β) is an active constraint set. Next, suppose we define allowed switching times as follows: $0 = N_1 < N_2 < \cdots < N_S < N$. For example, if $S = 3$, $N_1 = 0$, $N_2 = 3$ and $N_3 = 7$ there will be 3 subintervals $\{t, t+1, t+2\}$, $\{t+3, t+4, t+5, t+6\}$, and $\{t+7, t+8, t+9\}$ with associated fixed active constraint sets $(\alpha_1, \beta_1), (\alpha_2, \beta_2), (\alpha_3, \beta_3)$, respectively. In general, these active constraint sets lead to an *active constraint set sequence* $((\alpha_1, \beta_1), (\alpha_2, \beta_2), ..., (\alpha_{N_S}, \beta_{N_S}))$ that together with $(N_1, N_2, ..., N_S)$ and N define the active constraint set imposed at each sample on the horizon. This means that the constraints indexed by each active constraint set are imposed on the associated interval, leading to the following set of equality constraints:

$$\left.\begin{array}{c} H_{\alpha_1} u(t) = h_{\alpha_1} \\ H_{\alpha_1} u(t+1) = h_{\alpha_1} \\ \vdots \\ H_{\alpha_{N_S}} u(t+N-1) = h_{\alpha_{N_S}} \end{array}\right\} \tag{A.8}$$

and

$$\left.\begin{array}{c} G_{\beta_1}\left(Ax(t) + C_N \tilde{E}_1 \tilde{u}(t)\right) = g_{\beta_1} \\ G_{\beta_1}\left(A^2 x(t) + C_N \tilde{E}_2 \tilde{u}(t)\right) = g_{\beta_1} \\ \vdots \\ G_{\beta_{N_S}}\left(A^N x(t) + C_N \tilde{E}_N \tilde{u}(t)\right) = g_{\beta_{N_S}} \end{array}\right\} \tag{A.9}$$

We have introduced the matrix $C_\tau = (A^{\tau-1}B | A^{\tau-2}B | \cdots | B)$, the $rN \times rN$-matrix $\tilde{E}_\tau$ defined by

$$\tilde{E}_\tau \quad = \quad \begin{pmatrix} 0 & 0 \\ I_{r\tau \times r\tau} & 0 \end{pmatrix} \tag{A.10}$$

and applied the well known formula $x(t+\tau) = A^\tau x(t) + C_N \tilde{E}_\tau \tilde{u}(t)$ where $\tilde{u}(t) = (u^T(t),\ u^T(t+1),\ \cdots,\ u^T(t+N-1))^T$. Removing from (A.8) and (A.9) equations that are a priori known to be infeasible and duplicated equations, (A.8) and (A.9) may be stacked into the following set of equations

$$L_k \tilde{u}(t) \;\; = \;\; M_k x(t) + M_k^g g + M_k^h h \qquad \text{(A.11)}$$

where k is an index in the index set $\mathcal{C} = \{0, 1, 2, ..., N_K - 1\}$ enumerating the finite set of all active constraint set sequences generated by the constraints (A.5), (A.4) and the division into subintervals. For later use, let $k_0 \in \mathcal{C}$ be the index to the active constraint set sequence with no active constraints, and define the $r \times rN$ matrix $E_\tau = (0_{r\times r}, ..., 0_{r\times r}, I_{r\times r}, 0_{r\times r}, ...0_{r\times r})$ where the $I_{r\times r}$ is at the τ-th $r \times r$ block.

A.2.2 Decomposition of the HJB equation

In this section we consider the minimization problem on the RHS of (A.7) with the stated constraints, which is a strictly convex problem whose solution is characterized by the Karush-Kuhn-Tucker conditions. However, since these conditions involve inequalities, the Karush-Kuhn-Tucker conditions provide an implicit solution that does not lead to an explicit state-feedback implementation of the controller. This motivates a simple decomposition of the minimization in (A.7) into two nested parts where one part only involves equality constraints and the other part is a discrete optimization problem over all allowed active constraint set sequences. The part that involves equality constraints can then be solved explicitly offline, while the discrete optimization problem can also be solved offline or reduced to a simpler problem and then solved in real-time in a efficient manner. The following result is then evident from (Chmielewski and Manousiouthakis 1996):

Theorem 1 *(Nested HJB equation) Assume the minimum in the HJB equation (A.7) exists. With N sufficiently large and no restrictions on the active constraint set sequences allowed switching times ($S = N$), the HJB equation (A.7) is equivalent to*

$$\begin{aligned} 0 \;\; = \;\; \min_{k\in\mathcal{C}} \Bigg(& \min_{\substack{\tilde{u}(t)\in R^{rN} \\ L_k\tilde{u} = M_k x(t) + M_k^g g + M_k^h h}} \Big(V(x(t+N)) - V(x(t)) \\ & + \sum_{\tau=0}^{N-1} l_{QR}(x(t+\tau), E_{\tau+1}\tilde{u}(t)) \Big) \Bigg) \end{aligned} \qquad \text{(A.12)}$$

where the outer minimization is subject to the constraints

$$HE_\tau \tilde{u}_k^*(x(t)) \leq h \tag{A.13}$$

$$G(A^\tau x(t) + C_N \tilde{E}_\tau \tilde{u}_k^*(x(t))) \leq g \tag{A.14}$$

for all $1 \leq \tau \leq N$ *and* $\tilde{u}_k^*(x(t))$ *is the* $\tilde{u}(t)$ *solving the innermost optimization problem in (A.12).* □

Determining the optimal cost function V is in general a difficult problem, so similar to (Bemporad, Morari, Dua, and Pistikopoulos 2002; Rantzer and Johansson 2000) we utilize a lower bound $\underline{V}$ as a suboptimal approximation in the control design. Any loss of performance resulting from this approximation as well as sub-optimality due to restrictions on the allowed active constraint set switching times may be analyzed using the tools given in (Johansson and Rantzer 1998; Rantzer and Johansson 2000).

Lemma 1 *A lower bound on the optimal cost function is given by* $\underline{V}(x) = x^T \underline{P} x \leq V(x)$ *where the matrix* $\underline{P} = \underline{P}^T$ *is the positive definite solution of the algebraic Riccati equation corresponding to the unconstrained LQR problem:*

$$A^T \underline{P} A - \underline{P} - A^T \underline{P} B (B^T \underline{P} B + R)^{-1} B^T \underline{P} A + Q \quad = \quad 0$$

Proof. The result follows immediately from the observation that constraining the input will never decrease the value of the optimal cost function (Sznaier and Damborg 1990). □

Note that $\underline{V}(x) = V(x)$ for x in any compact set if N is sufficiently large (Chmielewski and Manousiouthakis 1996). For a given active constraint set sequence (with index $k \in \mathcal{C}$) this leads to the problem

$$\tilde{u}_k^*(x(t)) \quad = \quad \arg \min_{\substack{\tilde{u}(t) \in R^{rN} \\ L_k \tilde{u}(t) = M_k x(t) + M_k^g g + M_k^h h}} \underline{I}(\tilde{u}(t), x(t)) \tag{A.15}$$

where

$$\begin{aligned} \underline{I}(\tilde{u}(t), x(t)) \quad = \quad & \underline{V}(x(t+N)) - \underline{V}(x(t)) \\ & + \sum_{\tau=0}^{N-1} l_{QR}(x(t+\tau), E_{\tau+1}\tilde{u}(t)) \end{aligned} \tag{A.16}$$

and the outer finite discrete optimization problem of (A.12) is restated as

$$k^*(x) \quad = \quad \arg \min_{k \in \mathcal{C}} \varphi_k(x) \tag{A.17}$$

$$\varphi_k(x) \quad = \quad \underline{I}(\tilde{u}_k^*(x), x) \tag{A.18}$$

where for all $1 \leq \tau \leq N$ the minimization is subject to

$$\begin{aligned} HE_\tau \tilde{u}_k^*(x) &\leq h & \text{(A.19)} \\ G(A^\tau x + C_N \tilde{E}_\tau \tilde{u}_k^*(x)) &\leq g & \text{(A.20)} \end{aligned}$$

The problem (A.17)-(A.20) is feasible if and only if $x \in X^F$, where

$$X^F = \bigcup_{k \in \mathcal{C}} X_k^F \quad \text{(A.21)}$$

$$X_k^F = \{x \in R^n \mid HE_\tau \tilde{u}_k^*(x) \leq h, \; G(A^\tau x + C_N \tilde{E}_\tau^T \tilde{u}_k^*(x)) \leq g, \text{ for } 1 \leq \tau \leq N\Big\} \quad \text{(A.22)}$$

For $x \in X^F$, the suboptimal constrained LQR is given by $u^*(x) = E_1 \tilde{u}^*_{k^*(x)}(x)$. If $x \notin X^F$, we relax the problem by allowing minimum violation of some of the constraints according to some priority. Constraints that may be relaxed are called "soft" constraints (with indices in the constraint sets α_s and β_s), as opposed to "hard" constraints (with indices in the constraint sets α_h and β_h), which can not be relaxed under any circumstances. Hence, for $x \notin X^F$, we minimize the criterion

$$\begin{aligned} \nu_k(x) = & \sum_{\tau=1}^N \omega_{1,\beta_s}^T \max(0, G_{\beta_s}(A^\tau x + C_N \tilde{E}_\tau \tilde{u}_k^*(x)) - g_{\beta_s}) \\ & + \sum_{\tau=1}^N \omega_{2,\alpha_s}^T \max(0, H_{\alpha_s} E_\tau \tilde{u}_k^*(x) - h_{\alpha_s}) \quad \text{(A.23)} \end{aligned}$$

with respect to $k \in \mathcal{C}$, subject to "hard" constraints for $1 \leq \tau \leq N$

$$\begin{aligned} G_{\beta_h}\Big(A^\tau x + C_N \tilde{E}_\tau \tilde{u}_k^*(x)\Big) &\leq g_{\beta_h} & \text{(A.24)} \\ H_{\alpha_h} E_\tau \tilde{u}_k^*(x) &\leq h_{\alpha_h} & \text{(A.25)} \end{aligned}$$

The positive vectors ω_{1,α_s} and ω_{2,β_s} are weights that capture some prioritization among the soft constraints. The problem (A.23)-(A.25) is feasible when $x \in X^R$, where

$$X^R = \bigcup_{k \in \mathcal{C}} X_k^R \quad \text{(A.26)}$$

$$X_k^R = \Big\{x \in R^n - X^F \mid \text{such that } (A.24) - (A.25) \text{ holds}\Big\} \quad \text{(A.27)}$$

If $x \notin X^F \cup X^R$, i.e. no active constraint set sequence in $\mathcal{C}$ gives a control input that is feasible with respect to the hard (non-relaxable) constraints on the horizon, the controller fails. Let the solution to (A.23)-(A.25) be denoted $k^*(x)$ and the associated control input $\tilde{u}^*_{k^*(x)}(x)$. Furthermore, let $X = X^F \cup X^R$ and define for $x \in X$ the control input of the suboptimal constrained LQR:

$$u^*(x) = E_1 \tilde{u}^*_{k^*(x)}(x) \tag{A.28}$$

The resulting PWL control structure may be summarized as follows. There is a number of affine feedbacks where each affine feedback is designed with the objective of minimizing the LQ cost function subject to the state and input trajectories moving on a specific active constraint set sequence. The affine state feedbacks are designed offline by solving (A.15) as described in section A.3, so the real-time computations amount to selecting which affine state feedback to apply at a given state $x(t)$. This amounts to solving (A.17)-(A.20) (or (A.23)-(A.25) in case of infeasibility), which is addressed in section A.4.

A.3 Computing gain matrices

In this section, the solution to the optimization problem (A.15) is presented for a fixed active constraint set sequence. The expression (A.16) for $\underline{I}$ can be formulated as follows:

$$\underline{I}(\tilde{u}, x) = x^T S_1 x + 2x^T S_2 \tilde{u} + \tilde{u}^T S_3 \tilde{u} \tag{A.29}$$

where

$$\begin{aligned} S_1 &= Q + A^T Q A + (A^2)^T Q A^2 + ... + (A^{N-1})^T Q A^{N-1} \\ &\quad + (A^N)^T \underline{P} A^N - \underline{P} \\ S_2 &= A^T Q C_N \tilde{E}_1 + ... + (A^{N-1})^T Q C_N \tilde{E}_{N-1} \\ &\quad + (A^N)^T \underline{P} C_N \\ S_3 &= \tilde{R} + \tilde{E}_1^T C_N^T Q C_N \tilde{E}_1 + ... + \tilde{E}_{N-1}^T C_N^T Q C_N \tilde{E}_{N-1} \\ &\quad + C_N^T \underline{P} C_N \end{aligned}$$

and the block diagonal $rN \times rN$-matrix $\tilde{R}$ is defined by $\tilde{R} = \mathrm{diag}\,(R, R, ..., R)$.

Theorem 2 *(Gain matrices) Consider a fixed active constraint set sequence with index $k \in \mathcal{C}$. For any $x \in X^F$, the solution to the constrained quadratic optimization problem (A.15) is given by the affine state feedback*

$$\tilde{u}^*_k(x) = \begin{cases} K_{k,2} x, & \text{if } k = k_0 \\ K^g_{k,1} g + K^h_{k,1} h + K_{k,2} x, & \text{if } k \neq k_0 \end{cases} \tag{A.30}$$

where $K_{k,2} = -S_3^{-1} S_2^T$ *for* $k = k_0$*, and for* $k \neq k_0$

$$\begin{aligned} K_{k,1}^g &= S_3^{-1} L_k^T \left(L_k S_3^{-1} L_k^T \right)^{-1} M_k^g \\ K_{k,1}^h &= S_3^{-1} L_k^T \left(L_k S_3^{-1} L_k^T \right)^{-1} M_k^h \\ K_{k,2} &= -S_3^{-1} \left(\left(I - L_k^T \left(L_k S_3^{-1} L_k^T \right)^{-1} L_k S_3^{-1} \right) S_2^T \right. \\ & \qquad \left. - L_k^T \left(L_k S_3^{-1} L_k^T \right)^{-1} M_k \right) \end{aligned}$$

Proof. Note that (A.15) is strictly convex since $R > 0$, and it suffices to consider only first order optimality conditions, which is straightforward (Johansen, Petersen, and Slupphaug 2000b). □

Observe that in the case of no active constraints, (A.30) takes the form of the well known unconstrained LQR solution, $u(x) = -(B^T(Q + \underline{P})B + R)^{-1} B^T (Q + \underline{P})Ax$. The affine state feedback (A.30) is parameterized such that individual constraints can be deactivated and the constraint limits may be changed on-line without changing the gain matrices.

Example 1: Double integrator with input and state constraints. Consider a double integrator with the discretized model

$$A = \begin{pmatrix} 1 & T_s \\ 0 & 1 \end{pmatrix}, \qquad B = \begin{pmatrix} T_s^2 \\ T_s \end{pmatrix} \tag{A.31}$$

using a sampling-interval $T_s = 0.05$. The control objective is defined by the cost function $l_{QR}(x, u) = x_1^2 + u^2$ and the constraints $-0.5 \leq x_2 \leq 0.5$ and $-1 \leq u \leq 1$. Figure A.1 shows a simulation when the initial state is $x(0) = (-2, 0)^T$. Observe that initially the input constraint $u = 1$ is active. After $t \approx 0.5$, the state constraint $x_2 \leq 0.5$ is active, until $t \approx 2.85$ when the controller switches strategy once more, since it appears to be no longer optimal to stay on the constraint $x_2 = 0.5$. After this point the unconstrained LQ controller is used and the state is controlled to the origin. The switching strategy chosen by the controller is intuitive if x_1 is interpreted as position, x_2 as speed and u as acceleration: In order to reduce the position error the speed is first increased at a maximum rate (given by the input constraint). When the maximum speed allowed is reached, this speed is kept until the position error becomes so small that the speed must be reduced to stabilize the position at the setpoint. In this example we have chosen the smallest possible horizon, namely $N = S = 1$ since this is advantageous for computational reasons. The region of feasibility is seen to be $X^F = \{x \in R^2 \mid |x_2| \leq 0.55\}$ since the input constraints restricts x_2 to be changed by at most 0.05 units within one sample. Hence, the admissible region $|x_2| \leq 0.5$ can be reached in one sample from X^F. In order to efficiently handle cases when $|x_2| > 0.55$, we define the input constraints as hard (non-relaxable) constraints, and the state constraints as soft (relaxable) constraints. Furthermore, we define all the elements of the weight vector ω_{1,β_s} to be equal to one. Since the hard constraints are associated with the input only, $X^R = R^2$. The piecewise linear feedback control law is shown in Figure A.2. □

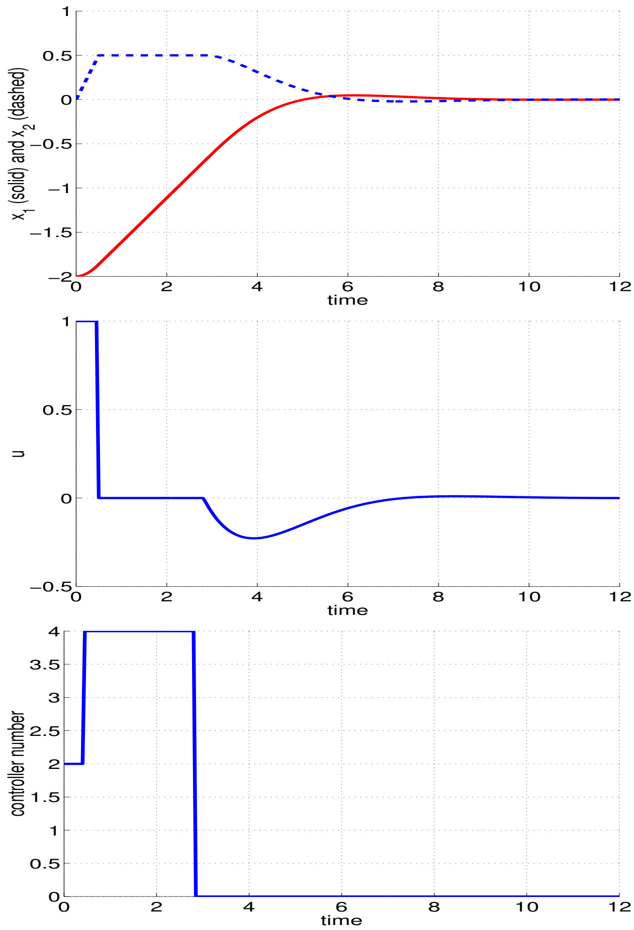

Figure A.1: Constrained control of a double integrator from initial state $x(0) = (-2, 0)^T$.

Effectively, the active state constraints $x_2 = \pm 0.5$ are enforced by a sliding-mode like strategy in the example above. This is mainly due to

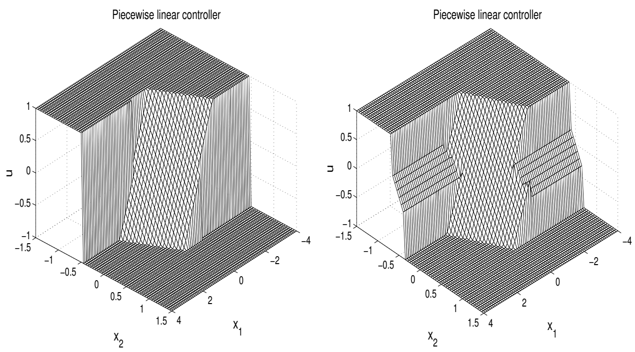

Figure A.2: PWL constrained LQ feedback controller for the double integrator (left) and with boundary layer around active state constraints (right).

the choice of a very small N, and will lead to poor robustness (Johansen, Petersen, and Slupphaug 2000b). However, the problem can be resolved by modifying the state constraints (A.9) such that they do not require the active state constraints to be fulfilled in a dead-beat manner (at the first possible sample), but rather attract the state asymptotically towards the active constraints. This is achieved by replacing every instant of the active state constraint equation $G_\beta x(t+\tau) = g_\beta$ by its asymptotic version

$$D_{\beta,\tau} G_\beta x(t+\tau) + \ldots + D_{\beta,1} x(t+1) + D_{\beta,0} G_\beta x(t) \quad = \quad g_\beta \tag{A.32}$$

where $D_{\beta,i}$ are diagonal matrices defined by pole placement such that $G_\beta x(t) \rightarrow g_\beta$ at a desired rate. In order take full advantage of this modification, it is convenient to introduce another modification, namely an ε-boundary layer near each active state constraint, similar to what is common in sliding mode control (Slotine 1984). Within this boundary layer, the controller is only allowed to switch to feedbacks that either makes the associated state constraints asymptotically active, or makes the state move away from the state constraint in the direction of the admissible region of the state space. Formally, this is achieved by adding the following constraint to the optimization problem (A.17)-(A.20)

$$G_{\beta(x)}(A^\tau x(t) + C_N \tilde{E}_\tau \tilde{u}_k^*(x(t))) \quad \leq \quad G_{\beta(x)} x(t) \tag{A.33}$$

if $\beta_k \subset \beta(x(t))$ for $1 \leq \tau \leq N$. $\beta(x)$ denotes the set of ε-active state constraints at x, i.e. $\beta(x) = \{l \in \{1, 2, ..., q\} \mid |(G_{l1}, ..., G_{ln})x - g_l| \leq \varepsilon_l\}$, where $\varepsilon_l > 0$ defines the boundary layer. Eq. (A.33) excludes non-attractive feedbacks that tend to move the state towards violation of active state constraints.

Double integrator example, cont'd. In order to reduce the gain near the active state constraints, a boundary layer of $\varepsilon_1 = \varepsilon_2 = \pm 0.15$ is defined around the constraints $x_2 = 0.5$ and $x_2 = -0.5$. Hence, when $0.65 \geq x_2 \geq 0.35$, the control strategy is allowed to switch and the controller takes the objective of attracting the state towards the surface $x_2 = 0.5$ while minimizing the LQ objective. The speed of the motion towards the surface $x_2 = 0.5$ is defined by $D_1 = 1/0.9$ and $D_2 = 1$. Comparing the piecewise linear controller surface of the modified controller (right part of Figure A.2) with the original controller (left part of Figure A.2), it is seen that the gain has indeed been reduced in an ε-boundary layer near the active constraints $x_2 = \pm 0.5$. $\square$

A.4 State space partitioning

The purpose of this section is to discuss how to solve the outer optimization problem (A.17)-(A.20), and in particular to derive an algorithm for computing a state space partitioning that can be used to decide which active constraint set sequence is optimal at a given state. The discrete minimizations in (A.17) and (A.23) can either be avoided completely in the real-time computations if the set of candidate optima is reduced to single elements within subsets of the state space, or at least reduced to a small subset of $\mathcal{C}$ within subsets of the state space. This can be exploited in the real-time implementation to reduce the processing capacity and memory requirements and also for computational analysis as considered in section A.5.

A.4.1 Activity region

The activity region $X_k \subset X$ is defined as the subset of the state space where the active constraint set sequence with index k is active, i.e. $X_k = \{x \in X \mid k = k^*(x)\}$. Together with the affine functions (A.30), the activity regions X_k, $k \in \mathcal{C}$ completely describes the PWL structure of the controller.

Double integrator example, activity regions. For the double integrator example, there are five constituent affine feedbacks with corresponding activity regions. Region/Feedback 0: unconstrained case ($k = 0$), Region/Feedback 1: input constraint $u = -1$ active ($k = 1$), Region/Feedback 2: input constraint $u = 1$ active ($k = 2$), Region/Feedback 3: state constraint $x_2 = -0.5$ active ($k = 3$), Region/Feedback 4: state constraint

$x_2 = 0.5$ active ($k = 4$). The activity regions for the suboptimal constrained LQ controller with boundary layer are shown in Figure A.3. We observe that in this case the regions can be characterized as unions of polyhedra. □

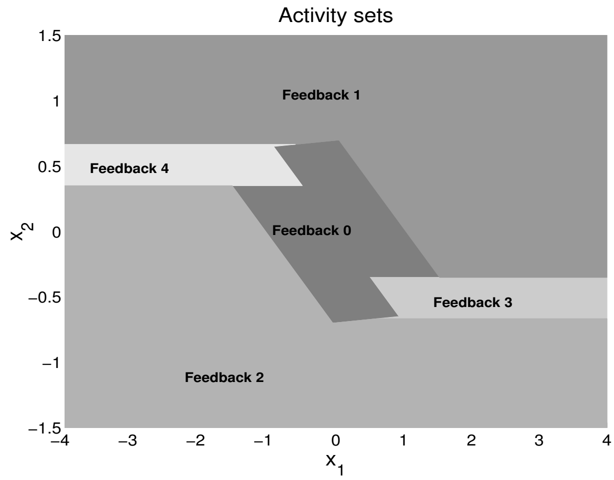

Figure A.3: Activity regions for the five constituent affine feedbacks in the constrained LQR for the double integrator with boundary layers.

In order to explicitly characterize the activity regions, it is natural to treat the feasible and relaxed feasible regions X^F and X^R separately, since the choice of optimal active constraint set sequence is based on different criteria in these cases. Thus, we define the activity regions contained in X^F as follows:

$$X_k^f = \{x \in X_k^F \mid k \text{ is optimal w.r.t. } (A.17) - (A.20) \text{ and } (A.33)\} \tag{A.34}$$

For $x \in X^R$, the controller objective changes to minimize the constraint violation and we define

$$X_k^r = \left\{x \in X_k^R \mid k \text{ is optimal w.r.t. } (A.23) - (A.25)\right\} \tag{A.35}$$

Hence, the activity region X_k where the feedback with index k is active is now $X_k = X_k^f \cup X_k^r$. A slightly more explicit characterization of X_k^f than (A.34) is

$$X_k^f = \left\{x \in X_k^F \mid \varphi_k(x) \leq \varphi_j(x), \quad j \in \mathcal{F}(x) \cap \mathcal{A}(x)\right\} \tag{A.36}$$

where $\mathcal{F}(x) = \{k \in \mathcal{C} \mid (x) \in X_k^F\}$ is a set containing the active constraint set sequences that are feasible at x, and $\mathcal{A}(x) \subset \mathcal{C}$ is a set containing the indices to the active constraint set sequences that are attractive or not currently active at x, cf. (A.33):

$$\begin{aligned}\mathcal{A}(x) \quad = \quad & \Big\{k \in \mathcal{C} \mid G_{\beta(x)}(A^\tau x + C_N \tilde{E}_\tau \tilde{u}_k^*(x)) \leq G_{\beta(x)} x \\ & \text{or} \quad \beta_k \not\subset \beta(x)\Big\}\end{aligned} \tag{A.37}$$

Furthermore, it follows that

$$X^F \quad = \quad \bigcup_{k \in \mathcal{C}} X_k^f \; = \; \bigcup_{k \in \mathcal{C}} X_k^F \tag{A.38}$$

Likewise, a slightly more explicit characterization of X_k^r than (A.35) is given by

$$X_k^r \quad = \quad \big\{x \in X_k^R \mid \nu_k(x) \leq \nu_j(x), \text{ for all } j \in \mathcal{R}(x)\big\} \tag{A.39}$$

where $\mathcal{R}(x) = \{k \in \mathcal{C} \mid x \in X_k^R\}$ is defined as the set of active constraint set sequences that are feasible with respect to the non-relaxable constraints, but not feasible with respect to the relaxable constraints at x. We also have

$$X^R \quad = \quad \bigcup_{k \in \mathcal{C}} X_k^r \; = \; \bigcup_{k \in \mathcal{C}} X_k^R \tag{A.40}$$

which is the set of states where there exists an active constraint set sequence that is feasible and optimal with respect to the non-relaxable constraints but not with respect to the relaxable constraints.

A.4.2 Outer Approximations to the Activity Regions

Since X_k^F and X_k^R are polyhedral, it is clear that X^F, X^R and $X = X^F \cup X^R$ are unions of polyhedra. However, because the optimality conditions in (A.36) are characterized by *quadratic* functions, the set $X_k \subset X$ may not be characterized only by the hyper-planes defined by feasibility, but possibly also by other hyper-planes or (convex or non-convex) quadratic surfaces due to the optimality conditions. Thus, X_k may in general not be a union of polyhedra and therefore difficult to characterize exactly in a more explicit manner than (A.36) and (A.39). Still, several explicit outer approximations of X_k can be computed in terms of sets that contain X_k. Here we develop an outer approximation $\overline{X}_k \supset X_k$ where $\overline{X}_k$ is a union of polyhedra. As the basic polyhedral building blocks in this characterization we consider the hyperplane partition $\mathcal{P}_X^{HP} = \{\mathcal{X}_l^{HP} \mid l \in \{1, 2, ..., N_P\}\}$ generated by all the hyper-planes involved in the characterization of X_k^F, X_k^R and X_k^A, for $k \in \mathcal{C}$:

$$HE_\tau K_{k,2}x = h - HE_\tau(K_{k,1}^g g + K_{1,k}^h h) \tag{A.41}$$

$$G(A^\tau + C_N\tilde{E}_\tau K_{k,2})x = g - GC_N\tilde{E}_\tau(K_{k,1}^g g + K_{k,1}^h h) \tag{A.42}$$

$$G(A^\tau + C_N\tilde{E}_\tau K_{2,k} - I)x = GC_N\tilde{E}_\tau(K_{1,k}^h h + K_{1,k}^g g) \tag{A.43}$$

for $1 \leq \tau \leq N$, with obvious interpretation when h or g are zero-dimensional. Let (A.41)-(A.43) be written in compact notation $Yx = y$. The set of half-spaces $\mathcal{Y}_i^+ = \{x \in R^n \mid Y_i x \geq y_i\}$ and $\mathcal{Y}_i^- = \{z \in R^n \mid Y_i x < y_i\}$ now defines the hyperplane partition $\mathcal{P}_X^{HP}$ of X as the set of all possible non-empty intersections of half-spaces: $\mathcal{X}_l^{HP} = \mathcal{Y}_1^* \cap ... \cap \mathcal{Y}_{N_z}^*$ where $*$ symbolizes any combinations of $+/-$. Note that this hyperplane partition will contain unnecessarily many elements in many cases and is introduced here in order to develop a theoretical understanding.

Lemma 2 *The hyperplane partition $\mathcal{P}_X^{HP}$ has the following properties:*

i. Each constituent region of the partition is uniquely associated with either the feasible region X^F or the relaxed feasible region X^R, i.e. $\mathcal{X}_l^{HP} \cap X^F = \emptyset$ and $\mathcal{X}_l^{HP} \cap X^R = \mathcal{X}_l^{HP}$, or vice versa $\mathcal{X}_l^{HP} \cap X^F = \mathcal{X}_l^{HP}$ and $\mathcal{X}_l^{HP} \cap X^R = \emptyset$, for all $l = 1, 2, ..., N_P$.

ii. For all $l \in \{1, 2, ..., N_p\}$ and $x \in \mathcal{X}_l^{HP}$ the sets $\mathcal{F}(x)$, $\mathcal{R}(x)$, $\mathcal{A}(x)$ and $\beta(x)$ are invariant such that each of them contain the same elements for all $x \in \mathcal{X}_l^{HP}$.

Proof. Follows from the fact that the hyperplane partition $\mathcal{P}_X^{HP}$ of X is generated by all hyper-planes involved in the characterizations of $\mathcal{F}(x)$, $\mathcal{R}(x)$, $\mathcal{A}(x)$ and $\beta(x)$. $\Box$

From the first part of Lemma 2 it is evident that each $\mathcal{X}_l^{HP} \in \mathcal{P}_X^{HP}$ is fully contained in either X^R or X^F. Thus, we define disjoint index sets

$$\mathcal{L}^F = \left\{l \in \{1, 2, ..., N_P\} \mid \mathcal{X}_l^{HP} \cap X^F \neq \emptyset\right\} \tag{A.44}$$

$$\mathcal{L}^R = \left\{l \in \{1, 2, ..., N_P\} \mid \mathcal{X}_l^{HP} \cap X^R \neq \emptyset\right\} \tag{A.45}$$

Assume $l \in \mathcal{L}^F$, i.e. $\mathcal{X}_l^{HP} \subset X^F$. One may now define a set $\mathcal{F}_l^f\{k \in \mathcal{C} \mid \mathcal{X}_l^{HP} \cap X_k^F \neq \emptyset\}$ of feasible active constraint set sequences in the region

$\mathcal{X}_l^{HP}$. Hence, for any $x \in X^F$ there exists a unique $l(x) \in \mathcal{L}^F$ such that $x \in X_{l(x)}^F$ and at least one of the feasible active constraint set sequences in $\mathcal{F}_l^f$ is optimal for all $x \in \mathcal{X}_l^{HP}$. We continue by characterizing the subset of $\mathcal{F}_l^f$ that is optimal for some $x \in \mathcal{X}_l^F$, aiming towards a definition of $\overline{X}_k^f \supset X_k^f$.

Lemma 3 *Let $l \in \mathcal{L}^F$ and $j, k \in \mathcal{F}_l^f$ be arbitrary. Suppose the active constraint set sequences $((\alpha_1^k, \beta_1^k)$, (α_2^k, β_2^k),..., $(\alpha_{N_S}^k, \beta_{N_S}^k))$ and $((\alpha_1^j, \beta_1^j)$, $(\alpha_2^j, \beta_2^j), ..., (\alpha_{N_S}^j, \beta_{N_S}^j))$ are different. If $\alpha_i^k \subset \alpha_i^j$ and $\beta_i^k \subset \beta_i^j$, for all $i = 1, 2, ..., N_S$, then the active constraint set sequence with index j is suboptimal for all $x \in \mathcal{X}_l^{HP}$.*

Proof. Because the active constraint set sequence with index k is a subset of the active constraint set sequence with index j and both are feasible, it follows immediately that $\varphi_k(x) \leq \varphi_j(x)$ for all $x \in \mathcal{X}_l^{HP}$ since adding a constraint to some constraint set sequence will not reduce the cost. $\square$

Lemma 4 *Let $l \in \mathcal{L}^F$ and $k \in \mathcal{F}_l^f$ be arbitrary, and define*

$$\gamma_{jk} = \max_{x \in \mathcal{X}_l^{HP}} (\varphi_k(x) - \varphi_j(x)) \tag{A.46}$$

$$\kappa_{jk} = \min_{x \in \mathcal{X}_l^{HP}} (\varphi_k(x) - \varphi_j(x)) \tag{A.47}$$

If $\gamma_{jk} \leq 0$ for all $j \in \mathcal{F}_l^f$, then the active constraint set sequence with index k is optimal for all $x \in \mathcal{X}_l^{HP}$. If $\kappa_{jk} \geq 0$ for all $j \in \mathcal{F}_l^f$, then the active constraint set sequence with index k is suboptimal for all $x \in \mathcal{X}_l^{HP}$.

Proof. Since $\gamma_{jk} \leq 0$ it follows that for all $x \in \mathcal{X}_l^{HP}$ and $j \in \mathcal{F}_l^f$, $\varphi_k(x) \leq \varphi_j(x)$. Note that due to Lemma 2, $\mathcal{F}_l^f = \mathcal{F}(x)$ for all $x \in \mathcal{X}_l^{HP}$, and the first part follows because $\mathcal{F}_l^f$ contains all feasible active constraint set sequences in $\mathcal{C}$. The second part of the lemma is analogous. $\square$

Both (A.46) and (A.47) are quadratic programs, for a fixed $l \in \mathcal{L}^F$ and fixed active constraint set sequences $k, j \in \mathcal{F}_l^f$, since $\mathcal{X}_l^{HP}$ is polyhedral and φ_k and φ_j are quadratic. Using the optimality characterizations in Lemmas 3 and 4, one will typically be able to exclude a large set of candidate active constraint set sequences from the set of feasible active constraint set sequences $\mathcal{F}_l^f$ in the region $\mathcal{X}_l^{HP}$. We define $\mathcal{O}_l^f \subset \mathcal{F}_l^F$ as the indices of those active constraint set sequences that are consistent with the optimality conditions in Lemmas 3 and 4 in $\mathcal{X}_l^{HP}$:

$$\mathcal{O}_l^f = \Big\{k \in \mathcal{F}_l^f \mid k \text{ is optimal w.r.t. (A.17)-(A.20), (A.33)} \quad \text{for some } x \in \mathcal{X}_l^{HP}\Big\} \tag{A.48}$$

We define the outer approximation to the activity region X_k^f as follows:

$$\overline{X}_k^f = \bigcup_{l \in \mathcal{L}^F} \mathcal{X}_l^{HP} \tag{A.49}$$

Next, assume $l \in \mathcal{L}^R$, i.e. $\mathcal{X}_l^{HP} \subset X^R$. One may now define a set $\mathcal{F}_l^r = \{k \in \mathcal{C} \mid \mathcal{X}_l^{HP} \cap X_k^R \neq \emptyset\}$ of relaxed feasible active constraint set sequences in the region $\mathcal{X}_l^{HP}$. Unlike the characterization of X_k^f, we now have the following result:

Lemma 5 *For all $k \in \mathcal{C}$, the set X_k^r is a union of polyhedra.*

Proof. Let $k \in \mathcal{C}$ be arbitrary. The region of relaxed feasibility X_k^R is polyhedral, cf. (A.27). Since the function $\nu_k(x) - \nu_j(x)$ is piecewise linear in x, the sets $\{x \in R^n \mid \nu_k(x) \leq \nu_j(x)\}$ that appear in the optimality condition in (A.39) are characterized using hyper-planes. Since all geometric objects characterizing X_k^r are hyper-planes, it is a union of polyhedral sets. □

According to Lemma 5 it is possible to obtain an exact and explicit characterization of X_k^r. However, for computational reasons it may be convenient with an outer approximation $\overline{X}_k^r \supset X_k^r$ in some cases. The following optimality lemma is useful in that respect:

Lemma 6 *Let $l \in \mathcal{L}^R$ and $k \in \mathcal{F}_l^r$ be arbitrary, and define*

$$\rho_{jk} = \max_{x \in \mathcal{X}_l^{HP}} (\nu_k(x) - \nu_j(x)) \tag{A.50}$$

$$\sigma_{jk} = \min_{(x) \in \mathcal{X}_l^{HP}} (\nu_k(x) - \nu_j(x)) \tag{A.51}$$

If $\rho_{jk} \leq 0$ for all $j \in \mathcal{F}_l^r$, then the active constraint set sequence with index k is optimal for all $x \in \mathcal{X}_l^{HP}$. If $\sigma_{jk} \geq 0$ for all $j \in \mathcal{F}_l^R$, then the active constraint set sequence with index k is suboptimal for all $x \in \mathcal{X}_l^{HP}$.

Proof. Analogous to Lemma 4. □

Note that (A.50) and (A.51) are piecewise linear programs. Using the optimality characterizations in Lemma 6, one will typically be able to exclude a large set of candidate active constraint set sequences from the set of feasible active constraint set sequences $\mathcal{F}_l^r$ in the region $\mathcal{X}_l^{HP}$. We define $\mathcal{O}_l^r \subset \mathcal{F}_l^R$ as the indices of those active constraint set sequences that are consistent with the optimality conditions of Lemma 6 in $\mathcal{X}_l^{HP}$:

$$\begin{aligned} \mathcal{O}_l^r \quad &= \quad \{k \in \mathcal{F}_l^r \mid k \text{ is optimal w.r.t. (A.23)-(A.25)} \\ &\qquad \text{for some } x \in \mathcal{X}_l^{HP}\} \end{aligned} \tag{A.52}$$

Finally, we define the outer approximation to the activity region X_k^r as follows:

$$\overline{X}_k^r \quad = \quad \bigcup_{l \in \mathcal{L}^R} \mathcal{X}_l^{HP} \tag{A.53}$$

We are now in position to define $\overline{X}_k = \overline{X}_k^f \cup \overline{X}_k^r$ and

$$\mathcal{F}_l = \begin{cases} \mathcal{F}_l^f, & l \in \mathcal{L}^F \\ \mathcal{F}_l^r, & l \in \mathcal{L}^R \end{cases}, \qquad \mathcal{O}_l = \begin{cases} \mathcal{O}_l^f, & l \in \mathcal{L}^F \\ \mathcal{O}_l^r, & l \in \mathcal{L}^R \end{cases} \tag{A.54}$$

A.4.3 Partitioning Algorithm

Algorithm 1

i. Let $\mathcal{E} := \emptyset$, and $\mathcal{U} := \{X\}$.

ii. If $\mathcal{U} = \emptyset$, the partition generated by this algorithm is $\mathcal{P} = \mathcal{E}$ and the algorithm terminates.

iii. Let $\mathcal{X}_0 \in \mathcal{U}$ be arbitrary.

iv. Let $\mathcal{O}_0$ contain the candidate optimal active constraint set sequences in $\mathcal{X}_0$, computed according to Lemmas 3-6.

v. If $\mathcal{O}_0$ contains a sufficiently small number of elements, add $\mathcal{X}_0$ to the set of explored subsets $\mathcal{E}$ and remove $\mathcal{X}_0$ from the set of unexplored subsets $\mathcal{U}$. Go to step 2.

vi. Select a hyperplane $Y_i x = y_i$ from $Yx = y$ and split $\mathcal{X}_0$ into non-empty $\mathcal{X}_0^+ = \mathcal{X}_0 \cap \mathcal{Y}_i^+$ and $\mathcal{X}_0^- = \mathcal{X}_0 \cap \mathcal{Y}_i^-$. If this is not possible for any hyperplane from $Yx = y$, add $\mathcal{X}_0$ to the set of explored subsets $\mathcal{E}$ and remove $\mathcal{X}_0$ from the set of unexplored subsets $\mathcal{U}$. Go to step 2.

vii. Add $\mathcal{X}_0^+$ and $\mathcal{X}_0^-$ to $\mathcal{U}$ and remove $\mathcal{X}_0$ from $\mathcal{U}$. Go to step 2.

The set $\mathcal{E}$ contains the set of explored subsets of X, while the set $\mathcal{U}$ contains the set of explored subsets of X. The algorithm will explore the candidate optimal active constraint sets associated with each element of $\mathcal{E}$ sequentially. The regions of X will be split using the hyper-planes from $Yx = y$ and explored individually until either a sufficiently small number of candidate optimal active constraint set remains in each region, or the region can not be split any further using hyper-planes from $Yx = y$. In order to reduce the computational complexity of Algorithm 1 one should implement heuristics in step 6 in order to select a "promising" hyperplane for splitting the region $\mathcal{X}_0$ such that unnecessary splitting is avoided. Note that the partition $\mathcal{P}_X$ generated by Algorithm 1 may be unnecessarily fine since at each step it is not known a priori if one can reduce the number of elements in $\mathcal{O}_0$ by further partitioning of $\mathcal{X}_0$. Hence, after the algorithm terminates, the number of constituent polyhedra in the partition of X can often be reduced considerably by aggregating pairs of neighboring polyhedra whenever their union remains polyhedral, see also (Bemporad, Fukuda, and Torrisi 2001).

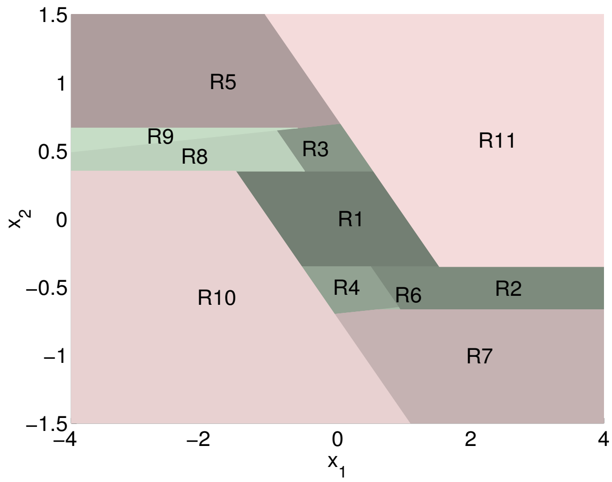

Figure A.4: Partition for the constrained LQR for the double integrator with boundary layers.

Double integrator example, cont'd. The partition computed using Algorithm 1 with a successive aggregation of neighboring regions is shown in Figure A.4. We observe that the number of regions is 11, which is the smallest possible number of polyhedral regions capable of characterizing the activity sets for this problem. Also, we observe that within each region, there is a single candidate optimal active constraint set sequence. Hence, the PWL feedback law is explicitly characterized by this partition. Feedback 0 (unconstrained case) is associated with R1, R3 and R4 in this partition. Feedback 1 ($u = -1$) is associated with R5 and R11. Feedback 2 ($u = 1$) is associated with R7 and R10. Feedback 3 ($x_2 = -0.5$) is associated with R2 and R6, while feedback 4 ($x_2 = 0.5$) is associated with R8 and R9. □

A.5 Optimality, complexity and real-time implementation

A.5.1 Upper and lower bounds on cost function

Define the closed loop performance of the suboptimal constrained LQR as follows:

$$\hat{V}(x(0)) = \sum_{t=0}^{\infty} \left(x^T(t)Qx(t) + (u^*(t))^T Ru^*(t) \right) \tag{A.55}$$

For example 1, upper and lower bound on cost $V(x(0))$ are illustrated in Figure A.5. These bounds are computed by solving LMIs with a continuous piecewise quadratic parameterization of the functions as described in (Johansson and Rantzer 1998; Rantzer and Johansson 2000), see (Johansen, Petersen, and Slupphaug 2000b) for details. Note that a continuous-time approximation is utilized due to restrictions in the available software implementation (Hedlund and Johansson 1999), and that the bounds have no direct meaning for $x \notin X^F$, except that the upper bound defines a Lyapunov function (under a detectability assumption).

A.5.2 Complexity reduction by sub-optimality

It was claimed initially that we expect that the restrictions introduced on the allowed active constraint set sequence switching times will reduce the computational complexity of the controller, i.e. lead to a partition of the state space with less regions. We illustrate this by an example.

Example 2, Double integrator (Bemporad, Morari, Dua, and Pistikopoulos 2002). Consider the double integrator

$$A = \begin{pmatrix} 1 & T_s \\ 0 & 1 \end{pmatrix}, \qquad B = \begin{pmatrix} T_s^2 \\ T_s \end{pmatrix} \tag{A.56}$$

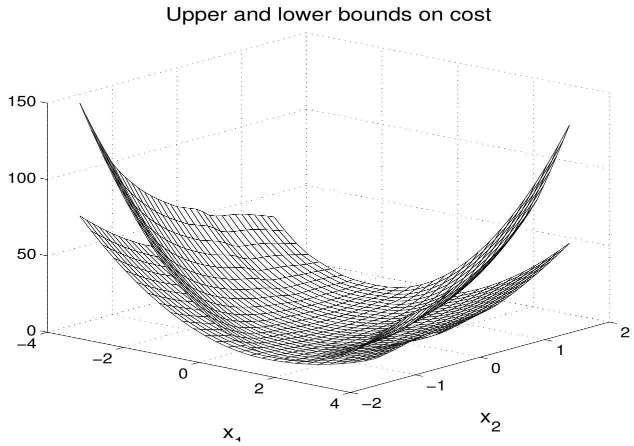

Figure A.5: Upper and lower bounds on the cost for the constrained LQR for the double integrator with boundary layers.

with sampling-interval $T_s = 0.05$. The control objective is defined by the cost function $l_{QR}(x,u) = x_1^2 + 0.1u^2$ and the constraints $-1 \leq u \leq 1$. We consider two cases

i. $N = 8$, with no restrictions on the number of active constraint set switches on the horizon, same as (Bemporad, Morari, Dua, and Pistikopoulos 2002).

ii. $N = 8$, $S = 2$, $N_2 = 3$, i.e. only one active constraint set switch allowed on the horizon

The second case leads to the following nine candidate active constraint set sequences that enumerates the set $\mathcal{C}$:

First 3 samples	Last 5 samples
$u = Kx$	$u = Kx$
$u = Kx$	$u = -1$
$u = Kx$	$u = 1$
$u = -1$	$u = Kx$
$u = -1$	$u = -1$
$u = -1$	$u = 1$
$u = 1$	$u = Kx$
$u = 1$	$u = -1$
$u = 1$	$u = 1$

The suboptimal strategy gives a reduction from 93 to 33 regions, which allows a significant reduction of the real-time processing and memory requirements. From Figure A.6 we observe that the differences in the closed loop trajectories for $x(0) = (-3, 3)^T$ are not very significant. $\square$

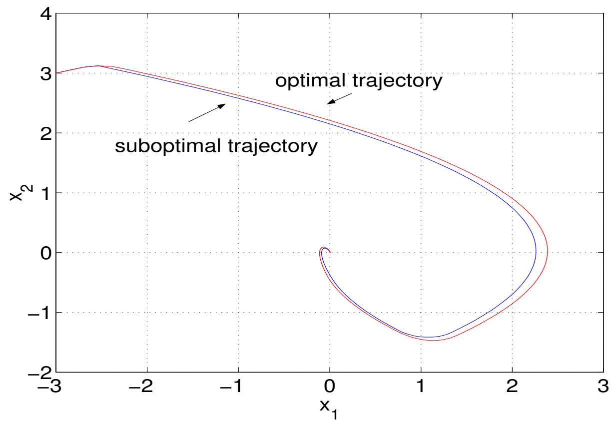

Figure A.6: Example of trajectories with and without active constraint set change restrictions.

A.5.3 Real-time Implementation

The suboptimal constrained LQR is a PWL function of the state. However, efficient evaluation of this PWL function in the real-time control system requires that one is able to efficiently compute in real time which affine feedback to associate with each vector x. The affine state feedbacks are computed offline and stored in real-time computer memory. Whether it is desirable to also compute offline an explicit characterization of the subsets of X where each affine feedback is active depends on several factors: Acceptable offline processing time, available real-time computer memory and real-time computer processing capacity. There exist at least two real-time implementation strategies that can be employed in order to address the above mentioned tradeoffs:

i. The discrete optimization problems (A.17)-(A.20) and (A.23)-(A.25) are solved in real time. Discrete search techniques such as branch-and-bound and A^* can be applied for this purpose (Korf 1990).

ii. A partitioning of X such that within each constituent region of the

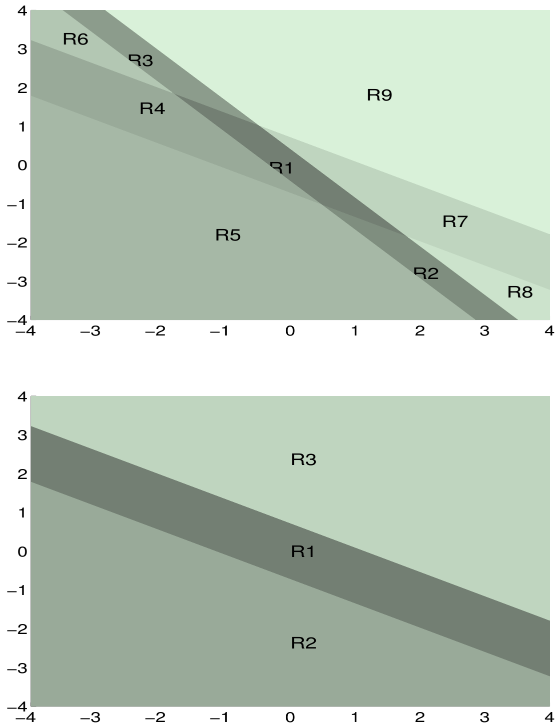

Figure A.7: Double integrator with input constraints and $N = 8$. Top: Simple partition where the maximum number of candidate state feedbacks in each region is 3. Bottom: Simple partition where the maximum number of candidate state feedbacks in each region is 5.

partition there are at most a given small number of affine feedbacks that may be optimal. A search among the small number of remaining candidates (if more than one) is then carried out in real time.

Example 2, continued. By early termination of the partitioning algorithm one can achieve for example the partitions shown in Figure A.7. In the first case there are 9 regions, each with a list of up to 3 affine feedbacks that are optimal at various states within each region, see Table A.1. In the second case there are 3 regions, with a list of up to 5 affine feedbacks that are optimal at various states in each region, see also Table A.1. Hence, one can reduce the complexity of the partition by comparing the values of a user-specified number of quadratic functions and linear constraints in real time.

In a sense, one has a method for partially solving the real-time quadratic program offline. □

	Region	Candidate optimal feedbacks
9 regions	R1	$\{1\}$
	R2	$\{3,6,9\}$
	R3	$\{2,5,8\}$
	R4	$\{7,8,9\}$
	R5	$\{9\}$
	R6	$\{2,8,9\}$
	R7	$\{4,5,6\}$
	R8	$\{3,5,6\}$
	R9	$\{5\}$
3 regions	R1	$\{1,4,5,7,9\}$
	R2	$\{3,5,6,9\}$
	R3	$\{2,5,8,9\}$

Table A.1: List of candidate optimal feedbacks for the simplified partitions of example 2.

Example 3, laboratory model helicopter. A laboratory model helicopter (Quanser 3-DOF Helicopter) with two DC-motor driven rotors is sampled with $T = 0.01s$, and the following state-space representation is obtained

$$A = \begin{pmatrix} 1 & 0 & 0.01 & 0 & 0 & 0 \\ 0 & 1 & 0 & 0.01 & 0 & 0 \\ 0 & 0 & 1 & 0 & 0 & 0 \\ 0 & 0 & 0 & 1 & 0 & 0 \\ 0.01 & 0 & 0 & 0 & 1 & 0 \\ 0 & 0.01 & 0 & 0 & 0 & 1 \end{pmatrix}, \quad B = \begin{pmatrix} 0 & 0 \\ 0.0001 & -0.0001 \\ 0.0019 & 0.0019 \\ 0.0132 & -0.0132 \\ 0 & 0 \\ 0 & 0 \end{pmatrix}$$

The states of the system are x_1 - elevation, x_2 - pitch angle, x_3 - elevation rate, x_4 - pitch angle rate, x_5 - integral of elevation error, and x_6 - integral of pitch angle error. The inputs are u_1 and u_2, the front and rear rotor voltages. Assume the system is to be regulated to some setpoint with the following constraints on the inputs, pitch and elevation rates $-1 \leq u_1 \leq 3$, $-1 \leq u_2 \leq 3$, $-0.25 \leq x_3 \leq 0.25$, and $-0.6 \leq x_4 \leq 0.6$. The LQ cost function is given by $Q = \text{diag}(100, 20, 40, 8, 1, 0.5)$ and $R = \text{diag}(1, 1)$. With $N = 1$ this leads to 33 active constraint sets. Comparing their quadratic cost function and evaluating the linear constraints requires in the worst case 320 microseconds on a 450 MHz Pentium II with our implementation. If necessary, this can be reduced by state space partitioning using Algorithm 1. The experimental results in Figure A.8 compares the performance along the elevation axis with unconstrained LQR. □

Another experimental case study utilizing this approach in an automotive application is reported in (Petersen, Johansen, Kalkkuhl, and Lüdemann 2001). Due to the exponential growth of the number of candidate active constraint set sequences as the number of states, horizon and constraints increases, the approach is restricted to problems of low and moderate complexity. As the problem complexity increases, the use of prior knowledge and simulation are the keys to restricting the number of candidate active constraint set sequences and the (offline and online) computational complexity.

A.6 Conclusions

A suboptimal strategy for explicit offline design of LQ controllers subject to state and input constraints is derived. It is demonstrated that allowing suboptimality in terms of restrictions on the number of allowed active constraint set changes on the horizon leads to significant reduction in the complexity of the state space partitioning. The method gives the user flexibility to address the tradeoff between real-time computer memory and processing capacity.

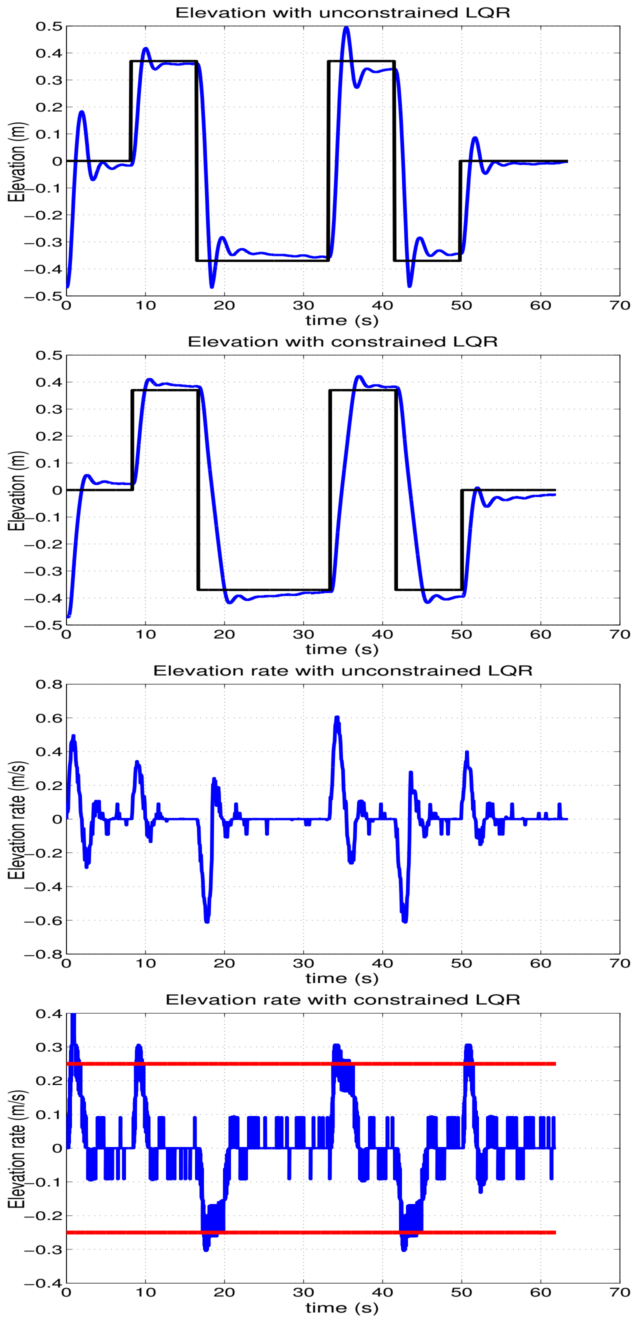

Figure A.8: Experimental results with 3-DOF laboratory model helicopter.

Appendix B

Details of Proof

In this section it is proven that (4.37) implies $D(v) > 0$ for all $v > 0$.

$$\dot{P}_{1,1}(v) = \frac{\partial P_{1,1}(v)}{\partial v}\dot{v} =$$
$$\frac{\left(\alpha_1^2 + \beta_1^2 R^{-1}\left(Q_{2,2}(v) + \frac{2\left(Q_{1,1}(v)/R^{-1}\right)^{1/2}}{\beta_1}v\right)\right)^{1/2}\frac{d}{dv}Q_{1,1}(v)}{2\beta_1\left(Q_{1,1}(v)R^{-1}\right)^{1/2}}\dot{v}$$
$$+\frac{\left(Q_{1,1}(v)R^{-1}\right)^{1/2}\beta_1\left(\frac{d}{dv}Q_{2,2}(v) + \frac{2\left(Q_{1,1}(v)/R^{-1}\right)^{1/2}}{\beta_1} + \frac{\frac{d}{dv}Q_{1,1}(v)}{\beta_1\left(Q_{1,1}(v)R^{-1}\right)^{1/2}}v\right)}{2\left(\alpha_1^2 + \beta_1^2 R^{-1}\left(Q_{2,2}(v) + \frac{2\left(Q_{1,1}(v)/R^{-1}\right)^{1/2}}{\beta_1}v\right)\right)^{1/2}}\dot{v} \tag{B.1}$$

$$\dot{P}_{1,2}(v) = \dot{P}_{2,1}(v) = \frac{\partial P_{1,2}(v)}{\partial v}\dot{v} =$$
$$\left(\frac{\left(Q_{1,1}(v)/R^{-1}\right)^{1/2}}{\beta_1} + \frac{\frac{d}{dv}Q_{1,1}(v)}{2\beta_1\left(Q_{1,1}(v)R^{-1}\right)^{1/2}}v\right)\dot{v} \tag{B.2}$$

$$\dot{P}_{2,2}(v) = \frac{\alpha_1 + \left(\alpha_1^2 + \beta_1^2 R^{-1}\left(Q_{2,2}(v) + \frac{2\left(Q_{1,1}(v)/R^{-1}\right)^{1/2}}{\beta_1}v\right)\right)^{1/2}}{\beta_1^2 R^{-1}}\dot{v}$$
$$+\frac{\left(\frac{d}{dv}Q_{2,2}(v) + \frac{2\left(Q_{1,1}(v)/R^{-1}\right)^{1/2}}{\beta_1} + \frac{\frac{d}{dv}Q_{1,1}(v)}{\beta_1\left(Q_{1,1}(v)R^{-1}\right)^{1/2}}v\right)v}{2\left(\alpha_1^2 + \beta_1^2 R^{-1}\left(Q_{2,2}(v) + \frac{2\left(Q_{1,1}(v)/R^{-1}\right)^{1/2}}{\beta_1}v\right)\right)^{1/2}}\dot{v} \tag{B.3}$$

Now

$$
\begin{aligned}
D(v) = & \frac{\left(\alpha_1^2 + \beta_1^2 R^{-1}\left(Q_{2,2}(v) + \frac{2\left(Q_{1,1}(v)/R^{-1}\right)^{1/2}}{\beta_1} v\right)\right)^{1/2} \frac{d}{dv} Q_{1,1}(v)\alpha_1}{2\beta_1 \left(Q_{1,1}(v)R^{-1}\right)^{1/2} \beta_1^2 R^{-1}} \\
& + \frac{\left(\alpha_1^2 + \beta_1^2 R^{-1}\left(Q_{2,2}(v) + \frac{2\left(Q_{1,1}(v)/R^{-1}\right)^{1/2}}{\beta_1} v\right)\right) \frac{d}{dv} Q_{1,1}(v)}{2\beta_1 \left(Q_{1,1}(v)R^{-1}\right)^{1/2} \beta_1^2 R^{-1}} \\
& + \frac{\frac{d}{dv} Q_{1,1}(v)\left(\frac{d}{dv} Q_{2,2}(v) + \frac{2\left(Q_{1,1}(v)/R^{-1}\right)^{1/2}}{\beta_1} + \frac{\frac{d}{dv} Q_{1,1}(v)}{\beta_1 \left(Q_{1,1}(v)R^{-1}\right)^{1/2}} v\right) v}{4\beta_1 \left(Q_{1,1}(v)R^{-1}\right)^{1/2}} \\
& + \frac{\left(Q_{1,1}(v)R^{-1}\right)^{1/2} \beta_1 \left(\frac{d}{dv} Q_{2,2}(v) + \frac{2\left(Q_{1,1}(v)/R^{-1}\right)^{1/2}}{\beta_1} + \frac{\frac{d}{dv} Q_{1,1}(v)}{\beta_1 \left(Q_{1,1}(v)R^{-1}\right)^{1/2}} v\right)}{2\left(\alpha_1^2 + \beta_1^2 R^{-1}\left(Q_{2,2}(v) + \frac{2(Q_{1,1}(v)/R^{-1})^{1/2}}{\beta_1} v\right)\right)^{1/2}} \frac{\alpha_1}{\beta_1^2 R^{-1}} \\
& + \frac{\left(Q_{1,1}(v)R^{-1}\right)^{1/2} \beta_1 \left(\frac{d}{dv} Q_{2,2}(v) + \frac{2\left(Q_{1,1}(v)/R^{-1}\right)^{1/2}}{\beta_1} + \frac{\frac{d}{dv} Q_{1,1}(v)}{\beta_1 \left(Q_{1,1}(v)R^{-1}\right)^{1/2}} v\right)}{2\beta_1^2 R^{-1}} \\
& + \frac{\left(Q_{1,1}(v)R^{-1}\right)^{1/2} \beta_1 \left(\frac{d}{dv} Q_{2,2}(v) + \frac{2\left(Q_{1,1}(v)/R^{-1}\right)^{1/2}}{\beta_1} + \frac{\frac{d}{dv} Q_{1,1}(v)}{\beta_1 \left(Q_{1,1}(v)R^{-1}\right)^{1/2}} v\right)^2}{4\left(\alpha_1^2 + \beta_1^2 R^{-1}\left(Q_{2,2}(v) + \frac{2(Q_{1,1}(v)/R^{-1})^{1/2}}{\beta_1} v\right)\right)} v \\
& - \left(\frac{\left(Q_{1,1}(v)/R^{-1}\right)^{1/2}}{\beta_1} + \frac{\frac{d}{dv} Q_{1,1}(v)}{2\beta_1 \left(Q_{1,1}(v)R^{-1}\right)^{1/2}} v\right)^2
\end{aligned}
$$

Define the following positive variables:

$$
\begin{aligned}
A &= \alpha_1^2 + D\left(Q_{2,2}(v) + \frac{2C}{D} v\right) = \alpha_1^2 + DQ_{2,2}(v) + 2Cv \\
B &= \frac{d}{dv} Q_{2,2}(v) + \frac{2C}{D} + \frac{\frac{d}{dv} Q_{1,1}(v)}{C} v \\
C &= \left(Q_{1,1}(v)R^{-1}\right)^{1/2} \beta_1 \\
D &= \beta_1^2 R^{-1}
\end{aligned}
$$

The above expression can then be rewritten to

$$D(v) = \frac{A^{1/2}\frac{d}{dv}Q_{1,1}(v)\alpha_1}{2CD} + \frac{A\frac{d}{dv}Q_{1,1}(v)}{2CD} + \frac{\frac{d}{dv}Q_{1,1}(v)Bv}{4C} + \frac{\alpha_1 BC}{2A^{1/2}D} + \frac{CB}{2D} + \frac{CB^2}{4A}v - \left(\frac{C}{D} + \frac{\frac{d}{dv}Q_{1,1}(v)}{2C}v\right)^2 \tag{B.4}$$

In (B.4) there are two possible negative factors involved: α_1 and the last quadratic term with a negative sign $(-P'_{1,2}(v)P'_{2,1}(v))$. To cancel $P'_{1,2}(v)P'_{2,1}(v)$, parts from the 3rd and 5th term in (B.4) are used which gives

$$\frac{\frac{d}{dv}Q_{1,1}(v)Bv}{4C} + \frac{CB}{2D} - \left(\frac{C}{D} + \frac{\frac{d}{dv}Q_{1,1}(v)}{2C}v\right)^2 = \frac{\frac{d}{dv}Q_{2,2}(v)\frac{d}{dv}Q_{1,1}(v)}{4C}v + \frac{d}{dv}Q_{2,2}(v)$$

The following inequality thus ensures $D(v) > 0$:

$$D(v) = \frac{A^{1/2}\frac{d}{dv}Q_{1,1}(v)\alpha_1}{2CD} + \frac{A\frac{d}{dv}Q_{1,1}(v)}{2CD} + \frac{\frac{d}{dv}Q_{2,2}(v)\frac{d}{dv}Q_{1,1}(v)}{4C}v + \frac{\alpha_1 BC}{2A^{1/2}D} + \frac{d}{dv}Q_{2,2}(v) + \frac{CB^2}{4A} > 0 \tag{B.5}$$

where only α_1 may have a negative value.